THE PLASMINOGEN RECEPTOR S100A10: STRUCTURE AND FUNCTION STUDIES

by

Victoria Ann Miller

Submitted in partial fulfilment of the requirements
for the degree of Doctor of Philosophy

at

Dalhousie University
Halifax, Nova Scotia

December 2019

CONTENTS

For Craig, for encouraging me to chase down my dreams…

LIST OF TABLES

LIST OF FIGURES

ABSTRACT

The critical role of the fibrinolytic system is the maintenance of vascular patency. Dysregulation ultimately leads to death; an inappropriate activation that causes excessive bleeding, or an inability to clear blood clots, leading to thrombosis, ischemia and death. Plasminogen receptors (PgR) are found on the surface of many cells, notably endothelial cells and lymphocytes. PgR bind plasminogen to the cell surface, promote directed proteolytic plasmin activity and protect bound plasmin from inhibition. This process is important for vessel patency, wound healing and inflammation. In addition to homeo- and hemostatic roles, PgR can be hi-jacked by cancerous cells for more nefarious roles. Oncogenic cells utilize focussed proteolytic activity of cell-bound plasmin to escape from primary tumours. Understanding how the PgR, plasminogen and activators interact may lead to targeted therapies for clot dissolution or cancer, among other diseases. Plasminogen contains kringle domains that bind to C-terminal lysine residues of fibrin and PgR. Studies were undertaken to explore how alterations in the C-terminal region of S100A10, a PgR, impact its ability to accelerate plasmin generation. S100A10 has 4 lysine residues in its C-terminal region, two at the C-terminus. Deletion of both C-terminal lysine residues results in the loss of up to 90% of the rate of plasmin generation. Substitution of the C-terminal lysines with isoleucine resulted in minimal activity loss. This led to the possibility that another lysine residue is a secondary binding site for kringles. Mutating internal sequence lysine residues to arginine resulted in little change in plasmin generation ability, however, changing a lysine to arginine at position 56 in addition to the substitution of C-terminal lysines to isoleucine resulted in a significant loss of plasmin generating ability.

Additionally, a study was initiated to explore a potential role of S100A10 in the demyelination of multiple sclerosis and other diseases whose hallmark is myelin loss. S100A10-null mice, 7 days post-demyelination event (lysophosphatidylcholine injection), had significantly larger lesion volumes than wild type mice injected concurrently. S100A10-null lesions had lower concentrations of microglia/macrophages within the borders of the lesion, indicating that the larger lesion possibly stemmed from a reduced ability to phagocytose degraded myelin.

µg	Microgram
µM	Micromolar
5-HT1B	SerotoninReceptor
A2PI	Alpha2 Plasmin Inhibitor
AIIt	Annexin A2 Heterotetramer
Arg	Arginine
Asn	Asparagine
Asp	Aspartic Acid
BAC	Bacterial Artificial Chromosome
BBB	Blood-Brain Barrier
C	Cysteine
CD	Circular Dichroism
CD-#	Cluster of Differentiation (with number)
CNS	Central Nervous System
CpB	Carboxypeptidase B
CpB2	Carboxypeptidase B2
CpN	Carboxypeptidase N
C-terminal	Carboxy-terminal
Cys	Cysteine
D	Aspartic Acid
DTT	Dithiothreitol
E. coli	*Escherichia coli*
EAE	Experimental Autoimmune Encephalitis
EGF	Endothelial Growth Factor
EGFP	Enhanced Green Fluorescent Protein
EGTA	Ethylene Glycol-bis(β-aminoethyl ether)-N,N,N′,N′-Tetra Acetic acid
FpA/FpB	Fibrinopeptide A or B
GABA	Gamma-Aminobutyric Acid
GFAP	Glial Fibrillary Acidic Protein
H	Histidine
h	Hour
His	Histidine
HMGB-1	High Mobility Group Box-1
HMW	High Molecular Weight
I	Isoleucine
Iba-1	Ionized Calcium Binding Adaptor Molecule 1
IFN-γ	Interferon-gamma
IL-#	Interleukin-(with number)

Ile	Isoleucine
K	Lysine
Kd	Dissociation constant
kDa	Kilodalton
Km	Michaelis constant
Kr	Kringle
L	Litre
LMW	Low Molecular Weight
Lys	Lysine
MBP	Myelin Basic Protein
mg	Milligram
MHC	Major Histocompatibility Complex
MHV	Mouse Hepatitis Virus
min	Minute
mL	Millilitre
mM	Millimolar
MMP	Matrix Metalloproteinase
MOG_{35-55}	Myelin Oligodendrocyte Glycoprotein$_{(33-55)}$
MS	Multiple Sclerosis
N	Asparagine
NG2	Neural/Glial Antigen 2
N-linked	Nitrogen-linked
nM	Nanomolar
OL	Oligodendrocytes
O-linked	Oxygen-linked
OPC	Oligodendrocyte Precursor Cells
PA	Plasminogen Activator
PAI	Plasminogen Activator Inhibitor
PBS	Phosphate Buffered Saline
Pg	Plasminogen
PgR	Plasminogen Receptor
$PLP_{139-151}$	Proteolipid Proteins
Pm	Plasmin
R	Arginine
RT	Room Temperature
S	Serine
SD	Standard Deviation
SDS-PAGE	Sodium Dodecyl Sulphate-Polyacrylamide Gel Electrophoresis
SEM	Standard Error of the Mean
Ser	Serine
SERPINS	Serine Protease Inhibitors

SP	Serine Protease Domain
T	Tyrosine
TAFI	Thrombin Activated Fibrinolysis Inhibitor
TBS-Tw	Tris Buffered Saline with 0.5% Tween 20
Thr	Threonine
TMEV	Theiler's Murine Encephalomyelitis Virus
tPA	Tissue-type Plasminogen Activator
Tyr	Tyrosine
uPA	Urokinase-type Plasminogen Activator
uPAR	Urokinase-type Plasminogen Activator Receptor
V	Volts
Val	Valine
WT	Wild Type
α_2-AP	Alpha2-antiplasmin
α2M	Alpha2 Macroglobulin
ε-ACA	Epsilon-Amino Caproic Acid

ACKNOWLEDGMENTS

A thesis is never completed in isolation. This one is no different in that regard.

This thesis would not have happened without the support and guidance of my supervisor, David Waisman. It has been a wonderful learning experience. Who knew a technician could become a student again….

Thank you to my supervisory committee, Alex Easton, Brent Johnston and Rob Liwski. I appreciated your enthusiasm for the projects I explored and enjoyed discussions in and out of the committee meetings.

Thank goodness for lab mates; they help make the whole thesis journey, never mind the day-to-day goings-on in the lab. Thank you to Dharini for helping me to hang on to my sanity. Big thanks to those lab mates that contributed to the data in this thesis; Dila and Jeffery were rocking honours students, Patricia helped me get off the ground with the initial mutations and Ryan provided some pivotal information on surface exposure.

A big thank you to the non-scientists of my world. You made sure I remembered there is more to life than lab work and the inevitable analysis. Big shout out to the Fireballs ringette team, Accel Physio hockey team and my Shimmy Sisters. An equal shout out to all those I am proud to call friend, both in Nova Scotia and in Ontario. We will be celebrating this accomplishment soon.

Lastly, but by no means last in my heart is my family. The encouragement, check-ins and reality checks were appreciated. A huge thank you to my biggest fan, Craig for never allowing me to quit. Love you huge bunches!

1.1 FIBRINOLYSIS

Maintenance of the patency of the vascular system is the crucial task of the fibrinolytic system. In the absence of fibrinolytic surveillance and clearing, occlusive thrombi would result, resulting in ischemia, thrombosis and eventual death of the organism. It is this underlying need for a well-regulated fibrinolytic system, whether coordinated through plasmin or some other proteolytic enzyme, that is absolutely required for vertebrate life.

Primary hemostasis initiates upon damage to the endothelial cells lining blood vessels, the vessel first releases endothelin, resulting in a short-lived vascular contraction. This is rapidly followed by the binding of von Willebrand Factor to the exposed collagen in the subendothelial space. The collagen-bound von Willebrand Factor binds to platelets via glycoprotein Ib, resulting in the activation of the platelets, which includes a shape change, release of their granules and a conformational change in the glycoprotein IIb/IIIa receptor on the platelet surface, allowing it to bind to fibrinogen (Winter et al., 2017). Secondary hemostasis or coagulation (Figure 1.1) is initiated by tissue factor expressed on the endothelial cell surface, leading to the eventual activation of prothrombin to thrombin, ultimately resulting in the production of fibrin from fibrinogen. This protein meshwork, further described in section 1.4, stabilizes the clot until tissue repair and remodelling can take place, preventing excessive blood loss. Once the clot is no longer required, fibrinolysis is the mechanism essential for its removal (Kumar et al., 2015; Lijnen and Collen, 1995; Longstaff and Kolev, 2015) (Figure 1.1).

As illustrated in Figure 1.1, the proteins involved in fibrinolysis include plasminogen and its active form plasmin. Plasminogen is activated by tissue-plasminogen activator (tPA) and urokinase plasminogen activator (uPA), and the

relevant primary inhibitors are α2-antiplasmin (for plasmin) and plasminogen activator inhibitor-1 (for tPA and uPA). Deficiencies or an over-abundance of any of these proteins can result in an upset of the fibrinolytic system, each of which is described in the section describing the particular protein.

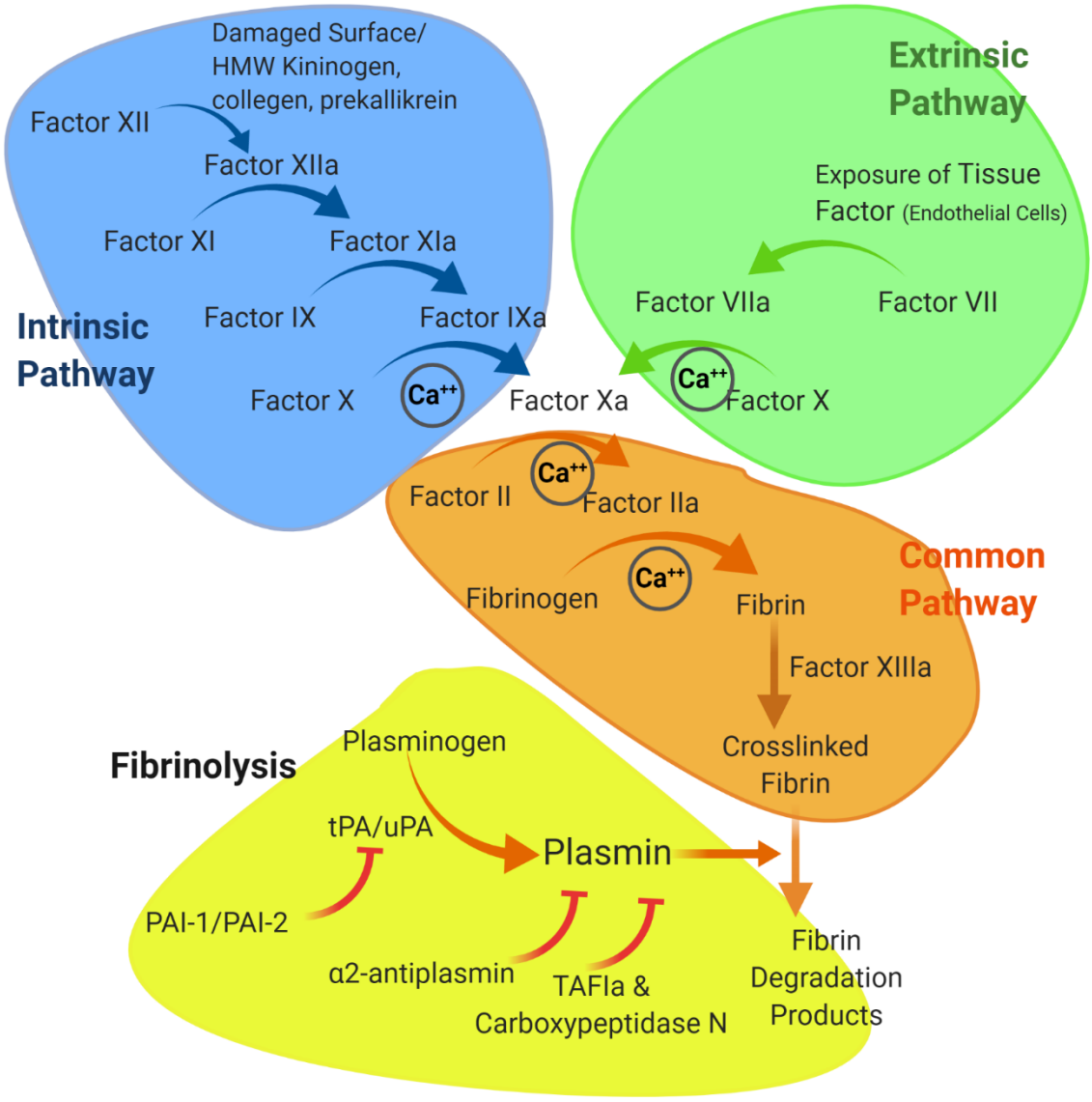

Figure 1-1 Simplified Coagulation Cascade and Fibrinolysis Cascade

Intrinsic or Contact pathway highlighted in blue, Extrinsic or Tissue Factor pathway highlighted in green. These pathways merge into the common pathway (orange background). The fibrinolysis pathway highlighted in yellow. Inhibitors are denoted by a red line. Active forms of coagulation factors are denoted by the addition of "a". Created with Biorender.com

1.2 PLASMINOGEN AND PLASMIN

Plasminogen is a 92-94 kiloDalton protein (dependent on glycosylation status) that circulates as zymogen in the blood. Plasminogen, like many hemostatic proteins, is produced in the liver and is found at a concentration of approximately 2 μM in the plasma (Ranson and Andronicos, 2003). It is a multi-domain protein, consisting of an amino(N)-terminal peptide domain (also referred to as the pan-apple domain), 5 kringle domains and the serine protease domain (Figure 1.2). The classical catalytic triad is located within the serine protease domain; Histidine (His) 603, Aspartic acid (Asp) 646 and Serine (Ser) 741. This domain has some homology with other serine proteases, such as trypsin and elastase (Castellino and McCance, 1997). Plasminogen is similar to trypsin, in it preferentially cleaves the peptide bond after a lysine or arginine residue. Glu-plasminogen (Glu-Pg) refers to the full-length protein; the N-terminal amino acid is glutamine. The removal of the N-terminal peptide at the peptide bond between lysine 76 and lysine 77 results in Lys-plasminogen (Lys-Pg). The active form of the protein, plasmin, performs this function.

There are two major glycoforms of plasminogen, Type I and Type II. Both have an O-linked sugar residue at Thr 346. Type I also has an N-linked sugar at Asp 289. Glycosylation status plays a role in plasminogen targeting; Type I plasminogen preferentially binds to and is activated on fibrin clots (Takada et al., 1985) while Type II plasminogen is targeted to the cell surface (Gonzalez-Gronow et al., 2002). These sites of glycosylation are identified in Figure 1.2.

The kringle domains are so-named due to their superficial physical resemblance to kringle pastries. The 3-dimensional structure of protein kringle domains is regulated by multiple intra-molecular disulphide bonds and can be a binding site for lysine residues. The current dogma states that it is C-terminal lysine residues that bind kringle domains. Interaction with the kringle domain is mediated by hydrophobic interaction as well as charge. Lysine (Lys) is a basic, charged aliphatic

amino acid; its side chain consists of a 4-carbon chain and a positively charged amine group. The amino group of lysine or interacts with negatively charged aspartic acid residues within the binding pocket of the kringle while the hydrocarbon chain, consisting of 4 methyl groups, interacts with the hydrophobic cleft of the kringle (Castellino and McCance, 1997). Figure 1.3 illustrates the binding of a lysine analogue, ε-aminocaproic acid within the binding pocket of kringle 4 of plasminogen. Each kringle is a triple loop structure of between 78 and 80 amino acids; the disulphide bonds within the polypeptide chain provides stability to the structure (Godier and Hunt, 2013). Of the 5 plasminogen kringles, kringle 3 is unable to bind to lysine; it contains a lysine residue at the position where other kringles have an aspartic acid residue that prevents lysine residues of binding proteins from binding (Christen et al., 2010).

Plasminogen circulates in a 'closed conformation', with the lysine 50 residue of the N-terminal activation peptide of the pan- apple domain inserted in the lysine binding site of kringle 5 (Law et al., 2012), noting this is an internal lysine motif interacting with a kringle domain. The closed conformation allows only kringle 1 to be available for lysine binding; all other kringles are engaged in intramolecular interaction, blocking any interaction with lysine moieties. The activation cleavage site is not easily accessible by its activators. Removal of the first 76 amino acids of Glu-plasminogen, the N-terminal activation peptide, results in Lys-plasminogen. Lys-plasminogen has a more relaxed conformation, enhancing its activation to Lys-plasmin(Gong et al., 2001).

Many studies have been performed to explore the interactions between Glu-plasminogen, Lys-plasminogen, lysine and lysine analogues (Kornblatt et al., 2001, 2007; V. A. Miller et al., 2017; Sun et al., 2002). Studies exploring the kinetics and mechanics of lysine analogs binding to plasminogen and the subsequent conformational changes in plasminogen revealed that the increase in activation rate induced by plasminogen activators results from a relaxation of the tight

confirmation that plasminogen primarily adopts while in circulation (Ranson and Andronicos, 2003).

The crystal structure of plasminogen has been recently solved (Law et al., 2013, 2012). This study confirmed that only Kr1 of circulating plasminogen is solvent-exposed and readily available for binding to lysine residues. It is Kr1 of plasminogen that mediates binding to both cell surface receptors as well as to fibrin. The crystal structure of plasminogen also revealed that the cleavage site for Lys-plasminogen is buried in the tight formation. This suggests that an intermediate conformation is required to reveal the Lys76-Lys77 bond prior to its hydrolysis. Binding to a cell surface receptor may help facilitate this conformation (Law et al., 2013; Miles and Parmer, 2013).

Plasmin, a serine proteinase, is the active form of the protein. It is formed after cleavage at Arg561/Val562 by tPA, uPA, or by previously activated plasmin. Plasmin is 83 kDa, with the heavy chain remaining associated with the light chain through disulphide bonds. These disulphide bonds are indicated in Figure 1.2 by light blue lines. Of particular importance are the bonds between Cysteine (Cys)548 of the heavy chain and Cys 666 of the light chain, as well as Cys 558 of the heavy chain and Cys 566 of the light chain (Castellino and McCance, 1997). It is these disulphide bonds that ensure the binding functionality of the kringles remains associated with the catalytic centre of the light chain.

Plasmin is a broad-spectrum proteinase, with targets that include plasminogen, cross-linked fibrin, matrix metalloproteinase (MMP)—1, -2, and -9, fibronectin, laminin, thrombospondin, and von Willebrand factor (Hermel et al., 2010; Lijnen and Collen, 2003; Schaller and Gerber, 2011; van der Vorm et al., 2018). The broad range of substrates results in an extensive range of processes, both physiologic and pathologic, in which plasmin participates. These processes include fibrinolysis, signalling pathways, cell migration, wound healing, inflammation, and oncogenesis (Andreasen et al., 2000).

Both the rate and location of plasmin formation is tightly controlled. To ensure homeo- and haemostasis, plasmin generation is typically restricted to sites of thrombosis, angiogenesis and sites of extracellular matrix remodelling. Unrestrained plasmin generation is a factor in the depletion of pro-coagulant proteins in disseminated intravascular coagulation (Plow et al., 1995). Indiscriminate plasmin generation is also a method tumour cells use to enable cell invasion and metastasis (Andreasen et al., 2000; Poddar et al., 2017).

Local surfaces play a part in plasmin generation; both fibrin surface and the cell surface carry out a similar regulatory role. Plasminogen receptors found on the cell surface, some of which also bind tPA, colocalize with receptors that specifically attract plasminogen activators. The plasminogen receptors provide the lysine residues for binding and protect the resulting plasmin from inactivation. Similarly, on the fibrin clot surface, C-terminal lysine residues are interspersed within the fibrin network. Restricting plasmin activation to either a cell surface or the clot surface allows for proteolytic targeting, as well as some protection from circulating inhibitors. There is limited evidence that kringles can interact with internal lysine domains (Knaust et al., 2007).

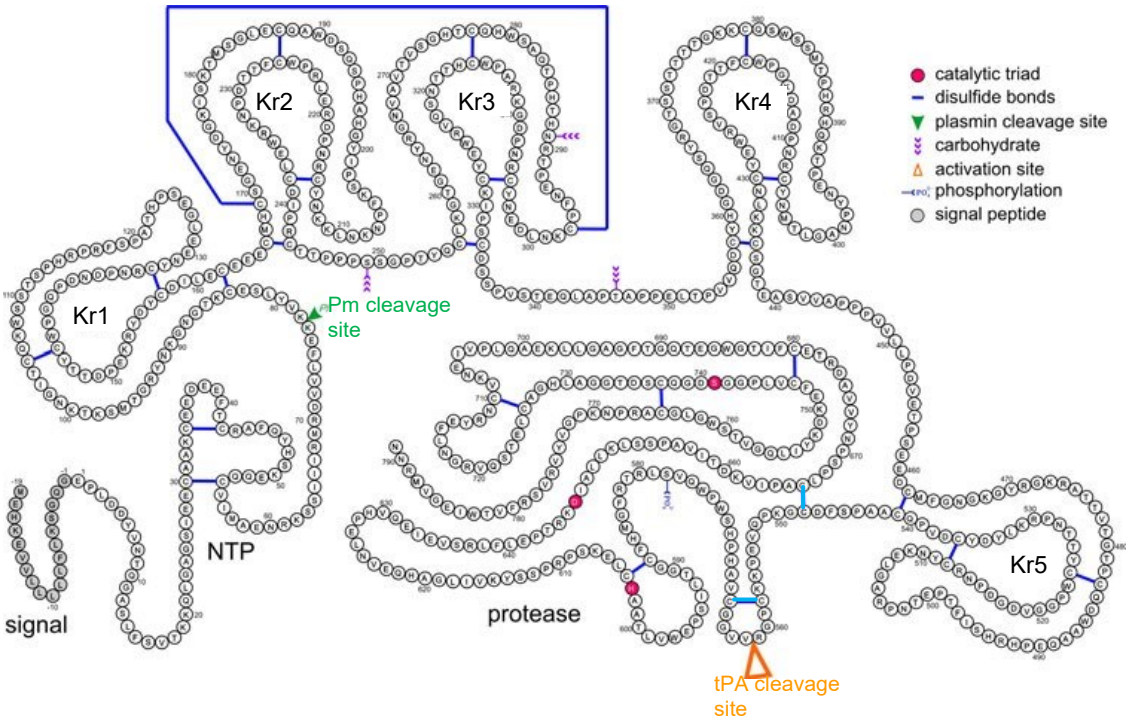

Figure 1-2 Graphic Representation of the Primary Structure of Plasminogen.

The activation cleavage site (tPA cleavage)is located at the orange triangle the catalytic site amino acids are denoted by red circles. The N-teminal peptide (NTP) and cleavage site of plasmin (green triangle), along with the signal peptide are on the left. The disulphide bonds that connect the heavy and light chain are highlighted in light blue, all other disulphide bonds are dark blue.The glycosylation sites, and kringles 1 through 5 are noted. Reproduced with permission from Schaller and Gerber, Cellular and Molecular Life Science 68:785-801 via Copyright Clearance Center.

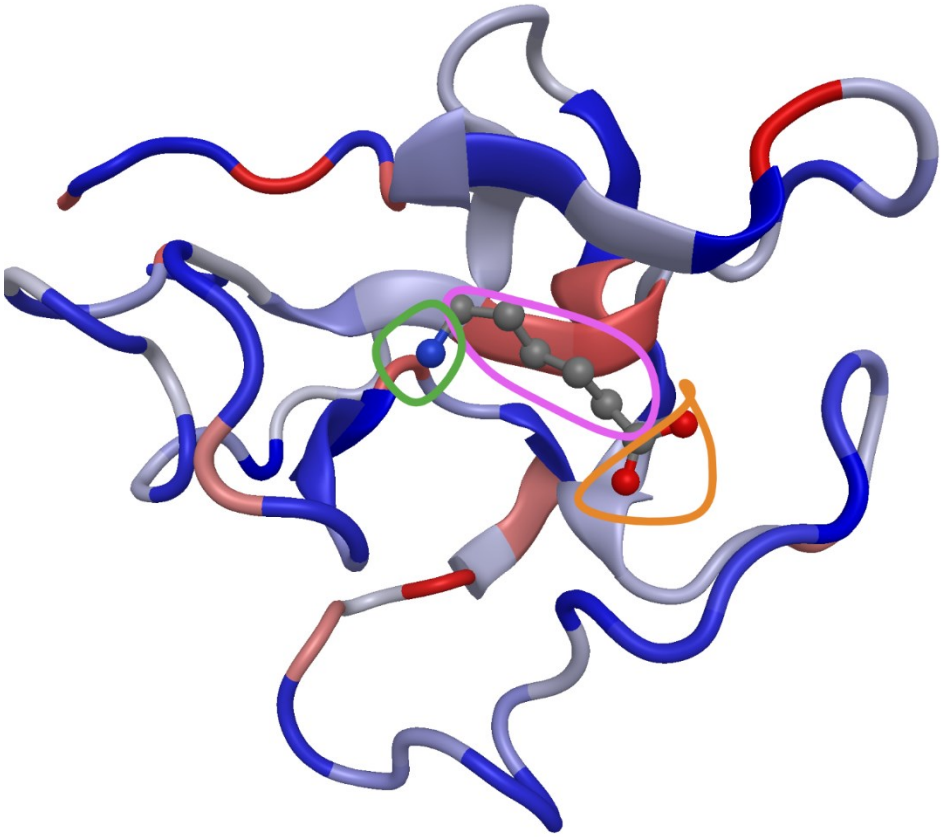

Figure 1-3 Schematic of ε-ACA in Lysine Binding Site of Kringle

The kringle domain is illustrated as a ribbon, while the lysine analogue, ε-ACA, the ligand is represented as a ball and stick. The carboxylate group of the ε-ACA interacts with a positively charged portion of the kringle (orange outline), while the amino group of the ε-ACA interacts with a negatively charged pocket (green outline). The carbon chain of the lysine analogue interacts with the hydrophobic cleft of the kringle (pink outline). Created with Biorender.com from X-ray crystal structure data generated by Wu, T.P., et al. Biochemistry 30: 10589–10594.

1.3 CONTROL OF FIBRINOLYSIS

1.3.1 PLASMINOGEN ACTIVATORS: TPA AND UROKINASE

Two physiologic activators of plasminogen exist: tissue-type plasminogen activator (tPA) and urokinase-type plasminogen activator (uPA). The mechanism of interaction of tPA with plasminogen is much better understood as it is used clinically as a thrombolytic therapeutic (Longstaff and Kolev, 2015). Both tPA and uPA are multi-domain proteases. The active forms of each of these enzymes are inhibited by plasminogen activator inhibitor- 1 (PAI-1) and PAI-2.

tPA is a 70kDa protein of 527 amino acids (Figure 1.4). It consists of 2 kringle domains, a finger domain, endothelial growth factor (EGF)-like domain and a serine protease domain (Hébert et al., 2016). Its activity is inhibited by PAI-1. tPA interacts with fibrin via its finger domain as well as kringle 2. Like most of the kringle domains of plasminogen, kringle 2 is a lysine binding site; however, kringle 1 has a serine residue at the site of a usual tryptophan residue within the hydrophobic cleft which alters its ability to bind to lysine residues (de Vos et al., 1992; Schaller and Gerber, 2011).

tPA is synthesized and secreted by endothelial cells, as well as many brain cells, including neurons, astrocytes, microglia, and oligodendrocytes (Hébert et al., 2016; Schaller and Gerber, 2011). In the brain, it is classified as an immediate-early response gene (Bardehle et al., 2015). The plasma protein concentration of tPA is in the range of 5-10 μg/L. The protein is synthesized as a pro-enzyme as a single chain, cross-linked polypeptide, glycosylated at threonine (Thr)61 (O-linked), asparagine (Asn)117, Asn184 and Asn448 (N-linked). The pro-enzyme has a low serine protease activity. This single-chain form is fully activated by cleavage of the arginine (Arg)275-isoleucine(Ile)276 bond by plasmin, kallikrein or coagulation factor Xa (Schaller and Gerber, 2011). This 2-chain form is held together by a single disulphide bond between Cys264 and Cys395.

tPA interacts with fibrin with high affinity, resulting in greater activation of plasminogen by the activator. The C-terminal lysine and, to a lesser extent, arginine residues found in the fibrin clot after proteolysis by plasmin, bind to the kringle 2 domain of tPA (de Vries et al., 1989; Hoylaerts et al., 1982).

The interaction of tPA with endothelial cells and vascular smooth muscle cells can lead to increased activation of plasminogen. Previous studies proposed that a C-terminal lysine or arginine residue on annexin A2, generated by an unknown protease as the binding site for kringle 2 of tPA (Cesarman et al., 1994; Hajjar et al., 1994). Subsequent studies have thrown doubt on the existence of proteolyzed annexin A2 as the binding site; it is more likely to be the binding partner of annexin A2, S100A10, which possesses a C-terminal lysine residue (Kwon et al., 2005; V. A. Miller et al., 2017). This is addressed further in this thesis.

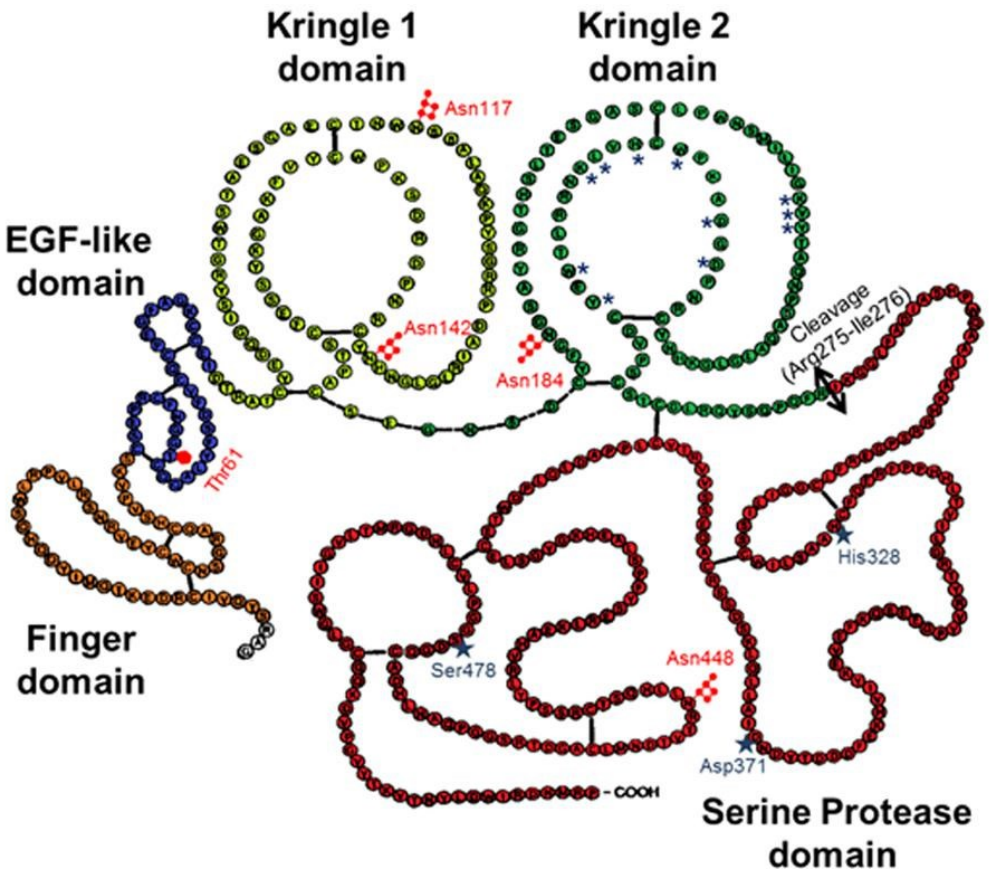

Figure 1-4 Structure of tPA

As noted in the text tissue plasminogen activator is a multi-domain serine protease. It consists of 5 domains: finger domain (orange), EGF-like domain (blue), 2 kringle domains (yellow and green) and a serine protease domain (red). Sites of N- (open red symbols) or O-glycosylation (filled red symbols) are indicated. The active site residues His322, Asp371, and Ser478 are marked by stars. The amino acids involved in the structure of the lysine binding site are noted with asterisks on kringle 2. The double-arrow indicates the cleavage site for conversion of sc-tPA to tc-tPA. Reproduced under terms of the Creative Commons Attribution License, which permits unrestricted use, distribution, and reproduction in any medium, provided the original author and source are credited. Chevilley A, et al (2015) Front. Cell. Neurosci. 9:415.

Like tPA, uPA is found in the plasma at approximately the same concentration, 5-10 μg/L, but it is produced by cells in the lung, kidney as well as keratinocytes and endothelial cells (Schaller and Gerber, 2011). uPA is synthesized as a single-chain protein, with a molecular weight of 55 kDa, consisting of 411 amino acids. This multidomain protein has an EGF-like domain, one kringle domain, and a serine protease domain. Also, like tPA, it is glycosylated: Thr18 (O-linked) and Asn302 (N-linked). Additionally, it has 2 phosphorylation sites: serine (Ser)138 and Ser303 (Figure 1.5). The secreted protein is a zymogen and requires cleavage of its Lys158-Ile159 bond to demonstrate its full activity. The two-chain form is held together by a single disulphide bond; between Cys148 and Cys279. The Lys-Ile bond is cut by plasmin, kallikrein, coagulation factor XIIa or cathepsin B (Schaller and Gerber, 2011; Stoppelli, 2013). This results in the high molecular weight (HMW) form of active uPA. Additionally, there is a low molecular weight (LMW) form, primarily found in the urine, and is generated by plasmin or self-proteolysis at the Lys135-Lys136 bond. This LMW form is lacking both the EGF-like and kringle domains and is unable to bind to the urokinase receptor (Schmitt et al., 1991).

uPA is primarily responsible for cell surface-associated plasminogen activation. This is accomplished by the binding of the single-chain pro-enzyme to the glycosylphosphatidylinositol (GPI)-anchored urokinase receptor (uPAR), where the pro-enzyme is activated by plasmin, cathepsin B or kallikrein (Stoppelli, 2013). The activation of cell-bound plasminogen (see plasminogen receptors in Section 1.5) by receptor-bound uPA is characterized by a 40-fold reduction in the Km for plasminogen activation (Ellis et al., 1991). The co-localization of uPAR with plasminogen receptors localizes the resultant plasmin activity to the cell surface. The cell membrane-bound plasmin activity created by cell-bound plasminogen is protected by inactivation from plasma-borne inhibitors, but its activity can be indirectly reduced by the plasminogen activator inhibitors 1 and 2 through the inhibition of tPA and uPA (Cubellis et al., 1990; Hall et al., 1991). In parallel,

plasmin bound to the surface of cells will cleave pro-uPA bound to uPAR at a rate 50-fold that of plasmin in solution (Ellis et al., 1989; Stephens et al., 1989). This directed activation on the cell surface gives those cells an invasive phenotype. Invasive cells make use of the broad substrate specificity of the resulting plasmin to degrade the various proteins of the extra-cellular matrix, including fibronectin, laminin, vitronectin and proteoglycans. Plasmin can also activate pro-MMPs, resulting in the degradation of collagen (Stoppelli, 2013).

The coordination of the uPA system: plasmin and uPA along with the inhibitors alpha2-antiplasmin and PAI-1 and PAI-2 (discussed in a later section), together with the receptor uPAR, plays an important role in the regulation of cancer progression and metastasis (Andreasen et al., 1997; Ranson and Andronicos, 2003; Stoppelli, 2013).

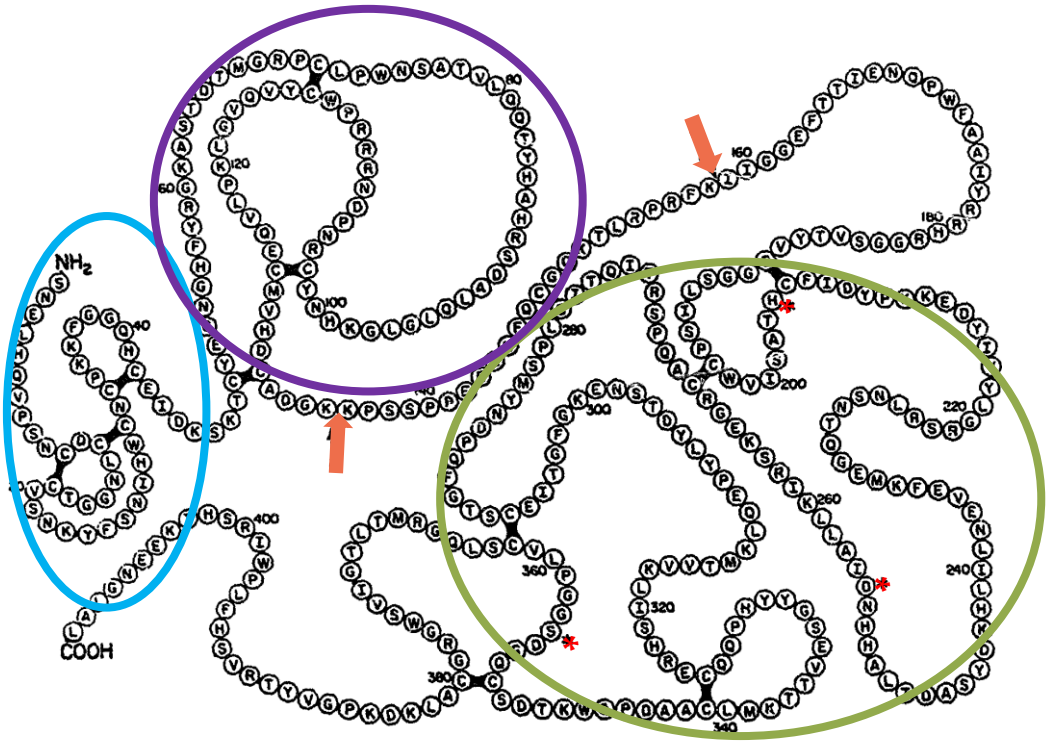

Figure 1-5 Structure of uPA

Cartoon structure of uPA. Amino acids encircled in blue denotes the EGF-like domain, in purple is the kringle domain and green is the serine protease domain. Arrow indicate cleavage site for LMW form (K135) and HMW form (K158). Red asterisks indicate active site residues. Reproduced with permission from Tebbe et al. (1995) J Am Coll Cardiol 26: 365-73 via Copyright Clearance Center.

1.3.2 SERINE PROTEASE INHIBITORS; SERPINS

Serine protease inhibitors (SERPINS) bind to and inactivate their target protease by initiating a large conformational change in the target protease, causing an irreversible inactivation.

1.3.2.1 PLASMINOGEN ACTIVATOR INHIBITORS

The two primary physiologic inhibitors of plasminogen activator are plasminogen activator inhibitor-1 (PAI-1) and plasminogen activator inhibitor-2 (PAI-2). PAI-1 and PAI-2 interact with tPA and uPA.

PAI 1 (50kDa), found in the plasma at approximately 20 µg/L, is produced by many different cells including endothelial cells, smooth muscle cells, and liver cells (Schaller and Gerber, 2011) and is also found in the α-granules of platelets (Flaumenhaft and Koseoglu, 2016). PAI-1 is an acute-phase reactant and its expression can increase rapidly in response to inflammatory cytokines, transforming growth factor-β, angiotensin II, and hypoxia (Tjärnlund-Wolf et al., 2012). In plasma and the extracellular matrix, PAI-1 is found bound to vitronectin, which helps to increase its active half-life (Tjärnlund-Wolf et al., 2012). PAI-1 binds to tPA and uPA with second-order rate constants of $10^6$and 10^7 $M^{-1}s^{-1}$ respectively (Dupont et al., 2009).

PAI-2 (47kDa), found a much lower plasma concentration of less than 5µg/L, is detectable only during pregnancy (Lecander and Astedt, 1986). It is produced by a variety of cells, including epithelial, monocytes, macrophages and keratinocytes. It is not efficiently secreted, and, as a result, accumulates in these cells (Schaller and Gerber, 2011).

There are 2 additional inhibitors with broader specificity: neuroserpin and glia-derived nexin. Neuroserpin (55kDa), found primarily in the brain, interacts with tPA, uPA and plasmin (Hastings et al., 1997; Mehra et al., 2016; Yepes and Lawrence, 2004). Neuroserpin is produced by neurons in those parts of the brain

where tPA is found (Yepes and Lawrence, 2004) and has been shown to protect against neurotoxic effects of tPA (Lee et al., 2017). Glia-derived nexin (43 kDa) interacts with a broad range of substrates, including uPA and plasmin, but also inhibits trypsin, and its key target, α-thrombin. It is produced by fibroblasts, heart muscle cells, kidney epithelial cells and in the brain (Buchholz et al., 2003; Eaton and Baker, 1983).

1.3.2.2 PLASMIN INHIBITORS: ALPHA$_2$-ANTIPLASMIN AND MACROGLOBULIN.

The primary inhibitor of plasmin is alpha$_2$-antiplasmin (α_2-AP) or alpha$_2$-plasmin inhibitor (A2PI). Plasmin activity can also be regulated by the general protease inhibitor α2-macroglobulin(α2M). α2-AP sequesters plasmin in the circulation to prevent wide-spread fibrinolysis and haemorrhage. α2-AP is a 67 kDa protein circulating at approximately 70 mg/L. It is a single chain glycosylated protein that is found in 2 different forms, which differ at the N-terminus. α2-AP inhibits plasmin in lysine dependent manner, interacting with kringles 1, 4 and 5(Wiman et al., 1979). The C-terminus of the protein contains the plasmin binding site, including a C-terminal lysine residue (Lys 452), which is thought to be the main binding site, with another lysine (Lys 436) contributing to the binding. There is some dissent in the field as some researchers have suggested that Lysine 436 is the main binding site, with no contribution from the C-terminus(Wang et al., 2006, 2003). The alpha$_2$-antiplasmin-plasmin interaction is irreversible.

Alpha-2-Macroglobulin is a broad-spectrum inhibitor, it is able to inactivate a range of proteinases (including serine-, cysteine-, aspartic- and metalloproteinases) (Garcia-Ferrer et al., 2017). It functions as an inhibitor of fibrinolysis by inhibiting plasmin and kallikrein (de Boer et al., 1993). It can also impede coagulation by inhibiting thrombin (de Boer et al., 1993).

1.3.3 CARBOXYPEPTIDASES

Plasma carboxypeptidases, such as carboxypeptidase B2 (CpB2); also referred to as thrombin activated fibrinolysis inhibitor (TAFI) or carboxypeptidase U, and carboxypeptidase N (CpN), are proteinases with specificity for C-terminal lysine and arginine residues. Carboxypeptidase B2 has approximately 50% sequence homology with pancreatic carboxypeptidase B1 (Nagashima et al., 2002). Carboxypeptidases are zinc-metalloproteases, of 2 types, A-like with a preference for hydrophobic amino acids and B-like with a preference for basic amino acids. The mode of action for CpB2, CpB1 and CpN is the removal of basic C-terminal amino acids. In a physiologic setting, CpB2 functions to keep haemostatic fibrin clot stable by removal of C-terminal lysine and arginine residues, preventing premature fibrinolysis and allowing for repair to occur, while CpN's role is primarily to decease anaphylatoxin activity within the complement cascade (Leung and Morser, 2018; Rijken and Lijnen, 2009). CpB2 circulates as an inactive form, requiring activation by either thrombin (with thrombomodulin for approximately a 1000-fold increase) or plasmin (in the presence of glycosaminoglycans for an enhanced rate). CpN circulates as an active molecule.

1.4 FIBRINOGEN AND FIBRIN

Fibrinogen is a soluble plasma protein and is the precursor to fibrin, the final protein in the coagulation cascade. Fibrinogen, the parent protein, is a 340 kDa protein and is synthesized in the liver. Normal plasma levels range from 1.5 to 4 g/L (Bardehle et al., 2015; Davalos and Akassoglou, 2011), with a half-life of up to 4 days (Tennent et al., 2007). Fibrinogen is an acute-phase reactant; after injury or in a disease state associated with blood vessel disruption, infection or inflammation, its plasma level can increase to several times the normal level, up to 7 g/L or more (Davalos and Akassoglou, 2011; Kattula et al., 2017; Tennent et al., 2007). Circulating fibrinogen is a protein complex that comprises 2 sets of non-identical disulphide crosslinked polypeptide chains, (Figure 1.6) known as Aα, Bβ and γ chains, and having molecular masses of 66.5, 52.0 and 46.5 kDa, respectively (Weisel, 2005). There are 29 disulphide bonds between the polypeptides (Kattula et al., 2017). The central part of the complex is termed the E region, while the outer ends are each called a D region and consist of the C-termini of the Bβ and γ chains (Jennewein et al., 2011; Köhler et al., 2015). Thrombin initiates clotting via enzymatic cleavage of fibrinopeptides A and B (FpA/FpB) from the N-terminus of the Aα or Bβ chains, respectively, at the E region (Jennewein et al., 2011; Kattula et al., 2017; Weisel, 2005; Weisel and Medved, 2001). The protein is glycosylated at asparagine residues on the Bβ and γ chains. The release of the 2 fibrinopeptides exposes the polymerization sites that bind to the outer ends of the protein complex, on the D region. The D regions spontaneous bind into complementary binding pockets on neighbouring fibrin molecules, creating the meshwork of the fibrin clot (Figure 1.7). Thrombin further stabilizes the fibrin clot by activating factor XIII which crosslinks between fibrin molecules. Each end of the fibrinogen molecule is able to bind with high affinity to the integrin receptor αIIbβ3 on the surface of activated platelets (Weisel, 2005). This results in the bridging of fibrinogen between platelets and ensures these cells are incorporated within the clot. The intermolecular interactions between alpha C domains are key to the stability of the

clot, increasing its mechanical strength. These domains are essential for the aggregation of adjacent fibrin molecules during polymerization. (Weisel and Medved, 2001) Several dysfibrinogenemias defined by amino acid substitutions in, or truncations of, the alpha C domains revealed that these changes can have dramatic effects on polymerization and clot structure. Clots formed using this mutated form of fibrinogen had very small pore sizes and were resistant to lysis.

Fibrin is the culmination of the coagulation cascade. This protein meshwork serves as the scaffold for assembly of the components of the fibrinolytic system, creating an environment for the dissolution of the fibrin clot/matrix. Fibrin can bind both plasminogen and tPA or tPA/PAI-1 (Bardehle et al., 2015; Weisel, 2005). Additionally, it also binds proteins that mediate its formation, and influence its structure (Lord, 2007). During clot formation, α2-AP, TAFI and fibronectin are incorporated into the clot, ensuring these proteins are within the clot during contraction and helping to protect against lysis (Pieters and Wolberg, 2019). Thrombin binds to the central E region of fibrinogen (Wolberg, 2007), where it is protected from inactivation by antithrombin.

Fibrin has recently been identified as a protein of interest in Multiple Sclerosis (MS) research (Petersen et al., 2018). Fibrin is an insoluble protein usually excluded from the brain parenchyma. Upon microinjury of the blood-brain barrier (BBB), fibrinogen enters the brain and is efficiently converted to fibrin after triggering of the coagulation cascade by endothelial cell tissue factor. The resulting insoluble fibrin matrix is the primary substrate for plasmin, the active form of circulating plasminogen. tPA is present in the brain where it has been shown to have a role in synaptic plasticity. Cleavage of soluble fibrinogen to the insoluble fibrin exposes a cryptic epitope that is a binding site for the CD11b/CD18 integrin, also known as MAC-1, complement receptor 3 and $\alpha_M\beta_2$ integrin (Davalos and Akassoglou, 2011; Petersen et al., 2018; Ryu et al., 2015). Leukocytes of the innate immune system, specifically microglia, macrophages and neutrophils, express this receptor on their

surface. Microglia activated by binding to fibrin via the CD11b/CD18 receptor secrete cytokines and chemokines that draw peripheral monocytes and macrophages to the site of fibrin deposition (Ryu et al., 2015).

While fibrinogen is a key player in the hemostatic processes, it also plays a major role in antimicrobial host defence (Gu and Lentz, 2018; Ko and Flick, 2016). As noted previously, fibrinogen, along with von Willebrand factor, coagulation factor VIII and PAI-1, is an acute-phase reactant, and the plasma concentrations of these proteins and others rise dramatically in a short time period in response to inflammation. As fibrinogen is rapidly upregulated and is also assembled into a matrix, it is exquisitely suited to play a role in limiting bacterial infiltration. Fibrin's mechanism of limiting bacterial infection is two-fold: 1) as a protective barrier and 2) the ability to directly, or indirectly, influence host protective immune function (Ko and Flick, 2016).

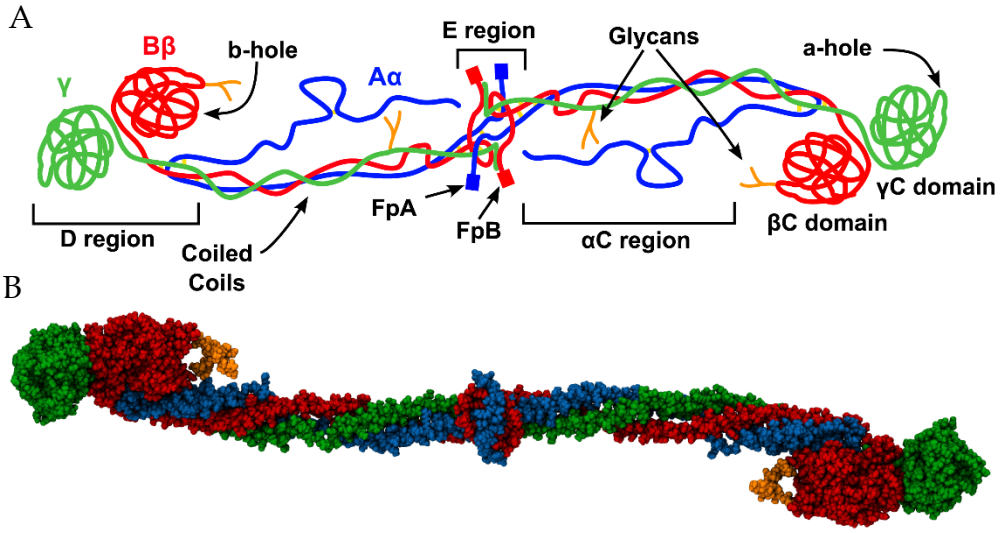

Figure 1-6 The Fibrinogen Molecule

Panel A) Schematic representation of the fibrinogen molecule. The three chains of Fg, Aα, Bβ and γ are shown in blue, red and green, respectively.

Panel B) Van der Waals representation of the crystallographic structure (pdb 3GHG) of Fg, color coded as in (A). Carbohydrates are in orange. The αC region and the FpA and FpB peptides were not resolved in the crystal structure . Reproduced under terms of the Creative Commons Attribution License, which permits unrestricted use, distribution, and reproduction in any medium, provided the original author and source are credited. Köhler et al., (2015) PLoS Comput Biol 11(9): e1004346.

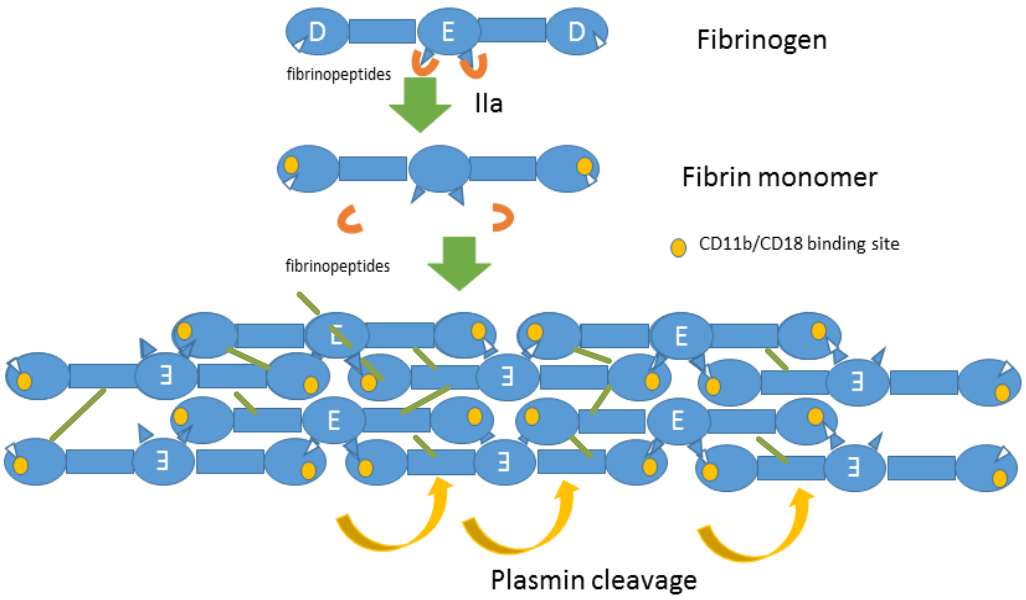

Figure 1-7 Fibrin Self-Assembly

Thrombin (IIa) cleaves the fibrinopeptides from the E region, allowing the insertion into the complementary binding site on the D domain of an adjacent fibrin monomer. Release of the fibrinopeptides reveals the cryptic CD11b/CD18 binding site. Factor XIII activated by IIa crosslinks the fibrin protofibrils (indicated by green lines). Adapted from Weisel, J.W., 2005. Fibrinogen and Fibrin, in: Chemistry, B.-A. in P. (Ed.), Fibrous Proteins: Coiled-Coils, Collagen and Elastomers. Academic Press, pp. 247–299.

1.5 PLASMINOGEN RECEPTORS

Plasminogen receptors are proteins found on the surface of cells and serve as anchoring sites for plasminogen. Binding of plasminogen to these receptors results in an increase in the rate of local plasmin generation. Characterization of these proteins initially indicated that a C-terminal lysine on the receptor was essential for plasminogen binding; treatment of these cells with carboxypeptidases caused a dramatic decrease in the capacity of these cells to bind plasminogen and to facilitate its conversion to plasmin. Plasminogen receptors are found on the surface of most cell types (except for red blood cells) at a fairly high density, that is somewhat dependent on cell type: 1-200 x 10^5/endothelial cell, 5 x 10^5/lymphocyte and 35000/platelet (Godier and Hunt, 2013; Plow et al., 1995).

Localizing plasmin activity at the cell surface grants the cell various abilities. The broad spectrum of plasmin activity means that in addition to direct extracellular proteolysis, plasmin can also activate other proteinases, increasing the overall proteolytic activity of the cell. Plasmin is also able to process latent growth factors and cytokines in the extracellular matrix, resulting in signalling events including cell migration.

Plasminogen receptors are often found co-localized with receptors for plasminogen activators or they also bind tPA themselves (Andronicos and Ranson, 2001; Felez et al., 1993). The co-localization of plasminogen and its activators aids in restricting the activity of the resulting plasmin to the cell surface.

The C-terminal lysine residue is thought to be the key site of binding to kringle domains of plasminogen, plasmin, and tPA. As discussed below, however, some plasminogen receptors do not have a C-terminal lysine residue.

Many proteins have been identified as potential plasminogen receptors. Most of these proteins have C-terminal lysines, but some do not. Those that have a C-terminal lysine include α-enolase (Miles et al., 1991), histone H2B (Das et al., 2007; Herren et al., 2006), S100A4 (Semov et al., 2005), the annexin A2 heterotetramer

(annexin A2 in complex with S100A10) (Kwon et al., 2005, p. 10), Plg-R_{KT} (Miles et al., 2012), TIP49a (Hawley et al., 2001), and cytokeratin 8 (Gonias et al., 2001). Examples of PgR that do not have the classic C-terminal lysine residue include high mobility group box-1 protein (HMGB-1) (Parkkinen and Rauvala, 1991) (which is also known as amphoterin) and integrins, primarily those of the beta2 integrin family (Godier and Hunt, 2013). Receptors that lack the typical C-terminal lysine may require processing, such as proteolytic cleavage, prior to the binding of plasminogen. These studies have not been completed (Miles and Parmer, 2013).

Many of the PgR are associated with cancer and are found on the surface of most tumours (Ceruti et al., 2013). Examples of PgR that are upregulated in cancer include S100A10 (see section 1.6) S100A4 (Bettum et al., 2014, p. 4; Klingelhöfer et al., 2012, p. 4), α-enolase (Capello et al., 2011), and cytokeratin K8 (Gonias et al., 2001). The PgR Histone H2B is found on the surface of activated macrophages (Das et al., 2007), as is S100A10 (section 1.6). Additionally, autoantibodies to Histone H2B are found in various autoimmune disorders, including systemic lupus erythematosus, systemic sclerosis scleroderma and human immunodeficiency virus-infection (Godier and Hunt, 2013). This illustrates that not only are PgR important for clot dissolution and as a potential target for cancer therapeutics but may also play a role in other disease processes.

1.6 S100A10

S100A10, also known as calpactin light chain or p11, is a member of the S100 family of calcium-binding proteins. The S100 proteins are low molecular weight, and each contains an EF-hand motif, which consists of a helix-loop-helix (Donato, 1999). The majority of the S100 proteins bind Ca^{2+} at this EF-hand motif. However, S100A10 has a mutation that does not allow for calcium-binding but does put the molecule in the 'calcium-present' conformation. The nomenclature S100 indicates the following: S= soluble, 100 = 100% (saturated) ammonium sulphate (Donato, 2001). The initial 2 proteins isolated were termed S100A and S100B. Subsequent family

members were assigned A + number with S100A being renamed S100A1, and other proteins with sequence homology sequentially numbered.

S100A10 is a 96 amino acid protein. The amino acid structure was published in 1992 by Gerke's group (Harder et al., 1992). Both residue 95 and 96 at the C-terminus are lysines; there are an additional 10 lysine residues throughout the molecule, with some, notably residue 56, being solvent-exposed. Lysine residues are often found to be solvent-exposed (Malleshappa Gowder et al., 2014), especially in alpha-helical structure. The relative solvent exposure for each lysine was determined to help predict which lysine residues are more likely to be involved in plasminogen receptor-kringle binding. Each S100A10 monomer is composed of 4 alpha-helical motifs (H-I, H-II, H-III and H-IV) joined by 2 linker regions and a hinge region. Hydrophobic amino acids located in helices H-I and H-IV and 2 amino acids in the hinge region are responsible for the interaction with Annexin A2. A cartoon representing the secondary structure of S100A10 and amino acids that participate in binding with Annexin A2 is presented in Figure 1.8.

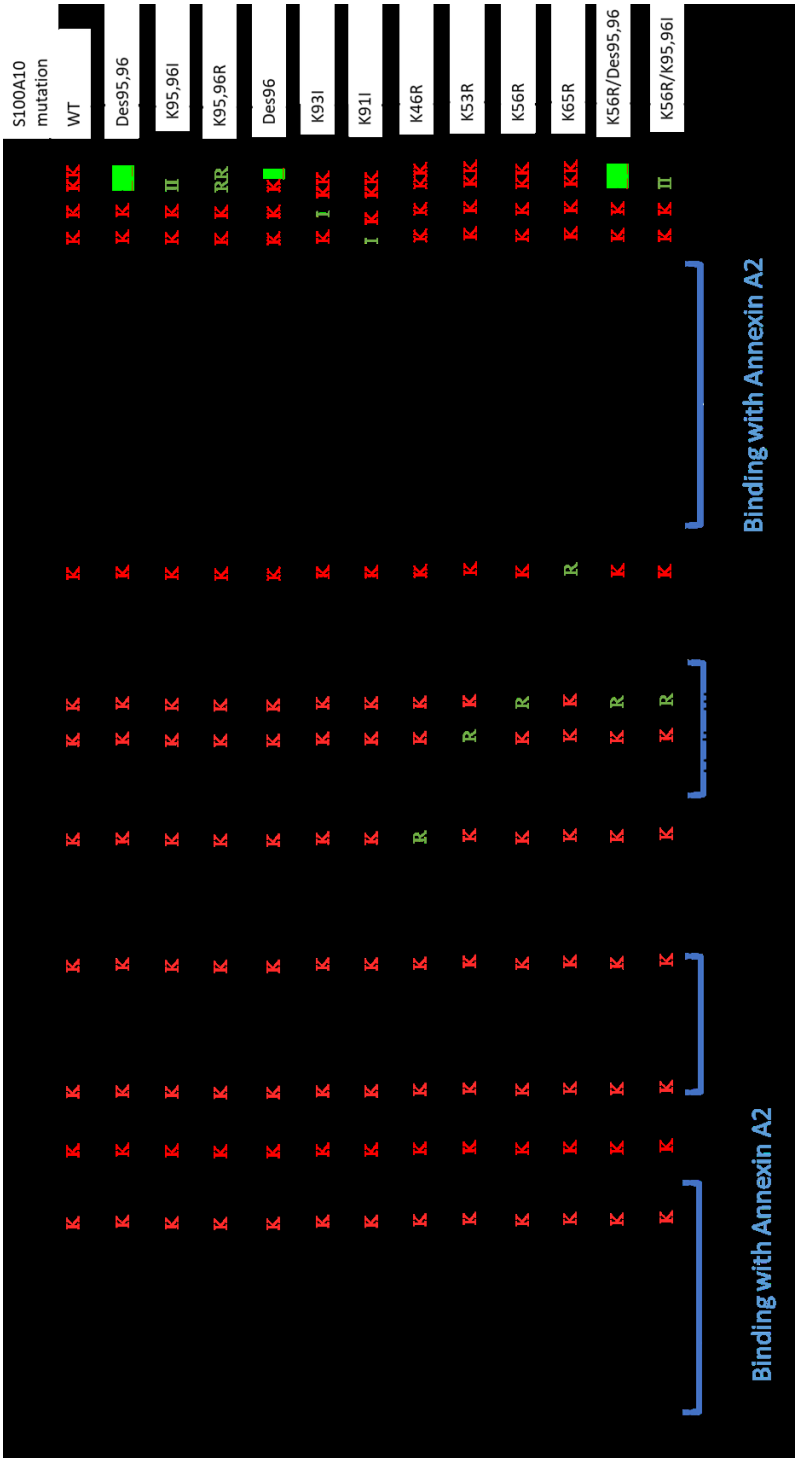

Figure 1-8 Structure and Sequence of Human S100A10

A cartoon of the unfolded structure of S100A10 is presented to show the location of mutated amino acids, as well as key secondary structure, and areas of interaction with annexin A2. Lyine residues are noted in red, mutated residues are green.

S100A10 is present in mammals, birds, reptiles, amphibians, and fish but absent from insects, nematodes, protozoa, fungi, or plants (Madureira et al., 2012). The amino acid sequence of S100A10 is well-conserved across these species; of interest is the conservation of the lysine at the C-terminus as well as the lysines at position 56 and 91- numbering for the human sequence. Figure 1.9 graphically illustrates the consensus sequence of S100A10 across 21 species. Prepared using the WebLOGO service at www.weblogo.berkley.edu (Schneider and Stephens, 1990). The taller the stack, the more conserved the residue. A single letter at the full height indicates all species share the same residue, while multiple 'short' letters indicate differences between species. The consensus sequence is read from the top amino acid in each position (Crooks et al., 2004). It is interesting that the C-terminal lysine residue is not fully conserved over the entire 21 species list, but the lysine residues that correspond to human sequence positions 56 and 91 are fully conserved.

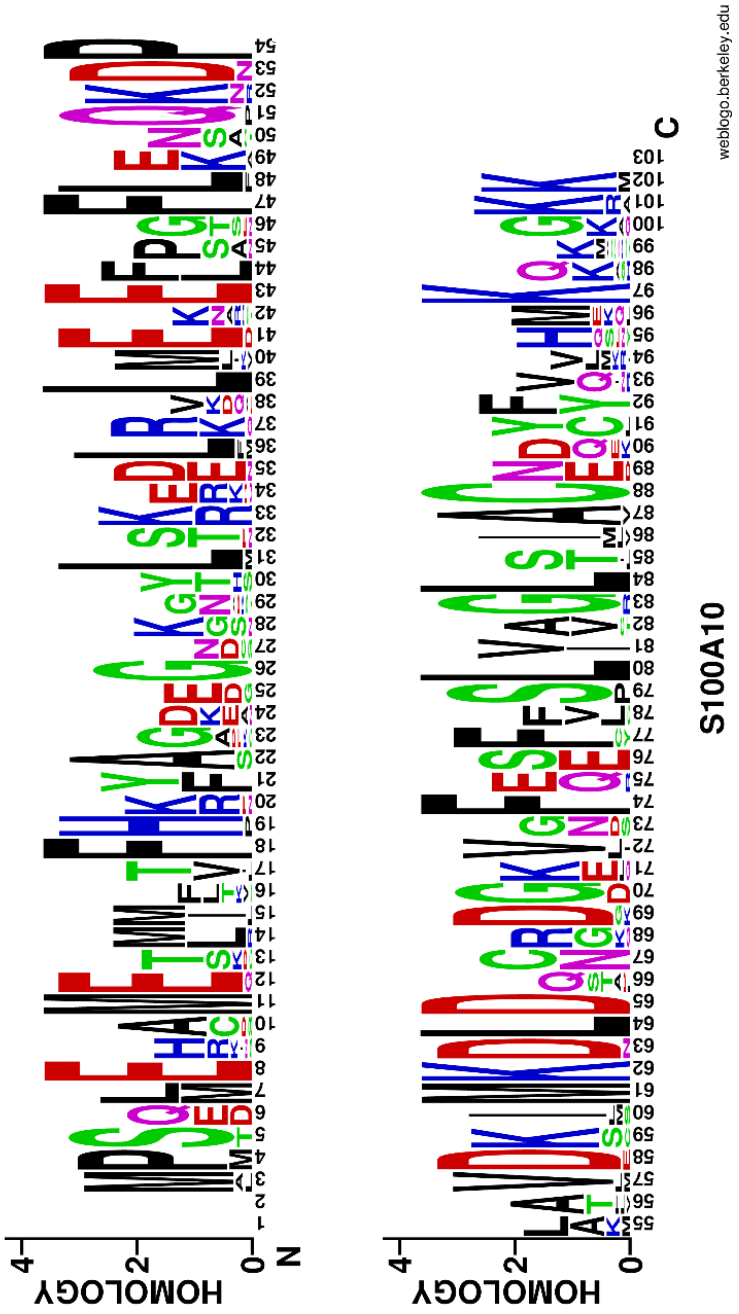

Figure 1-9 Canonical Sequence of S100A10

The amino acid sequence of 21 organisms from humans to swamp eel was input into WebLOGO at https://weblogo.berkeley.edu/ The generated logo consists of stacks of amino acid symbols, one stack for each position in the sequence. The overall height of the stack indicates the sequence conservation at that position, while the height of symbols within the stack indicates the relative frequency of each amino acid at that position.

S100A10 is found as a monomer, a dimer or as part of a heterotetramer with annexin A2. It is localized on the outside of cells as the heterotetramer, or inside the cytoplasm as the monomer, dimer or heterotetramer. The heterotetramer consists of a dimer of S100A10 interacting with a dimer of Annexin A2. Annexin A2 is a calcium-binding protein, also known as lipocortin 1, calpactin 1 or p36. It localizes S100A10 to the plasma membrane (Kwon et al., 2005).

S100A10 has been identified as a plasminogen receptor. As a homodimer, it possesses 2 binding sites for plasminogen and/or tPA and is usually anchored to the cell surface via a dimer of annexin A2, forming the annexin A2 heterotetramer (AIIt) (V. A. Miller et al., 2017). The binding site for S100A10 on annexin A2 is the first 14 amino acids of the N-terminus of annexin A2 (Réty et al., 1999), while annexin A2 associates with a hydrophobic region in the N-terminal portion of S100A10.

S100A10 is found in a wide range of tissues, with the highest expression found in the lungs, kidney and intestine (Madureira et al., 2012). The protein is also found on the surface of various cell types, including endothelial cells, macrophages, fibroblasts and various cancer cells.

In the brain, S100A10 co-localizes with the serotonin receptor (5-HT1B) (Egeland et al., 2011; Svenningsson et al., 2006), and low levels of the protein have been associated with depression. S100A10-null mice exhibit a depressed phenotype and show a decreased response to selective serotonin reuptake inhibitors, such as fluoxetine (Egeland et al., 2010).

S100A10 can stimulate plasmin autoproteolysis, further regulating plasmin activity (Kwon et al., 2005). Multiple degradation products result and are classified as angiostatins. These biologically active antiangiogenic molecules contain the kringle 1-3 domains and serve to block tumour growth and metastasis by limiting endothelial cell proliferation required for tumour vascularization (Kassam et al., 2001; Kwon et al., 2001).

S100A10 is a key regulator of plasminogen dependent macrophage invasion, which is mediated in part by MMP-9 activation (O'Connell et al., 2010). Using thioglycollate to stimulate the movement of macrophages into the peritoneal cavity of wild type and S100A10-null mice, those mice lacking S100A10 had over a 50% reduction in the number of macrophages into the peritoneal cavity (O'Connell et al., 2010). Using an *in vivo* model of invasion into a Matrigel plug, the S100A10-null mice had fewer macrophages infiltrate into the plug (Madureira et al., 2012; O'Connell et al., 2010).

There have been many studies that have linked S100A10 with oncogenesis. Cancer cells use plasmin as well as other proteases such as cathepsin B and the MMPs to breakdown the extracellular matrix and the basement membrane to get access to the vasculature (Poddar et al., 2017; Stoppelli, 2013). The same proteases are then used by the malignant cells to enter other tissues to form metastatic cores. Tumour-associated cells, such as macrophages, also use these proteases to enter the tumour site (Phipps et al., 2011). S100A10 co-localizes with uPAR on the cell surface, which facilitates plasminogen activation, as well as activation of pro-uPA to its active form (Zhang et al., 2004). uPAR is also upregulated on the surface of many types of cancer cells (Andreasen et al., 2000, 1997). Additional studies that explored the role of S100A10 include the use of an anti-sense vector to deplete HT1080 fibrosarcoma cells of S100A10 (Choi et al., 2003). When these cells were injected into mice there was a 3-fold decrease in the number of metastatic foci in the lung compared to mice injected with control cells. Conversely, when mice were injected with HT1080 cells over-expressing S100A10, mice had a 16-fold increase in the number of metastatic lesions in the lungs (Choi et al., 2003). Similar studies were performed with colorectal cells and RNA interference to deplete the cells of S100A10 (Zhang et al., 2004), which resulted in a significant decrease in plasminogen binding as well as plasmin generation and a diminution of the ability of these cells to invade through an artificial basement membrane (Matrigel). Up-regulation of cellular S100A10 has been associated with poorer outcomes and/or

chemoresistance in ovarian (Lokman et al., 2016; Noye et al., 2018), pancreatic (Bydoun et al., 2018), breast (Browne et al., 2013; Johansson et al., 2015; Myrvang et al., 2013), colorectal (Suzuki et al., 2011), and lung carcinomas (Katono et al., 2016; K. Sato et al., 2018) as well as leukemia, specifically acute promyelocytic leukemia (Holloway et al., 2018; Huang et al., 2017; O'Connell et al., 2010).

The loss of S100A10 from the surface of macrophages dramatically decreased both the tumour size compared to wild type mice injected with the same number of Lewis lung carcinoma cells (Phipps et al., 2011). Tumours in the S100A10-null mice reached their maximum size at day seven, while tumours in wild type animals continued to grow. Examination of the resulting tumours revealed very few macrophages within the tumours of the S100A10-null mice. When wild type macrophages were injected into the tumours of S100A10-null mice, the tumour growth approached that of wild type mice. This study highlights the importance of S100A10 in tumour associated cells and how the tumour microenvironment influences tumour growth.

S100A10 plays a role in fibrinolysis. In a study exploring the role of S100A10 in fibrinolysis using the S100A10-null mouse, Surette et al. (2011) found that S100A10-null mice had increased levels of fibrin deposition in the lung, liver, spleen and kidney, as determined by western blot, as well as through measurement of radio-labelled fibrinogen. No differences in coagulation or fibrinolytic parameters between the wild type and S100A10 were revealed. This finding is similar to fibrin deposition in plasminogen-null mice (Bugge et al., 1995; Ploplis et al., 1995).

A clinical study involving critically injured trauma patients found that individuals with a low mean lysis time in a viscoelastic measure of fibrinolytic potential coupled with a high D-dimer (fibrin degradation product), had higher levels of S100A10 in the plasma (Gall et al., 2018). These patients had poorer outcomes and were more likely to have suffered a traumatic head injury.

1.7 MULTIPLE SCLEROSIS

Multiple Sclerosis (MS) is a chronic inflammatory disease characterized by demyelination of the central nervous system. The immune system attacks the myelin of nerve cells eventually resulting in deficits in the motor, visual, sensory and autonomic systems (Simmons et al., 2013). Although specific causes of MS are not fully understood, it is currently thought that MS pathology results from interactions between genetics, microbial infection and auto-immunity (Rahmanzadeh et al., 2018; F. Sato et al., 2018). Most researchers agree that genetic, environmental, and lifestyle aspects all influence disease progression and the disease is usually classified as an autoimmune condition (Thompson et al., 2018). Animal models, discussed below, have led to the identification of treatment targets, leading to some successful treatment protocols.

There are four main sub-types of MS: relapsing-remitting, secondary progressive, primary progressive, and clinically isolated syndrome (Rahmanzadeh et al., 2018). The majority of those diagnosed with MS first present with a clinically isolated syndrome, where there is the involvement of the brain stem, optic nerve or spinal cord that resolves over time. Individuals are classified as having relapsing-remitting MS when they experience a second episode that also resolves over time. Many of these individuals go on to have multiple episodes, with varying amounts of time between each episode. A certain percentage of those with relapsing-remitting MS will develop secondary progressive disease where there is no resolution of the symptoms between episodes. Approximately 15% of those diagnosed with MS have primary progressive MS, experiencing no reduction of MS symptoms (Rahmanzadeh et al., 2018; Thompson et al., 2018).

The clinical signs and symptoms of MS include double/blurry vision, lack of muscle control and coordination, diminished skin sensation and progressive paralysis. As noted above, some individuals experience resolution of their clinical symptoms, though not to non-pathologic levels. The pathological process of MS

consists of a breakdown of the blood-brain barrier, multifocal inflammation, demyelination, oligodendrocyte loss, reactive gliosis (colloquially referred to as scarring) and loss of axons (Baecher-Allan et al., 2018). Inflammation and the immune system are major players in the progression of MS (Baecher-Allan et al., 2018; Rahmanzadeh et al., 2018; Thompson et al., 2018). Many of the current drug protocols target specific immune cells or molecules. At a minimum, the following immune cells have a potential role in the pathogenesis of MS: cells from the adaptive immune system, such as B cells and specific effector T cell populations, and cells of the innate immune system including natural killer and microglial cells (Baecher-Allan et al., 2018; Buzzard et al., 2017).

The effector CD4 T cells are believed to be causative in MS. Specifically, autoreactive CD4 T cells migrate from the periphery into the central nervous system (CNS) and reactivate to initiate the disease. This is referred to as the "outside-in hypothesis" (Malpass, 2012). Once inside the CNS, the reactivation by antigen-presenting cells results in the recruitment of more T cells and macrophages, creating the inflammatory lesion (Baecher-Allan et al., 2018). These CD4, as well as CD8 T cells, cause myelin loss, oligodendrocyte loss and damage axons, leading to an imbalance in neurological function (Baecher-Allan et al., 2018). CD4 T cells are often myelin reactive and cells secrete interferon-γ (IFN-γ) and interleukin- 17 (IL-17) which are thought to be at the heart of the pathologic damage (Buzzard et al., 2017). IFN- γ activates microglial cells, while IL-17 and IFN- γ activate microglia and macrophages.

Demyelination is one of the hallmarks of multiple sclerosis. Understanding how various proteins interact in the brain during this process, as well as during endogenous repair, is crucial to identifying druggable targets for future treatments, as well as for identifying potential biomarkers for diagnosis. Demyelination marks an active relapse; the remission is the repair. Eventually, the

oligodendrocytes are damaged beyond their ability to repair the demyelinated axons, and the damage is permanent.

Myelin basic protein (MBP), an important component of the myelin sheath, protects the integrity of the nerve impulse along the neuron axon. Previous research suggested that plasmin can degrade MBP (Cammer et al., 1981, 1978; Law et al., 1985). Early reports of this phenomenon linked the loss of myelin to the presence of macrophages (Cammer et al., 1978; Norton et al., 1978). The researchers linked the protease activity to a plasminogen activator secreted by the macrophages. Predictably, plasmin was found to lyse MBP after a lysine or arginine residue, distributed throughout the protein sequence (Law et al., 1985). The loss of MBP results in a loss of the structure of the myelin sheath, exposing the axon to further injury. In MS, fibrin deposition has been illustrated in CNS lesions; the presence of fibrin deposits has been shown to precede lesion formation (Akassoglou et al., 2004; Wakefield et al., 1994).

1.8 BLOOD-BRAIN BARRIER

The tissues of the brain are segregated from most substances found in the blood by the blood-brain barrier (BBB) or neurovascular unit. Usually, the brain is protected from toxins and most blood components, such as cytokines and chemokines (Obermeier et al., 2016; Sharif et al., 2018; Sweeney et al., 2018). The BBB comprises endothelial cells connected by tight junctions and adherens junctions. Tight junctions are closely associated areas on adjacent cell membranes, located at the apical site between brain endothelial cells, and consist of three integral protein types: claudins, occludin, and junctional adhesion molecules (East et al., 2008). The adherens junctions consist of cadherins, platelet endothelial cell adhesion molecule and the junctional adhesion molecules (Sweeney et al., 2018). The tight junctions and adherens junctions seal the cells of the BBB, helping to regulate the flow of molecules into the central nervous system. The balance of nutrients in and waste products out is controlled by the BBB. This selective cell-

matrix also serves to keep toxins and other pathogens out of the brain and CNS, rendering it an 'immune-privileged site'. It is the endothelial cells of the vasculature, with the important contribution of the pericytes and astrocytic end-feet, that control access through the BBB (Andreone et al., 2017; Boer and Gaillard, 2006; Sweeney et al., 2018).

The tightly controlled BBB can be damaged; tight junctions between cells can be disrupted, cells can increase transport across or damage may occur to the vessel (Dvorak et al., 1985). This loss of integrity of the BBB may occur during the course of many neuropathologies, such as stroke, traumatic brain injury, epilepsy and in diseases of chronic neuroinflammation and neurodegeneration, such as multiple sclerosis and Alzheimer's disease (Adams et al., 2004). However, there is also loss of BBB integrity as a part of normal ageing; scans of individuals showed BBB breakdown in the hippocampus (Montagne et al., 2015). These conditions all show either transient or chronic BBB opening.

1.9 Plasminogen Activation System and Multiple Sclerosis

Under normal physiological conditions, the blood proteins plasminogen and fibrinogen are not found in the brain parenchyma (Davalos et al., 2019; Petersen et al., 2018). In cases when the blood-brain barrier is compromised – in stroke, epilepsy, traumatic brain injury or when chronic inflammation and neurodegeneration are present- such as multiple sclerosis and Alzheimer's disease - plasminogen, fibrinogen and other blood components, such as immune cells can then enter the brain (Bardehle et al., 2015). The plasminogen activation system can influence the BBB. tPA can open the BBB through various mechanisms. This includes activation of platelet-derived growth factor-CC (Su et al., 2008), astrocytic remodelling through plasmin (Niego et al., 2012), and promotion of phosphorylation of claudin-5 and occludin, both BBB proteins (Kaur et al., 2011). PAI-1 appears to promote BBB tightness in *in vitro* models (Dohgu et al., 2011). There is clinical evidence of tPA influencing BBB integrity; individuals treated

with tPA for thrombotic stroke are at risk of increased bleeding in the brain (Fugate and Rabinstein, 2014).

Fibrinogen, a major substrate of plasmin, has been shown *in vitro* to increase endothelial cell permeability, partially by reducing the expression of tight junction proteins (Patibandla et al., 2009; Tyagi et al., 2008). It is possible that conditions that cause fibrinogen and/or fibrin to accumulate on the vessel wall may lead to the weakening of the BBB. Additionally, the transient weakening of the BBB allows blood proteins to enter the brain, which may result in the activation of both the fibrinolytic and coagulant systems in the CNS. The presence of these blood proteins may lead to further conditions or reinforcement of conditions where the BBB is further weakened. As fibrin lies at the interface of the fibrinolytic and coagulant pathways, researchers are targeting it as a potential diagnostic or therapeutic target.

The plasminogen activation system in the brain has benefits to the brain, as tPA is found within the normal brain parenchyma (Melchor et al., 2003; Melchor and Strickland, 2005). Fibrin plays a pivotal role in stopping bleeding, and the plasmin removes that clot once the necessary repairs to the vasculature are complete, restoring blood flow. However, if either process is dysregulated, inflammation is the likely outcome, and if inflammation persists, pathology follows; in the brain, that includes multiple sclerosis (East et al., 2005; Marik et al., 2007), Alzheimer's disease and vascular dementia (Paul et al., 2007; van Oijen et al., 2005), and traumatic brain injury (Chodobski et al., 2011; Muradashvili et al., 2017).

Fibrin has been found in histologic studies of MS lesions, both human (Marik et al., 2007) and mouse (Ryu et al., 2015; Ryu and McLarnon, 2009). Specifically targeting fibrin either genetically, in the fibrinogen knock-out mouse, or by administering an antibody to the CD11b/CD18 binding site on fibrin) has been shown to lessen the severity of disease in mouse models of MS (Ryu et al., 2018).

PAI-1 levels in active MS lesions are increased compared to normal-appearing white matter (Gverić et al., 2003).

In 2003, a study by Craner et al. (2003) explored S100A10 levels in Purkinje cells in the cerebellum. These gamma-aminobutyric acid-(GABA)ergic neurons express the sodium channel $Na_v1.8$ at low levels. S100A10 binds to the N-terminus of this protein which aids in its membrane localization. These researchers found that S100A10 levels and $Na_v1.8$ sodium channel levels were both up-regulated in human MS lesions, as well as in the mouse Experimental Autoimmune Encephalitis (EAE) model.

In 2005, Gveric et al. (2005) investigated tPA receptors in MS lesions. They found that Annexin A2 and S100A10, and low-density lipoprotein receptor-related protein 1 were co-localized with macrophages and astrocytes in active lesions. In normal-appearing white matter, Annexin A2 and S100A10 were found at low levels, primarily on endothelial cells. This result was corroborated with Western blot analysis of sample tissue from acute lesions. Additionally, in an earlier study using the same samples (Gverić et al., 2003), they also found that these lesions had increased concentration of PAI-1 and increased concentrations of PAI-1 – tPA complex, resulting in a decrease in tPA activity in tissue samples assayed for fibrinolytic activity.

In models of EAE (see next section for further information) and demyelination in plasminogen deficient mice (Shaw et al., 2017), the disease course is altered. Researchers expected to find that the loss of plasminogen, either genetically in the plasminogen-null mouse or by the administration of the plasmin generation inhibitor tranexamic acid, would enhance the disease compared to wild type animals, as fibrin deposition at the sites of BBB breakdown is correlated to disease severity (Akassoglou et al., 2004). However, the time to disease onset is longer in plasminogen-deficient mice, and these also had a reduced disease score when

demyelination was initiated (Shaw et al., 2017). These changes were not due to differences in the T-cell response between the animal groups.

1.10 Animal Models of MS

There are a variety of animal models used to explore the many aspects of MS. MS, described in the previous section, is a complicated condition with no clear cause. There is a complicated interplay of many systems, as well as a lack of complete understanding of the exact nature of the initiating factor(s), genetic condition(s) and exacerbating aspect(s) which makes the creation of one animal model that adequately addresses all potential influencers of the initiation and progression of MS nearly impossible (Procaccini et al., 2015). As a result, a variety of animal models are in use in MS research, depending on which disease aspect the researcher desires to explore. This brief summary focuses only on mouse models. Mice are a very attractive model for many disease states. They are relatively low cost and many transgenic strains are available or can be experimentally produced. However, the differences between the human and murine immune systems do limit the direct transferability of findings (Mestas and Hughes, 2004). Most notably for MS research, mice and humans have differing white blood cell makeup (Doeing et al., 2003); mice have 75-90% lymphocytes in their peripheral circulation, while humans have only 30-50%. Neutrophils are also found in different proportions; mice have 10-25% and humans 30-50%. In humans, interferon-γ worsens MS symptoms, while in mice it is protective (Heremans et al., 1996; Lublin et al., 1993; Panitch et al., 1987). Other models used in MS research are rats, zebrafish and non-human primates.

There are three categories of mouse models for the study of MS systems (Procaccini et al., 2015). Each of these categories is useful for the study of discrete factors that affect MS. EAE is a model of immune-mediated inflammation and is primarily induced by autoreactive CD4+ T-cells (F. Sato et al., 2018). However, in humans, the data show that CD8+ T- and B cells may play larger roles in MS

(Buzzard et al., 2017). Viral models mirror some key factors of MS (Lassmann and Bradl, 2017; Procaccini et al., 2015; F. Sato et al., 2018), most importantly inflammatory demyelination. But the models are complex; there are effects from both the virus and the immune response it elicits. Additionally, the role of virus infection in MS is currently one of debate, as no one virus has been shown to be causative in all cases (Oleszak et al., 2004). The final category is toxic models, which are most valuable for the study of de- and remyelination mechanisms (Kipp, 2016; Kipp et al., 2017; Lassmann and Bradl, 2017). Their application to MS is limited, as no other aspect of MS is incorporated in this model, and most importantly, the role of autoimmunity is not addressed (Lassmann and Bradl, 2017).

1.10.1 Experimental Autoimmune Encephalitis

EAE is the most commonly used animal model of MS (Procaccini et al., 2015). The use of this model has helped to develop many of the first line therapeutics that target the inflammatory stage of the disease. EAE uses various central nervous system antigens as the immunogen. Antigens used are proteolipid protein, spinal cord homogenate, myelin basic protein or myelin oligodendrocyte glycoprotein (Lassmann and Bradl, 2017; F. Sato et al., 2018). To activate the immune system of the mouse, the antigen is suspended in complete Freund's adjuvant. Pertussis toxin is often added to the EAE protocol to disrupt the blood-brain barrier (Procaccini et al., 2015). The use of an immunization approach to replicate a portion of the MS disease process results in the activation of myelin-specific T cells. These T cells express integrins that allow them to cross the BBB; once in the CNS, they are re-activated by antigen-presenting cells that are specific for myelin (R. H. Miller et al., 2017; Procaccini et al., 2015; F. Sato et al., 2018). This results in the release of proinflammatory cytokines such as interferon-γ (INF-γ), interleukin-17, tumour necrosis factor and granulocyte-macrophage colony-stimulating factor; which ultimately results in the recruitment of γδ T cells, macrophages, monocytes

and neutrophils to the CNS (Becher et al., 2017; Lassmann and Bradl, 2017). The end result is the destruction of myelin. Symptomatically, the mice exhibit progressive paralysis, first the tail, followed by the hind limbs, then the forelimbs (Burrows et al., 2018).

EAE symptoms are species- and strain-specific. C57BL/6 mice are one of the most commonly used mouse strains, even though they are considered to be EAE-resistant. EAE can be generated by a dose of 300μg of myelin oligodendrocyte glycoprotein$_{(33-55)}$ (MOG$_{35-55}$), resulting in a chronic non-remitting condition that shows its first symptoms around 2 weeks after the immunization, with no recovery for up to 4 months (Burrows et al., 2018; Procaccini et al., 2015). Immune cells attack the cortex, spinal cord and cerebellum, staying for up to 50 days, with axon loss seen only in the spinal cord (Burrows et al., 2018). At lower doses of MOG$_{35-55}$ some relapsing-remitting disease results, but with reduced loss of myelin, less axon damage and smaller lesion size (Burrows et al., 2018). SJL mice injected with proteolipid protein$_{139-151}$ (PLP$_{139-151}$) develop a chronic relapsing model of MS approximately 2 weeks after immunization, with a relapse 2-3 weeks after the first clinical symptom (Burrows et al., 2018). This model exhibits much variability, which may better mimic the human version of the disease.

1.10.2 Models of Demyelination

Demyelinating models are useful for exploring factors that impact both the loss of myelin and the innate repair mechanisms of the brain. There are two distinct types of demyelination models in animals; virus-induced inflammatory demyelination and toxic demyelination.

1.10.2.1 Viral Models of Demyelination

There are two viruses used to induce inflammatory demyelination; Theiler's virus and Mouse Hepatitis Virus (MHV) (Burrows et al., 2018). These models are somewhat hampered by their complex pathogenesis, as there are direct virus-

induced effects, as well as antiviral immunity and some autoimmune mechanisms (Oleszak et al., 2004). As a result, the outcomes specific to these exacerbating effects can be difficult to dissect out. The similarities between the demyelinating disease and MS were somewhat surprising, as there has been little evidence that links a human virus to the onset of MS, although there is some indirect evidence supporting a possible role for Epstein Barr Virus (Ascherio and Munger, 2016; Wingerchuk, 2011) or activation of an endogenous retrovirus (Nexø et al., 2016). The virus-induced models have some advantages over other models. The disease involves both B and T cells and there is a genetic linkage of the MHC type of the animal (Oleszak et al., 2004). The researcher has the option to control both the dosage and the virulence of the virus, and thus the host response can be altered.

In the model that uses Theiler's virus (Theiler's Murine Encephalomyelitis Virus or TMEV), the demyelination is induced by infecting the animal's brain with the virus. An acute encephalomyelitis follows in most animals. The exact pathogenesis and mortality depend on the strength of the virus preparation used, as well as the ability of the animal to mount a specific anti-viral T-cell response (R. H. Miller et al., 2017). The two primary strains of the virus used are Daniel's or BeAn strain, and susceptible animals must have specific MHC haplotypes (H-$2^{q,r,s,v,f,p}$)- found in the SJL strain of mice. The extent of demyelination is greater than in EAE mice and functional deficits last longer, allowing the researcher to better study the mechanisms that control remyelination. The development of the disease has been well documented and depends on the genetics of the animal (Oleszak et al., 2004). In susceptible animals, the disease course follows a two-phase process. First, there is an acute early phase followed by a chronic phase. The acute phase develops 3-12 days post-infection, followed by the chronic phase 30-40 days post-infection (Lassmann and Bradl, 2017; R. H. Miller et al., 2017). The disease in susceptible animals is terminal. In resistant strains (C57BL/6), only the early acute phase is evident, and the virus is cleared approximately 3 weeks post-infection (Oleszak et al., 2004).

The model that uses Mouse Hepatitis Virus was first developed after the isolation of the virus from a paralyzed mouse that presented with widespread encephalomyelitis and demyelination (Lassmann and Bradl, 2017). This virus was further developed into a model for MS, utilizing a neurovirulent strain of MHV (Bailey et al., 1949; Lassmann and Bradl, 2017). The virus is introduced intracranially or nasally. As with Theiler's virus, the disease is biphasic; the first phase begins just days after infection, resulting in a panencephalitis. After recovery, a second phase may appear approximately 4 weeks later and is characterized by a neuroparalytic disease with inflammatory demyelinating lesions (Lassmann and Bradl, 2017). The animals experience chronic inflammation and develop plaques of demyelination, with variable axon injury or loss. T-cells and activated macrophages/microglia infiltrate the lesions. B-cells and plasma cells also contribute to the inflammation. Compared to EAE, these animals experience a greater extent of microglial activation throughout the entire brain and spinal cord. This is linked to the expression of oxygen free radicals produced by the NADPH oxidase and iNOS in the microglia (Schuh et al., 2014) leading to extensive oxidative injury in the active lesions. Astrocyte loss may also be present, leading to a loss of oligodendrocytes and demyelination (Lassmann and Bradl, 2017).

1.10.2.2 TOXIC MODELS

The last group is classified as toxin-mediated demyelination. There are two types: systemic cuprizone administration or focal administration of either lysophosphatidylcholine or ethidium bromide (Procaccini et al., 2015).

Cuprizone is a copper -chelating drug, and when administered in the chow to mice, it causes apoptosis in the oligodendrocytes, eliciting demyelination by oxidative injury (Lassmann and Bradl, 2017). Inflammation follows, modulated by microglia and astrocytes. The usual course is a 4-week treatment with 0.2% cuprizone in rodent chow (Gudi et al., 2014) in C57BL/6 mice. Remyelination

occurs upon return to normal mouse chow. Other mouse strains can be used, and the technique has been successfully used in rats, guinea pigs and hamsters (Burrows et al., 2018). The usual short course of treatment consists of supplementation of the chow with the cuprizone for 4-6 weeks. Remyelination begins upon return to regular chow. A more chronic demyelination model involves exposure to cuprizone in the chow for 12 weeks, with little remyelination occurring upon return to regular chow (Lassmann and Bradl, 2017).

Demyelination occurs predictably in the corpus callosum. The short-term model has limited use; the remyelination is very quick and does not model the human condition well. This drawback has been addressed by long term administration of cuprizone, resulting in chronic demyelination with little repair noted (Lassmann and Bradl, 2017). The long term exposure to cuprizone results not only in apoptosis of mature oligodendrocytes but also changes in cytokines and chemokines that are involved with the proliferation of the OPCs, their differentiation or which inhibit the migration of the progenitor cells to the site of injury (Lassmann and Bradl, 2017). These aspects have been put forward as possible reasons for the eventual remyelination failure in MS.

Focal toxin-induced demyelination provides a lens to study the mechanisms involved in de- and remyelination. Lysophosphatidylcholine (LPC) and ethidium bromide are the two most commonly used agents to induce local demyelination in a known white matter tract of the central nervous system. LPC causes focal plaques of demyelination caused by the direct effects due to the toxin; resulting in detergent-like damage of the lipid membrane of the myelin sheath. In a recent publication, Plemel et al (2018) explored the early events following lysophosphatidylcholine injection and confirmed that the LPC does, in fact, integrate into the membrane of the myelin sheath and cause its degeneration. They found the lesion had formed within 4 hours of the injection, reaching its maximum size within 24 hours.

Other researchers have reported that the age of the animals can impact the speed and degree of remyelination; older animals are slower to remyelinate and may not completely remyelinate a lesion (Crawford et al., 2013; Franklin et al., 2002). These age-related effects may be reflective of the mechanisms at play in progressive MS, as the majority of those with progressive MS, either primary progressive or after a period of relapsing/remitting to secondary progressive, are older adults (Lassmann and Bradl, 2017).

The injection of ethidium bromide into white matter tracts (either corpus callosum or in the spinal cord) results in the degeneration of oligodendrocytes and astrocytes (R. H. Miller et al., 2017; Procaccini et al., 2015). The presence of astrocytes is necessary for the oligodendrocyte remyelination process, so in the absence of astrocytes in the spinal, remyelination is provided by Schwann cells. This mechanism - the reliance of oligodendrocytes on astrocytes - may explain why in individuals with Neuromyelitis Optica, there is evidence of primarily Schwann cell remyelination (Ikota et al., 2010).

These de- and remyelination models offer a method for understanding the molecular mechanisms of, as well as a possibility to explore potential remyelination therapies.

No single animal model can recapitulate the disease course of human MS. Given the complexity of the disease, until the exact etiology of the disease in humans is delineated, the use of multiple animal models to explore discrete aspects of MS will continue to be used in the field.

1.11 RATIONALE

The current dogma states that a C-terminal lysine residue is critical for plasminogen receptor status (Miles et al., 1991; Miles and Parmer, 2013), however receptors without a C-terminal lysine exist. Using an *in vitro* model of plasmin activation, the use of a mutagenesis approach will allow us to determine the role the C-terminus plays in plasmin generation.

Recent studies have pointed to fibrin as a potential player in the development of demyelinated plaques in MS (Davalos and Akassoglou, 2011; Petersen et al., 2018). Studies have also revealed S100A10 and its binding partner annexin A2 as present in established MS lesions (Gverić et al., 2005; Han et al., 2008). The presence of fibrin usually results in an increase in fibrinolysis in the absence of a signal indicating the clot or thrombus is required. Examining the potential role of S100A10 in the initial demyelination steps is the first step to a better understanding of why S100A10 may be localized within an MS plaque.

1.12 THESIS HYPOTHESIS

I hypothesize that the C-terminal lysine residues are critical for the interaction of S100A10 with both plasminogen and tPA and that loss of these 2 lysine residues, either by deletion or mutation, will lead to decreased ability of S100A10 to accelerate tPA-mediated generated plasmin from the pro-enzyme plasminogen.

I also hypothesize that like fibrin, the plasminogen receptor S100A10 interacts with the finger domain of tPA and kringle 1 of plasminogen.

I hypothesize that S100A10 functions to generate plasmin, degrade fibrin and MBP which results in increased axonal damage. In MS lesions, S100A10 functions to generate plasmin, which degrades fibrin, but as collateral damage, it also degrades MBP.

2.1 INTERACTION OF S100A10, PLASMINOGEN AND TPA

2.1.1 MUTANT S100A10

The pAED4.91-S100A10 construct was mutated using the QuikChange II mutagenesis kit (Agilent, Mississauga ON). Lysine (K) residues located in the C-terminal region (residues 91, 93, 95 and 96) were mutated to isoleucine (I) or arginine (R) (95 and 96 only), and internal (residues 17, 22, 27, 36, 46, 53, 56 and 65) were mutated to arginine (R). In addition to the lysine to arginine mutants, lysine residues 95 and 96 were both mutated to isoleucine, and the deletion mutants, K95 and K95,96 were also produced. Additionally, the pAED4.91-S100A10^{K95,96I} and pAED-S100A10^{Des95,96} constructs were mutated to also contain the mutation K56R. Primers were designed using the Agilent QuikChange Primer Design Tool available online at https://www.agilent.com/store/primerDesignProgram.jsp. Resulting plasmids were sequenced to confirm the inclusion of the desired mutation, then used to transform competent bacteria for protein expression.

The mutants were generated using the forward and reverse primers listed in Table 2-1. In each case, an adenine base was changed to a guanine base, using a primer pair. The deletion mutants were similarly prepared, introducing an early stop codon. Patricia Madureira prepared the C-terminal region lysine mutants in the pAED4.91 vector, and the author prepared the remaining mutant vectors.

Table 2-1 Primers Utilized in PCR Reactions to Introduce Mutations in S100A10 Plasmid Constructs

The nucleotide mutation in each primer is highlighted in red. The complementary primer is not shown. The parent plasmid was sequenced past the inserted nucleotide sequence stop codon to mutate amino acids at the C-terminus.

Mutation	Primer 5′-3′
K17R	gaaaccatgatgtttacatttcacagattcgctggggataaagg
K22R	tttcacaaattcgctggggatagaggctacttaacaaagg
K27R	ggggataaaggctacttaacaagggaggacctgag
K36R	ggacctgagagtactcatggaaagggagttccctgg
K46R	ccctggatttttggaaaatcaaagagaccctctggc
K53R	cctctggctgtggacagaataatgaaggacccg
K56R	tctggctgtggacaaaataatgagggacctggacca
K65R	ggaccagtgtagagatggcagagtgggcttcc-
K91I	gcaatgactattttgtagtacacatgatccagaagggaaagaagtag
K93I	gcaatgactattttgtagtacacatgaagcagatcggaaagaagtag
K95R	ctattttgtagtacacatgaagcagaagggaaggaagtag
K96R	ctattttgtagtacacatgaagcagaagggaaagaggtag
K95,96R	gactattttgtagtacacatgaagcagaagggaaggaggtag
K95,96I	gcaatgactattttgtagtacacatgaagcagaagggaatcatcta
DesK96	gactattttgtagtacacatgaagcagaagggaaagtagtag
DesK95,96	gactattttgtagtacacatgaagcagaagggatagaagtag

2.1.2 EXPRESSION AND PURIFICATION

The pAED4.91-S100A10 construct was transformed into BL21(DE3)pLysS competent *Escherichia coli*, expressed and purified according to Ayala-Sanmartin et al. (Ayala-Sanmartin et al., 2000) with modifications. Bacterial cell pellets were lysed either by sonication (60 seconds [s] for 3 pulses) or by French press (1000 psi). Lysis was performed in 100 mM HEPES, (pH 7.5), 400 mM NaCl, 10 mM $MgCl_{2'}$, and 2 mM DTT (dithiothreitol) with 0.1 mg/mL soybean trypsin inhibitor, 2.25 mg/mL benzamidine, 1 mM phenylmethylsulfonyl fluoride, 1 mM 4-benzenesulfonyl fluoride hydrochloride, 10 µg/mL aprotinin, 10 µg/mL leupeptin, and centrifuged at 30,000 × g for 60 minutes (min). The supernatant was precipitated with the addition of an equal volume of saturated $(NH_4)_2SO_4$ and centrifuged at 27,000 × g for 45 min. The supernatant was applied to a Butyl-Sepharose column (GE Healthcare Life Sciences, Piscataway, NJ, USA) equilibrated with 50% saturated $(NH_4)_2SO_4$ in 50mM HEPES, pH 7.5 200 mM NaCl, 1 mM DTT.

The S100A10 was eluted with a linear gradient from 50% to 0% saturated $(NH_4)_2SO_4$ in 50mM HEPES (pH 7.5), 200 mM NaCl,and 1 mM DTT. The eluate was dialyzed against 40 mM Tris (pH 7.4), 150 mM NaCl, 0.5 mM EGTA (ethylene glycol-bis(β-aminoethyl ether)-N,N,N′,N′-tetraacetic acid), and 0.5 mM DTT and subjected to gel permeation chromatography on a HiLoad 16/600 Superdex 75 (GE) column. All chromatography steps were performed at 4°C using the BioLogic DuoFlow system (BioRad) controlled by BioLogic DuoFlow Software (version 5.3). In cases where the mutant S100A10 could not be isolated using this procedure, a lower concentration of ammonium sulphate was used, determined empirically where the mutant S100A10 remained in solution. This procedure was altered to match the starting ammonium sulphate concentration, and the linear gradient started at half the starting concentration. Wild-type (WT) and mutant S100A10 eluted as a single peak in size exclusion chromatography.

2.1.3 PRODUCTION OF RECOMBINANT ANNEXIN A2

The pAED4.91-Annexin A2 (Kang et al., 1997) construct was transformed into BL21(DE3) pLysS competent *E. coli*, and the resulting protein was expressed and purified according to Khanna et al. (Khanna et al., 1990) with modifications. Bacterial cell pellets were subjected to lysis by French press (1000 psi). Lysis was performed in 20 mM imidazole (pH 7.5), 150 mM NaCl, 5 mM EGTA, and 3 mM DTT with 0.1 mg/mL soybean trypsin inhibitor, 2.25 mg/mL benzamidine, 1 mM phenylmethylsulfonyl fluoride, 1 mM 4-benzenesulfonyl fluoride hydrochloride, 10 μg/mL aprotinin, 10 μg/mL leupeptin and the suspension was centrifuged at 30 000 × g for 40 min.

The NaCl concentration was reduced to 50 mM prior to loading the supernatant onto a DEAE ion-exchange column (MacroPrep DE, BioRad, Hercules, CA, USA) equilibrated in 20 mM Imidazole (pH 7.5), 25 mM NaCl, and1 mM DTT. Ten mM phosphate was added to the flow-through fraction and applied to a CHT™ Ceramic Hydroxyapatite (BioRad) column equilibrated in 10 mM potassium phosphate pH 7.0. Annexin A2 was eluted with a linear gradient from 0.01 to 1 M KPi pH 7.0. The eluate was dialyzed against 40 mM Tris, (pH 7.4), 150 mM NaCl, 0.5 mM EGTA, and 0.5 mM DTT and subjected to gel permeation chromatography on a HiLoad 16/600 Superdex 75 (GE Healthcare, Pittsburgh, PA, USA) column.

2.1.4 PRODUCTION OF RECOMBINANT ANNEXIN A2 CYS 8 SER MUTANT

The pAED4.91-Annexin A2 Cys 8 Ser expression plasmid was constructed by point mutation of the Annexin A2 gene in the pAED4.91-Annexin A2 vector using the QuikChange II Site-directed mutagenesis kit (Agilent Technologies). The primer used to introduce the point mutation in the Annexin A2 gene was the following:5'-GTT CAC GAA ATC CTG AGC AAG CTC AGC TTG GAG GG-3'. The pAED4.91-Annexin A2 Cys 8 Ser construct was transformed into BL21(DE3) pLysS competent *E. coli*, the protein expressed and purified as reported for WT annexin A2.

2.1.5 Preparation of Recombinant Annexin A2 Heterotetramers

Equal molar ratios of purified annexin A2 (WT or C8S mutant) and S100A10 were incubated o ice for 1 hour before gel filtration chromatography to separate the heterotetramer from the excess of either constituent protein. The fractions containing the heterotetramer were pooled and concentrated.

2.1.6 Plasminogen Domain Mutants

Truncated human plasminogen derivative proteins were a gift from Dr. Girish Sahni (Institute of Microbial Technology, Chandigarh, India). The proteins consisted of the following regions of human plasminogen; K1–Kr5SP (residues 78–791), Kr2–Kr5SP (residues 163–791), Kr4Kr5SP (residues 350–791), Kr5SP (residues 440–791), and SP (residues 543–791), where Kr refers to kringle and SP refers to serine protease domain. Proteins were expressed in Pichia pastoris and purified according to the methods of (Joshi et al., 2012).

2.1.7 tPA-Domain Mutants

Domain-switched/deleted variants of tPA were a gift from Dr. Colin Longstaff (Haemostasis Section, Biotherapeutics Group, National Institute for Biological Standards and Control, South Mimms, Herts, UK). The WT tPA (F-G-Kr1-Kr2-P, where F = finger domain, G = EGF-like domain, Kr1= kringle 1, Kr2 = kringle 2, SP =serine protease domain), a replacement domain variant: K1K1tPA (F-G-Kr1-Kr1-PS) and a domain deleted variant: FdeltPA (G-Kr1-Kr2-SP) that lacks the finger domain were expressed and purified from Sf9 insect cells as detailed in Longstaff et al. (Longstaff et al., 2011).

2.1.8 Sources of Other Proteins and Reagents

Glu-plasminogen was prepared according to the methods of Deutsch and Mertz (Deutsch and Mertz, 1970), with some minor alterations. Briefly, human plasma was exposed to lysine-Sepharose equilibrated in phosphate buffered saline (PBS). The column was washed in 0.8 M NaCl in PBS pH 7.3 to remove any non-specific

binding proteins. The bound plasminogen was eluted with an ε-aminocaproic acid (εACA) gradient (0 to 25 mM) in PBS. The plasminogen eluted at 12.5 mM εACA in a sharp peak. The fractions were tested for plasmin contamination by their ability (or absence of ability) to cleave the plasmin specific substrate S2251 (H-D-Valyl-L-leucyl-L-lysine-p-Nitroaniline dihydrochloride) (Chromogenix (distributed by Diapharma, West Chester OH) or Molecular Innovations (Novi, MI)), and any fractions containing plasmin activity were discarded. Remaining fractions were pooled, concentrated and dialyzed in PBS to remove εACA. Aliquots were prepared and subsequently frozen at -80°C.

Lys-plasminogen was obtained from Enzyme Research Labs (South Bend IN, USA). Single chain recombinant tPA was obtained from Genentech (South San Francisco CA). Recombinant plasminogen receptors were sourced as follows: S100A4 from Novus Biologicals Canada (Oakville ON), α-enolase from Creative BioMart (Shirley NY), cytokeratin K8 from Progen Biotechnik GmbH (Heidelberg, Germany), high mobility group box-1 protein (HMGB-1) from Prospec-Tany Technogene Ltd (East Brunswick NJ), and Histone H2B from GenWay Biotech (San Diego, CA). Porcine pancreatic carboxypeptidase B1 was purchased from Worthington Biochemical (Lakewood, NJ).

2.1.9 ACTIVITY ASSAYS

2.1.9.1 PLASMIN GENERATION ASSAY

The kinetics of tPA- dependent plasminogen activation were determined by measuring the amidolytic activity of the plasmin generated during activation of plasminogen as described previously(Geetha Kassam et al., 1998). The reaction was performed at 37°C, in 0.2 ml final reaction volume of a buffer consisting of 50 mM Tris-HCl (pH 7.4), 50 mM NaCl, 5 mM $CaCl_2$, and 10 nM or 0.1 nM tPA with the substrate S-2251 (H-D-Valyl-L-leucyl-L-lysine-p-Nitroaniline dihydrochloride) (Chromogenix-Diapharma Group, Inc., West Chester, OH or

Molecular Innovations Novi, MI) at a final concentration of 360 µM, or as noted in the figure legend. The concentration of tPA was dependent on which batch was used, and the actual concentration used is noted in the figure legends. The reaction was initiated by the addition of 0.15 µM Glu-plasminogen (or concentrated noted in the figure legend) and the reaction progress monitored at 405 nm in a Molecular Devices SpectraMAX M3 microplate reader (Sunnyvale, CA). Initial rates of plasmin generation were calculated using linear regression analysis of plots of A405 nm versus time^2 utilizing data points at a low extent of substrate conversion as outlined in Kassam et al. (Geetha Kassam et al., 1998). Specifically, the rate of plasmin generation was calculated using the equation A405 nm = B + Kt^2. Where K is the slope and rate constant for the acceleration of plasmin generation and B is the y-intercept (G. Kassam et al., 1998).

2.1.9.2 tPA Activity

Assays were performed in 100 mM Tris (pH 8.4), 106 mM NaCl, 0.1 g/L Triton-X100. tPA activity was directly measured with the substrate S-2288)H-D-Isoleucyl-L-prolyl-L-arginine-p-nitroaniline dihydrochloride) (Chromogenix via Diapharma Group, Inc.) at a concentration of 0.1–2.0 mM at 37 °C in a reaction volume of 0.2 mL. Ten nM tPA in the presence and absence of 1 µM S100A10 was incubated in each of the substrate concentrations. The reaction progress was monitored at 405 nm and the rate was calculated using linear regression analysis of plots of A405 nm versus time (in minutes).

2.1.10 Circular Dichroism Spectroscopy

A Jasco J-810 spectropolarimeter (Jasco Inc., Easton, MD, USA) was used to obtain circular dichroism (CD) spectra by the methodology described in Kassam et al. (Kassam et al., 1997). S100A10 (18.2 µM) was incubated in PBS (pH 7.5) at room temperature (RT) and scanned in a quartz cuvette (0.5 mm path length) from 190 nm to 260 nm at a rate of 20 nm/s, using a bandwidth of 1 nm and a response time

of 1 s. CD spectra of proteins were obtained by averaging five wavelength scans and were corrected by subtracting buffer scans. The data are expressed as mean residue ellipticity where the raw ellipticity value was converted into mean residue ellipticity ([θ]) by the formula: [θ]= (0.1) (molecular weight)/ (number of residues) (pathlength [cm]) (protein concentration [mg/mL]). Spectra were analyzed using DichroWeb software (Whitmore and Wallace, 2008, 2004).

2.1.11 Fluorescence Spectroscopy

All fluorescence experiments were performed using a Spectra-MAX M3 multi-mode plate reader at RT, using the integrated cuvette port. A quartz cuvette with a path length of 5 mm was used. Plasminogen (1 μM), S100A10 (1 μM) or both were incubated in 0.2 mL PBS (pH 7.4) and excited at 280 nm and the intrinsic fluorescence emission spectra were measured from 310–450 nm. These particular settings for intrinsic fluorescence will specifically target tryptophan residues, as the peak emission for a 280 excitation for tryptophan is 330-350 (Lakowicz, 2006). Tyrosine emits at approximately 300 with an excitation of 280 while phenylalanine is excited at 270 with an emission maximum of about 290 (Eftink, 2000; Lakowicz, 2006).

2.1.12 SDS-PAGE and Western Blotting

Proteins were separated by sodium dodecyl sulphate-polyacrylamide gel electrophoresis (SDS-PAGE) at 100 V until suitable protein separation, monitored by the movement of pre-stained electrophoresis protein standards, was achieved. Gel concentrations ranged from 10 to20%, depending on the proteins separated. The Laemmli buffer system was used exclusively (Laemmli, 1970). For total protein staining the gel was briefly incubated in deionized water to remove as much SDS as possible, then incubated for 2 h to 18 h at RT (RT) in Coomassie Blue staining solution, consisting of 0.1% Coomassie Blue G-250 in 30% methanol and 10% acetic acid. The gel was then destained in 30 % methanol and 10% acetic acid

until the background was clear. Gels were imaged using a Licor™ Odyssey scanner (Lincoln NE). Images were processed using Image Studio Lite Software (Licor, Lincoln NE).

For gels that underwent western blotting, the staining procedure was omitted and the proteins were transferred to 0.2 μm nitrocellulose in Towbin's buffer (Towbin et al., 1979) for either 1 h at 100V or 16 h at 20V. The blots were blocked in Licor™ Odyssey Blocking Buffer for a minimum of 1 h at RT with agitation, washed in Tris-buffered saline with 0.5% Tween 20 (TBS-Tw), then incubated in antibody specific primary antibody solutions in TBS-Tw for 1 h with agitation. The blots were again extensively washed in TBS-Tw, then incubated with the appropriate secondary DyLight(Thermo Fisher Scientific Whitby ON) or IRDye (Licor) infrared tagged antibody. The blots were again washed before imaging on Licor™ Odyssey infrared scanner. The image was processed using Image Studio Lite Software (Licor).

2.2 Role of S100A10 in Demyelination

2.2.1 In vitro Proteolysis of Myelin Basic Protein

Plasminogen (30μM) was mixed with tPA (1.6 or 0.2 nM) in the presence and absence of S100A10 (0.2 or 0.05 nM) for 20 minutes at 37°C. This mixture either was preincubated for 60 minutes prior to the addition of 10μg MBP (Sigma, Oakville ON) or the MBP was added immediately after mixing. The reaction was stopped by the addition of an equal volume of 2X SDS-PAGE loading buffer and boiled for 5 minutes. The resulting reaction products were separated on a 20% SDS-PAGE gel.

2.2.2 Animal Care

All animals used were 6-8 weeks of age and were bred and housed in the Carleton Animal Care facility at Dalhousie University. Mice were fed a standard diet of

rodent chow and water *ad libitum* and housed in a 12-hour light/dark cycle. The demyelination study was approved by the Dalhousie University Committee on Laboratory Animals and was performed following guidelines of the Canadian Council on Animal Care.

Two mouse strains were used in this study, wild type (WT) which were C57BL/6 or *S100A10*$^{-/-}$ on a C57BL/6 background. The mice were generously provided by Per Svenninsson (Egeland et al., 2011) and colonies maintained in the Carleton Animal Care Facility.

2.2.3 INJECTION OF LYSOPHOSPHATIDYLCHOLINE

Female mice, either wild type (C57BL/6) or S10A10null (on a C57BL/6 background) were anesthetized via continuous inhaled isoflurane. Mice were immobilized on a Kopf model 940 digital stereotaxic frame. A mid-line incision on the skull exposed the bone and connective tissue was gently cleared. Two small holes were drilled, 1 mm bilaterally, 2.3 mm anterior to the bregma and 2.7 mm deep. Hamilton syringes (10 μL) retrofitted with Neuros syringe needles were used to inject with 1 μL of 1% lysophosphatidylcholine (LPC)(Sigma) in PBS on the animal's left, and PBS on the right (Figure 2.1). Volumes were injected slowly, over 60 s, and the needle held in place for 2 min to minimize backflow. The wound was sutured and mice were allowed to recover and then sacrificed 7 days post-injection by anesthetic overdose and perfused with 10% formalin. The brains were removed and placed in 10% buffered formalin (Fisher) for a minimum of 4 days. The cerebellum was removed, and the right side (PBS-treated) notched for orientation. The remaining tissue was post-fixed in 70% ethanol, then embedded by Dalhousie Histology Research Services. Brains were sectioned in 5 μm slices using a Leica RM2255 microtome and sequentially mounted on serially numbered slides (Fisherbrand Superfrost Plus).

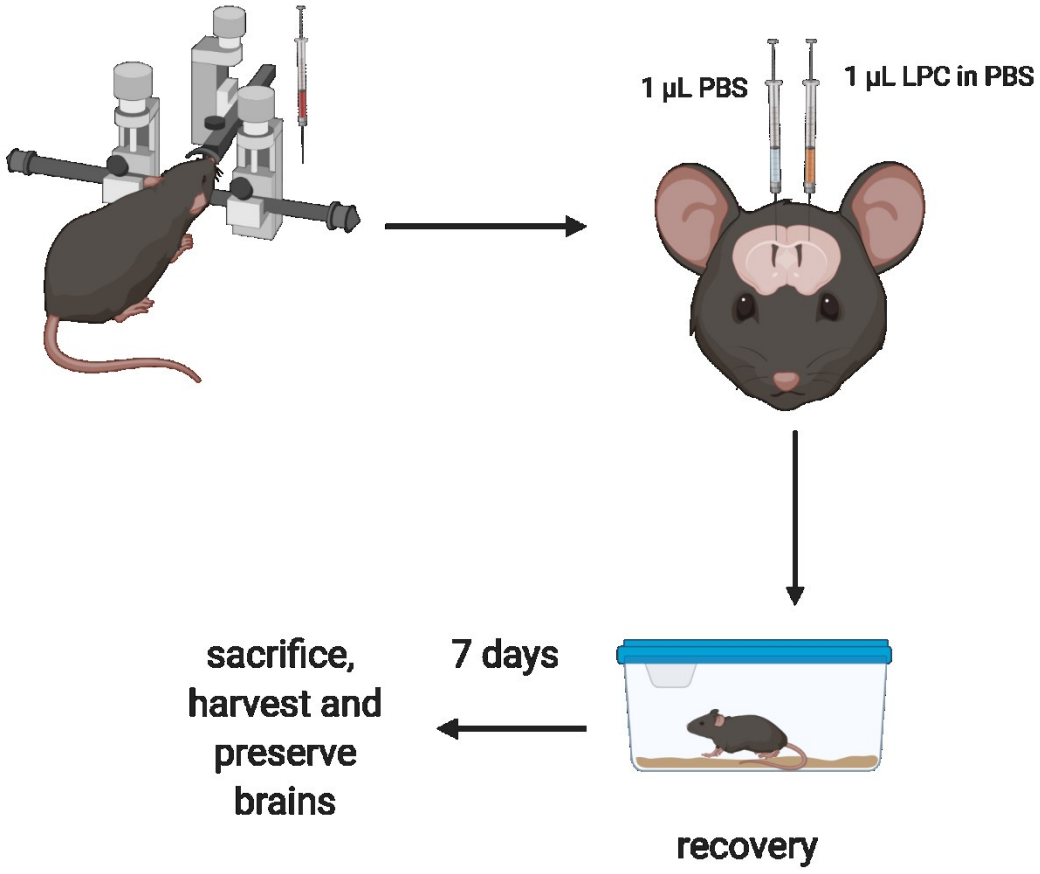

Figure 2-1 Demyelination Model Injection Protocol

Schematic for injection of PBS (sham) and 1% lysophosphatidylcholine. Mice were prepared for surgery, anesthetized and maintained on isoflurane and immobilized on a stereotaxic frame. After exposure of the skull, a small hole was drilled in the bone, then 1 µL of either sterile PBS or 1% lysophosphatidylcholine was injected using a 10 µL Hamilton syringe retro-fitted with a Neuros syringe needle. The needle was left in place for at least 60 seconds to minimize back-flow. The wound was sutured, the animal allowed to recover, then sacrificed 7 days later. Brains were extracted and preserved as described in the text. Created with Biorender.com

2.2.4 HISTOLOGY

All brains were stained for demyelination. Every fifth slide from the initial limit of the corpus callosum was stained with eriochrome cyanine and neutral red counterstain to determine the limits of the resulting lesion. Briefly, slides were deparaffinized with xylene, then brought to 70% ethanol and rinsed with tap water before incubating in eriochrome cyanine for 15 minutes. Tissues were differentiated in 0.5% (w/v) NH_3OH, followed by counterstain with 0.5% (w/v) neutral red (Rowley Biochemical, Danvers, MA). Sections were dehydrated and coverslipped with CytoSeal 60 (Thermo Scientific™- Richard-Allen™ Scientific, San Diego. CA).

Slides were imaged, both left and right sides, using a Zeiss Axioplan II outfitted with Axiocam HRC Colour Camera (both Carl Zeiss Canada Ltd, Toronto ON). Images were obtained at 5X or 10X magnification. The lesion area was measured using ImageJ (Schneider et al., 2012) utilizing the Fiji plugin bundle (Schindelin et al., 2012). Each slide contained three 5µm sections (notes were made if a section was unusable, or if more or less than 3 sections were present). At least one image/imaging session was processed using a scale bar to set the measurements in Fiji.

2.2.4.1 LESION QUANTITATION

Lesions were traced using the freehand tool, and the area inside the trace calculated by Fiji (Schindelin et al., 2012). Volume was determined by plotting the areas of adjacent sections vs accumulated thickness (calculated as the number of sections per slide multiplied by the 5µm section thickness.

2.2.5 IMMUNOFLUORESCENCE

Slides adjacent to slides with a confirmed lesion were subjected to immunofluorescent staining for Ionized Calcium Binding Adaptor Molecule 1 (Iba-1) to assess the presence of microglia cells and recruited peripheral

macrophages (Ito et al., 1998; Plemel et al., 2018) and were also stained for Glial fibrillary acidic protein (GFAP) marker for the presence of astrocytes (Briens et al., 2017; Plemel et al., 2018; Sofroniew and Vinters, 2010). Slides were deparaffinized with xylene, then brought to 70% ethanol. Antigen retrieval was performed in Tris-EDTA buffer with 0.1% Tween 20 using a Biocare (Pacheco, CA) Decloaking Chamber™, then samples were blocked with normal donkey serum (Sigma). After washing, the slides were incubated with a 1:500 dilution of primary rabbit polyclonal Iba-1 (product 013-27691, Wako, Osaka Japan) at 4°C overnight in a humid chamber. The following day, the secondary antibody, donkey anti-rabbit AlexaFluor 488 (1:500 dilution) (A21206 Life Technologies Carlsbad CA) was added in combination with the primary mouse monoclonal anti-GFAP conjugated with Cy3, diluted 1:500 (C9205, Sigma), and incubated for 2 hours in a humid chamber. Slides were treated with a 1X solution of True Black® Lipofuscin Autofluorescence Quencher (Biotium, Fremont CA) then coverslips were applied using Fluoromount G with DAPI (Electron Microscopy Sciences, Hatfield, PA). Images were obtained using a Zeiss AxioPlan microscope fitted with AxioCam503 camera and the total fluorescence of the field containing the full lesion was quantitated using Fiji software(Schindelin et al., 2012). Control slides omitting the primary were treated identically, substituting a Cy3 conjugated mouse monoclonal antibody for the Cy3 conjugated anti-GFAP primary.

2.3 Statistical Analysis

Analysis using student t-test, one-way ANOVA followed by Dunnett's multiple comparisons test or two-way ANOVA followed by Tukey multiple comparison test (as noted) was performed using Prism version 7.02 for Windows, (GraphPad Software (La Jolla, CA, www.graphpad.com).

Data are shown as mean ± standard deviation (SD) or standard error of the mean (SEM) as noted in the figure legend. Statistical significance was defined as * $p <$

0.05, ** p < 0.01, *** p < 0.001, ****p< 0001. All experiments were repeated independently at least three times.

3.1 PUBLICATIONS ARISING FROM THIS WORK

Section 3.2 Miller et al Thrombosis and Haemostasis 117:1058

3.2 INTERACTION OF S100A10, PLASMINOGEN AND TISSUE PLASMINOGEN ACTIVATOR; C-TERMINAL LYSINE RESIDUES OF S100A10

3.2.1 RESULTS OF EXPRESSION AND PURIFICATION OF C-TERMINAL REGION LYSINE S100A10 MUTANTS

The C-terminal mutants of S100A10 were all expressed and purified using the same protocol as for wild type S100A10. No alterations in the protocol were required for efficient expression or purification of these mutants (Figure 3.1).

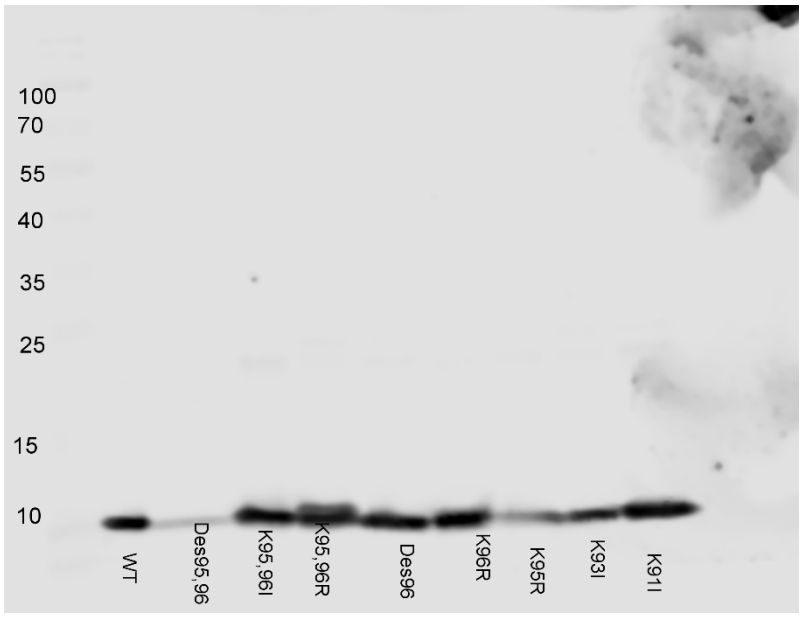

Figure 3-1 SDS-PAGE of S100A10 C-terminal Region Lysine Mutations

Select C-terminal region mutants (0.1µg) were loaded onto a 15% SDS-PAGE, subjected to electrophoresis and then blotted to nitrocellulose. The resulting blot was bloked with Licor Blocking buffer then probed with mouse monoclonal antibody (BD Biosciences) (1/2000) followed by detection with Goat anti-mouse IgG-DyLight8000 (Thermo) (1/15000) and imaged with LiCor Odyssey imaging system.

3.2.2 KRINGLE-2 OF TPA IS CRITICAL FOR COMPLEX FORMATION WITH TPA, PLASMINOGEN AND S100A10

Initially, experiments were undertaken to determine which domains of tPA participate in the tPA-dependent plasminogen activation acceleration by the PgR S100A10. tPA mutants were incubated with plasminogen and S100A10 to determine the ability of S100A10 to enhance tPA-dependent plasmin generation. The tPA constructs tested included a recombinant wild type: (F-G-Kr1-Kr2-SP, where F = finger domain, G = EGF-like domain, Kr1= kringle 1, Kr2 = kringle 2, SP = protease domain), a replacement domain variant: K1K1tPA (F-G-Kr1-Kr1-SP) and a domain deleted variant: F_{del}tPA (G-Kr1-Kr2-SP). S100A10 amplified plasmin generation by both rWTtPA and F_{del}tPA, but plasmin generation in the presence of K1K1 tPA was not enhanced in the presence of S100A10 (Figure 3.2.)

To confirm that substituting Kr2 with another Kr1 motif did not alter the base rate of plasmin generation, (i.e. to confirm that the decrease in acceleration of plasmin generation was not due to a lower overall activity of the K1K1tPA mutant), the rate of conversion of plasminogen to plasmin in the absence of S100A10 for each of the tPA variants was analyzed. WTtPA had the highest activity, while K1K1tPa and F_{del}tPA had progressively lower activity (Figure 3.3). This result agrees with the original published data (Longstaff et al., 2011), where the authors suggested that the finger domain of tPA plays a role in regulating its activity. This suggests the loss of the ability of S100A10 to stimulate plasminogen activation in the presence of K1K1tPA was not due to a decrease in the ability of the K1K1tPA to activate its substrate plasminogen. Additionally, the activity of each of the tPA mutants towards the tPA-specific amidolytic substrate S2288 was determined. If the baseline activity of each of the mutants varied from the WTtPA then the difference in the presence of S100A10 could be attributed to the intrinsic activity of the tPA construct. Holding the tPA concentration constant at 10nM revealed no differences in the rate of cleavage of the tPA-specific substrate over the range of

0.1 to 1.0 mM substrate (Figure 3.4). At higher substrate concentration, the FdeltPA had a higher activity, opposite to the effect observed in the presence of S100A10. The decreased rate of plasmin generation by K1K1 tPA in the presence of S100A10 is not due to differences in the ability of the mutant tPA to cleave plasminogen.

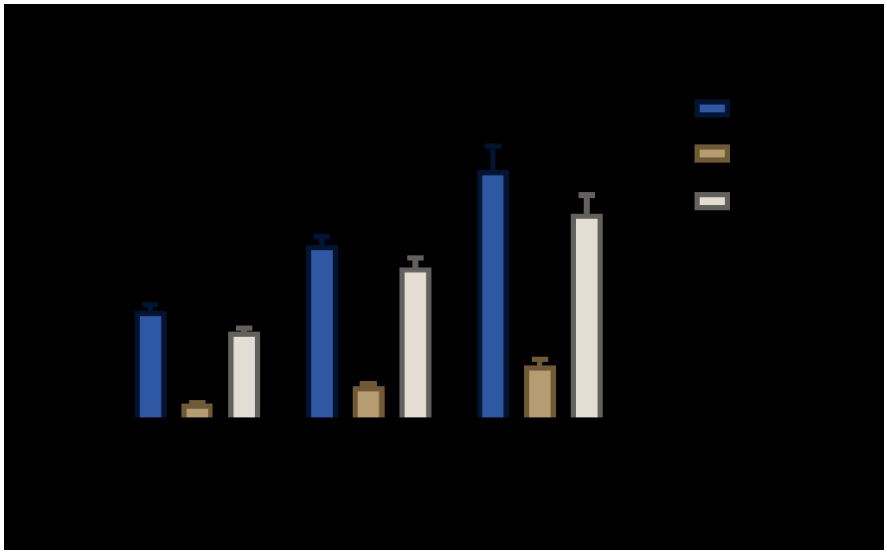

Figure 3-2 The Role of tPA Domains in Acceleration of Plasmin Generation by S100A10

Plasmin formation was measured at 405 nm using the plasmin specific substrate S-2251 (0.36 mM) in the presence of 1 μM recombinant human S100A10, different concentrations of Glu-plasminogen (0.075, 0.15 and 0.30 μM) and 10 nM tPA mutants. The rate of plasmin generation was calculated from the equation: A 405 nm = B + K*t ^{2}, where K, the slope, is the rate constant for the acceleration of plasmin generation and B is the y-intercept and is expressed as A405 nm/min^2. The results are the mean ± SD of triplicate measurements, repeated at least three times. * $p < 0.05$, ** $p < 0.01$, *** $p < 0.001$, **** $p < 0.0001$ (two-way ANOVA, Tukey multiple comparisons test). Reproduced with permission from Miller et al. (2017) Thrombosis and Haemostasis 117, 1058–1071 via Copyright Clearance Center.

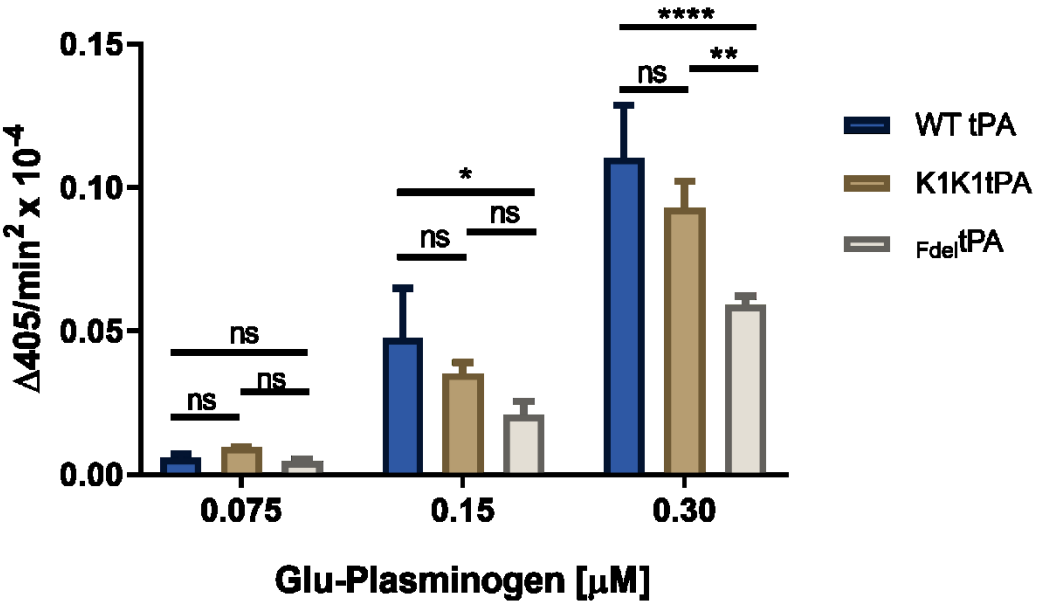

Figure 3-3 Kringle 2 Domain of tPA is Not Required for Plasmin Generation in the Absence of S100A10

The rate of plasmin formation in the absence of S100A10 and in the presence of the various constructs of tPA was also determined. The results are the mean ± SD of triplicate measurements, repeated at least three times. * $p < 0.05$, ** $p < 0.01$, *** $p < 0.001$, **** $p < 0.0001$ (two-way ANOVA, Tukey multiple comparisons test). Reproduced with permission from Miller et al. (2017) Thrombosis and Haemostasis 117, 1058–1071 via Copyright Clearance Center.

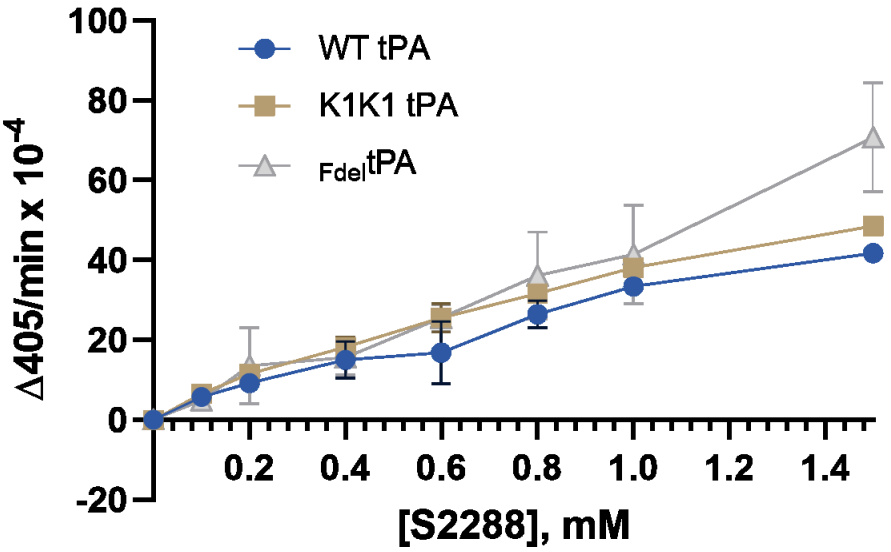

Figure 3-4 Mutant tPA Constructs Possess Similar Activity Towards tPA-Specific Amidolytic Substrate

WT tPA and mutants (K1K1tPA and Fdel tPA) were assayed for the ability to cleave the tPA-specific substrate S2288. Increasing concentrations of the tPA-specific amidolytic substrate S2288 was added to 10 nM tPA (either WT or mutant) in TBS with 0.1% Trition X-100 and the reaction monitored at A405 nm. The rate at each substrate concentration was determined by plotting the absorbance vs time elapsed in minutes. Reperesentative experiment shown, mean of 3 replicate values +/- SD, the experiment was repeated at least 3 times.

Previous publications have shown that tPA binds to S100A10 (Kwon et al., 2005; MacLeod et al., 2003). It is possible that the stimulation in plasmin generation is due to S100A10 interacting with tPA, causing a conformational change and increasing its catalytic rate towards plasminogen. To explore this, the activity of WT tPA towards a tPA-specific chromogenic substrate, S2288 (H-D-Ile-Pro-Arg-pNA) in the presence and absence of S100A10 was tested over varying substrate concentrations. The catalytic activity of tPA remains the same in the presence of S100A10. The addition of S100A10 to tPA and its amidolytic substrate does not increase the ability of tPA to cleave said substrate (Figure 3.5). S100A10 does not appear to increase the catalytic activity of tPA.

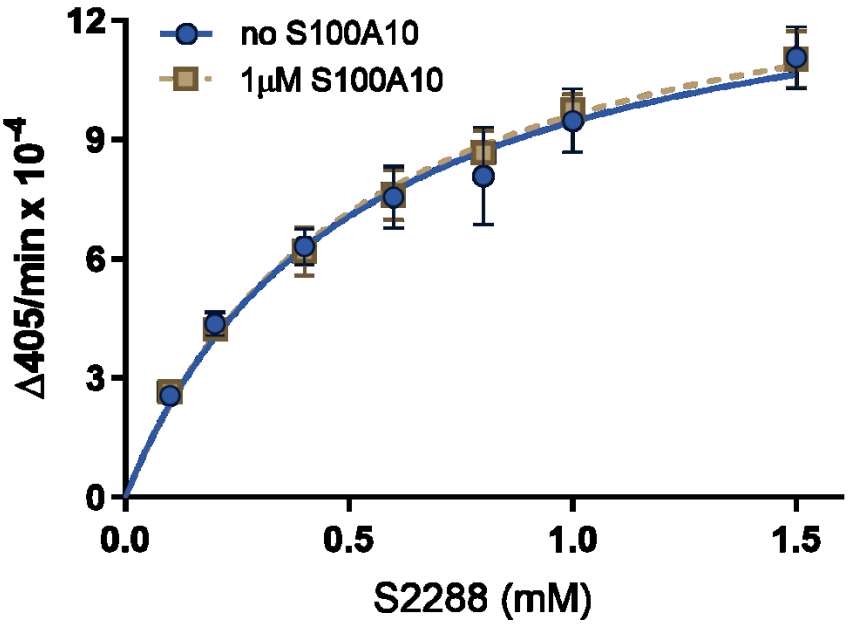

Figure 3-5 S100A10 Does Not Increase the Activity of tPA

To assess the effect of S100A10 on the ability of tPA to cleave a substrate, 10 nM tPA was incubated in the presence and absence of 1μM S100A10. Increasing concentrations of the tPA-specific amidolytic substrate S2288 was added and the reaction monitored at A405 nm. The rate at each substrate concentration was determined by plotting the absorbance vs time elapsed in minutes. Reperesentative experiment shown, mean of 3 replicate values +/- SD, the experiment was repeated at least 3 times. Reproduced with permission from Miller et al. (2017) Thrombosis and Haemostasis 117, 1058–1071 via Copyright Clearance Center.

3.2.3 KRINGLE-2 OF TPA IS IMPORTANT FOR BINDING OF MANY CELLULAR PLASMINOGEN RECEPTORS

S100A10 is one of many cellular PgR, many of which bind both tPA and plasminogen (Felez et al., 1993). The interaction between plasminogen kringles and the PgR has been established (Miles and Parmer, 2013); the mechanism of interaction of tPA and the PgR has not been thoroughly investigated. The initial results of the interaction of tPA and 2 domain mutants have suggested that it is Kr2 of tPA that interacts with S100A10. To determine if the interaction appears to be the same as with other PgR, several other PgR were incubated with each of the tPA mutants and subsequent plasmin generation was measured. The PgR substituted for S100A10 were α-enolase, S100A4, histone H2B, cytokeratin 8 and HMGB-1. These PgR were tested at concentrations chosen to optimize the *in vitro* activity, and not to mirror their comparative involvement in plasmin generation *in vivo*. For α-enolase only, an increased concentration of the PgR was required for a similar activation acceleration. All the PgR tested accelerated plasmin generation by both the WT tPA and the F_{del}tPA, but a comparable increase was not seen in the presence of K1K1tPA (Figure 3.6). This suggests that the interaction between tPA and many PgR occurs via the Kr2 domain of tPA.

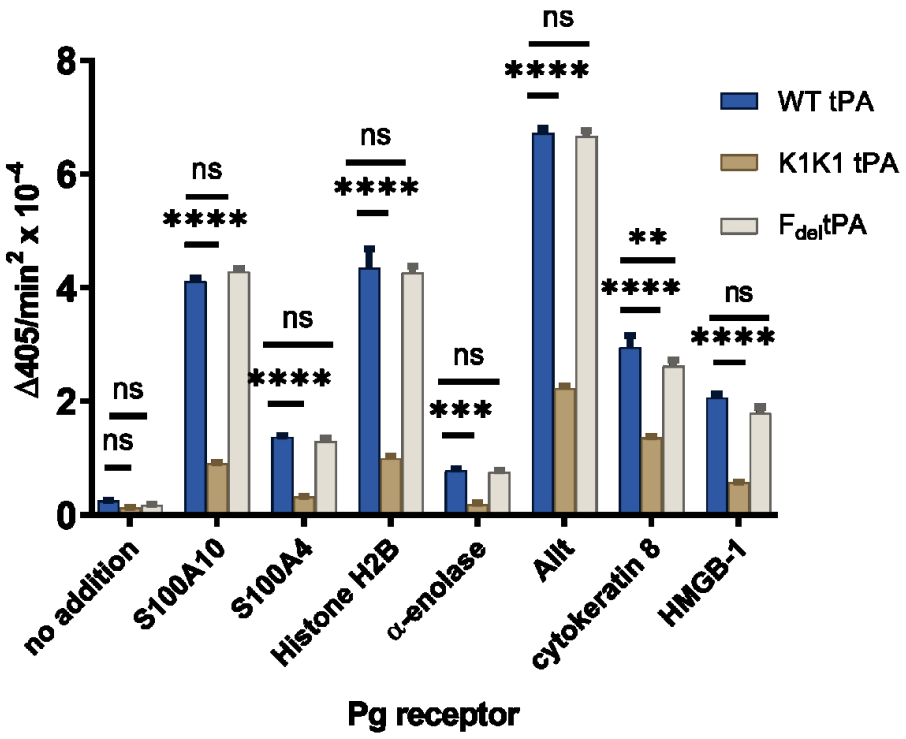

Figure 3-6 Role of tPA Domains in Plasminogen Activation Acceleration by Plasminogen Receptors

Plasmin generation was measured at 405 nm using the plasmin specific substrate S2251 (0.36 mM) in the presence of 0.15 μM plasminogen, 10 nM tPA variants and 0.5 μM (or 2.0 μM α-enolase) recombinant plasminogen receptors. The rate of plasmin generation was calculated as described in section 2.1.8.2. Results shown are the mean ± SD of triplicate measurements. Twoway ANOVA with Dunnett's multiple comparison test, p values ns ≥ 0.05, * < 0.05, ** < 0.01, *** < 0.001, **** <0.0001. Reproduced with permission from Miller et al. (2017) Thrombosis and Haemostasis 117, 1058–1071 via Copyright Clearance Center.

3.2.4 ANNEXIN A2/S100A10 COMPLEX AND ITS INTERACTION WITH KRINGLE-2 DOMAIN OF TPA

On the surface of cells, S100A10 is found in a heterotetramer consisting of a dimer of S100A10 interacting with 2 molecules of annexinA2. The annexin A2 molecules anchor the complex to the phospholipids of the cell surface in a calcium-dependent manner (Madureira et al., 2011). This complex is termed Annexin A2 heterotetramer or AIIt and induces a more potent acceleration of plasmin generation than S100A10 alone (Figure 3.6). This increase in plasmin generation was also noted when WTtPA was substituted with FdeltPA but a much lower rate of plasmin generation was observed with K1K1tPA (Figure 3.6). The loss of tPA-dependent plasmin generation with the K1K1 mutant was more striking for S100A10 alone than AIIt. In the presence of S100A10, the rate increased by 16.28 with WT tPA, while the rate increased to 6.88 with K1K1tPA. When AIIt was present, the rates increased by 26.66 and 16.86 fold respectively. The most straightforward cause for this difference was that since both S100A10 (MacLeod et al., 2003) and annexin A2 (Hajjar et al., 1998; Roda et al., 2003) possess tPA binding sites, the tPA-binding site on annexin A2, which reportedly uses the cysteine residue at position 8 to interact with tPA (Jacovina et al., 2009; Roda et al., 2003), might interact differently with the domains of tPA than S100A10. Annexin A2 potentially forms a covalent bond with tPA (Jacovina et al., 2009). The activity of recombinant AIIt made with WT S100A10 subunits was compared to either WT annexin A2 ($AIIt^{WT}$) or mutant annexin A2 in which the putative tPA binding site was inactivated ($AIIt^{Cys8Ser}$). If the interaction/binding site for tPA on annexin A2 is Cysteine 8, the loss of this binding site should result in a loss in the ability of $AIIt^{Cys8Ser}$ to accelerate plasmin generation. Examination of the rate of plasmin produced by tPA-dependent plasminogen activation by these the $AIIt^{WT}$ and $AIIt^{Cys8Ser}$ showed that $AIIt^{Cys8Ser}$ in fact accelerated tPA-dependent plasminogen activation to a higher level than $AIIt^{WT}$ (Figure 3.7). This suggests that the Cys-8

residue of annexin A2 does not play an important role in the acceleration of tPA-dependent plasminogen activation by the annexin A2 heterotetramer.

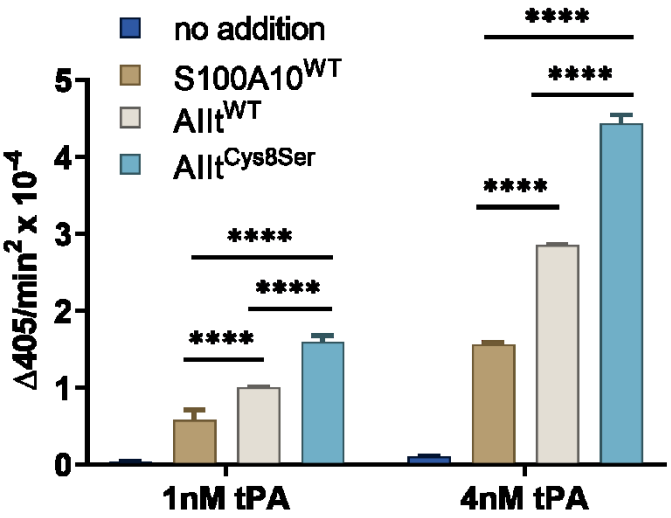

Figure 3-7 tPA Does Not Require the Cysteine Residue at Position 8 to Interact with the Annexin A2 Component of AIIt

Plasmin formation was measured at 405 nm using the plasmin-specific substrate S-2251 (0.36 mM) in the presence of 0.15 µM plasminogen, 1, or 4 nM tPA and 1 µM recombinant heterotetrameric complex consisting of WT annexin A2/WT S100A10 ($AIIt^{WT}$), annexin $A2^{Cys8Ser}$/WT S100A10 ($AIIt^{C8S}$) or 1 µM $S100A10^{WT}$ alone. Plasmin formation is expressed as A405 nm/min^2. The results are the mean ± SD of triplicate measurements, repeated at least three times. **** $p < 0.0001$ 2 Way ANOVA, with Dunnett's multiple comparison test. Reproduced with permission from Miller et al. (2017) Thrombosis and Haemostasis 117, 1058–1071 via Copyright Clearance Center.

3.2.5 THE ROLE OF THE PLASMINOGEN KRINGLE DOMAINS IN S100A10-ACCELERATED PLASMIN GENERATION

As discussed in the introduction, plasminogen consists of seven domains: an N-terminal peptide domain, five kringle domains and the serine protease domain. Plasminogen adopts a range of conformations that fluctuate from closed to open. Within the circulation, Glu-plasminogen is primarily present in the closed conformation which is poorly activated by tPA (Suenson and Petersen, 1986) Glu-plasminogen will adopt a more open conformation when bound to fibrin or cell surface plasminogen receptors. Loss of the amino-terminal peptide domain (residues 1-77) by plasmin lysis produces an alternative zymogen form called Lys-plasminogen. Biochemical and structural studies suggest that kringle-1 enables the initial interaction of plasminogen with fibrin or the cell surface via binding to a carboxyl-terminal lysine (Miles et al., 1988). Crystallographic analysis has shown that in the closed conformation, kringle-1 is the only kringle domain available for binding (Law et al., 2012). However, it is unclear which of the kringle domains play a role in the interaction of Lys-plasminogen with its binding partners. Recently, Sahni's group developed a series of truncated derivatives of Lys-plasminogen with progressive removal of kringle domains (Joshi et al., 2012). These mutants were used to identify which plasminogen kringles interact with S100A10. The ability of S100A10 to accelerate tPA-dependent activation of the Kr2-Kr5SP plasminogen mutant was reduced compared to the parent molecule, Lys-plasminogen (Figure 3.8 panel A). This suggests that kringle-1 (Kr1) of Lys-plasminogen plays an important role in the stimulatory function of S100A10. S100A10 accelerated the rate of activation of Glu-plasminogen to a greater extent than that of Lys-plasminogen. These data are best illustrated by examining the fold increase over the rate in the absence of S100A10 (Figure 3.8 panel B).

Figure 3-8 Loss of Kringle 1 of Plasminogen Results in a Loss of S100A10 Mediated Plasmin Generation

Plasmin formation was measured at 405 nm using the plasmin-specific substrate S-2251 (0.36 mM) in the absence (no addition) or presence of 1 μM S100A10 or annexin A2/S100A10 complex (AIIt), 4 nM tPA and 0.15 μM Glu-plasminogen, Lys-plasminogen, or Lys-plasminogen mutants consisting of residues 78–791 (Lys-plasminogen) (Kr1–Kr5SP), residues 163–791 (Kr2–Kr5SP), residues 350–791 (Kr4Kr5SP), residues 440–791 (Kr5SP), and residues 543–791 (SP). Kr refers to the kringle domain and SP, the serine protease domain of plasminogen.

Plasmin formation is expressed as A405 nm/min^2 (A) or as the fold increase (B) where the fold increase is defined as the rate in the presence of S100A10 or AIIt (as appropriate) divided by the rae in the absence. The results are the mean ± SD of triplicate measurements, repeated at least three times. * $p<0.05$, ** $p < 0.01$, *** $p < 0.001$, **** $p < 0.0001$ (2-way ANOVA, with Tukey's multiple comparison test). Reproduced with permission from Miller et al. (2017) Thrombosis and Haemostasis 117, 1058–1071 via Copyright Clearance Center.

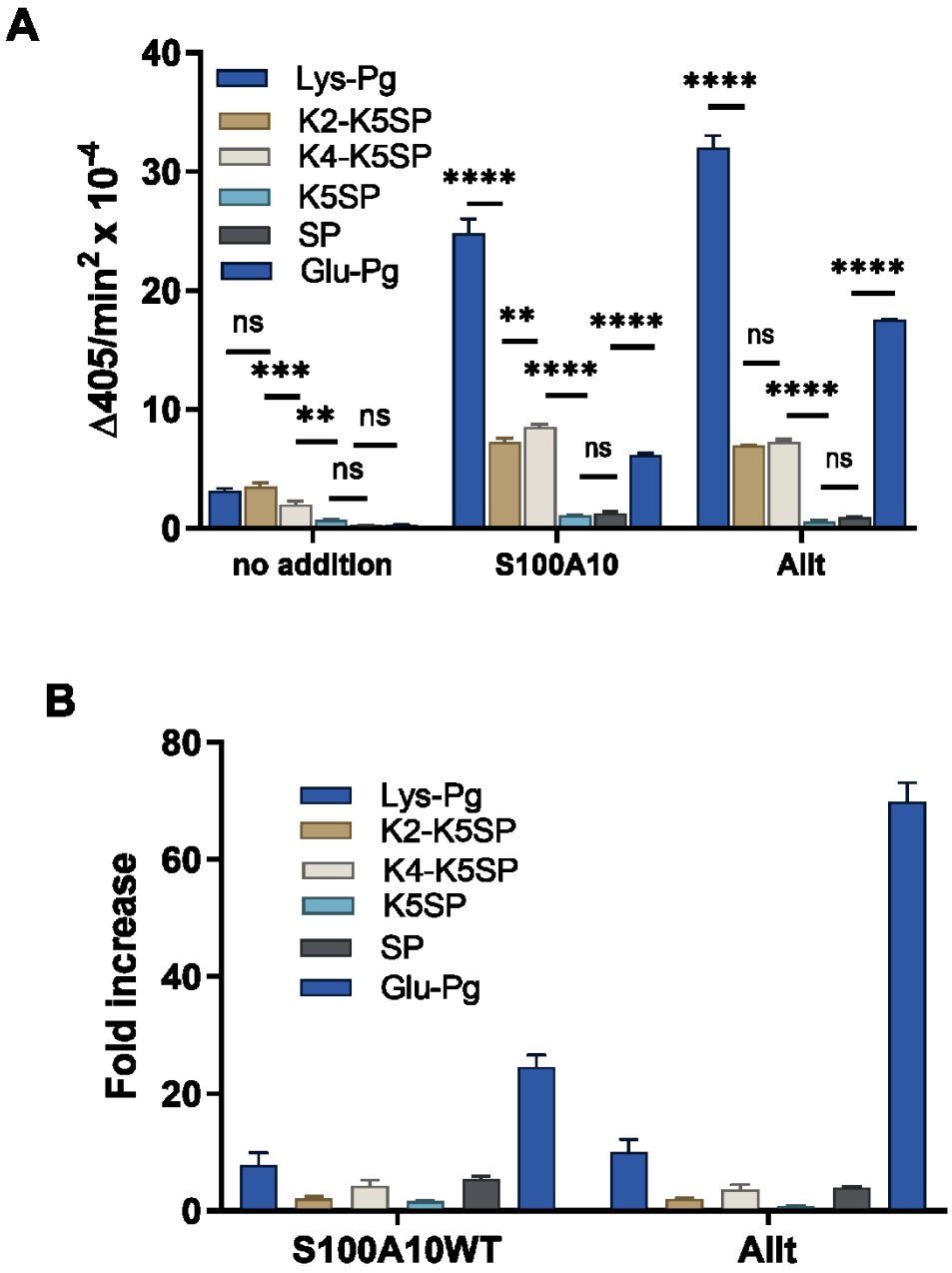
A
Δ405/min² x 10⁻⁴
40
30
20
10
0
Lys-Pg
K2-K5SP
K4-K5SP
K5SP
SP
Glu-Pg
ns
***
**
ns
ns
****
**
****
ns
****
****
ns
****
ns
no addition
S100A10
Allt
B
Fold increase
80
60
40
20
0
Lys-Pg
K2-K5SP
K4-K5SP
K5SP
SP
Glu-Pg
S100A10WT
Allt

3.2.6 IMPORTANCE OF THE C-TERMINAL LYSINE DOMAINS OF S100A10 IN PLASMIN GENERATION

It has long been accepted that the carboxyl-terminal lysine residues found in fibrin and many cell-surface plasminogen receptors are essential for plasminogen activation (Miles et al., 1988). Prior work published by the Waisman laboratory showed that the loss of the carboxy-terminal lysine residues of S100A10 resulted in a loss of plasminogen binding, along with a decrease in the rate of plasminogen activation (Fogg et al., 2002; Geetha Kassam et al., 1998; MacLeod et al., 2003). This supports the hypothesis that it is the lysine residue on the C-terminus of S100A10 that is the plasminogen binding site. As shown in Figure 3.9, and consistent with previous data published by the Waisman lab (Fogg et al., 2002), the loss of the carboxyl-terminal lysine residues ($S100A10^{des95,96}$) results in a loss of about 90% of the activity of S100A10. When just one of the last two lysines was deleted, S100A10 lost about 10 % of activity suggesting that the presence of both carboxyl-terminal lysines was not required for activity. Furthermore, the $S100A10^{K95R}$ and $S100A10^{K93I}$ mutants showed an approximate 50% loss in activity suggesting a change in conformation, or a less robust interaction. Since the C-terminus of S100A10 is missing from the X-ray crystal structure (Réty et al., 1999), and the researchers hypothesized that it may have been due to molecular motion, it's possible that altering the C-terminus results in an unstable structure, not able to consistently interact with plasminogen. The substitution of the last and next to last carboxyl-terminal lysines of S100A10 with isoleucine ($S100A10^{K95,96I}$) resulted in only an approximate 10% loss in activity whereas a similar substitution with arginine resulted in an approximate 25% loss in activity. The observation that $S100A10^{K95,96I}$ retained much of its activity was inconsistent with the proposed role of the carboxyl-terminal lysine residue as the only residue responsible for the plasminogen activator activity of S100A10.

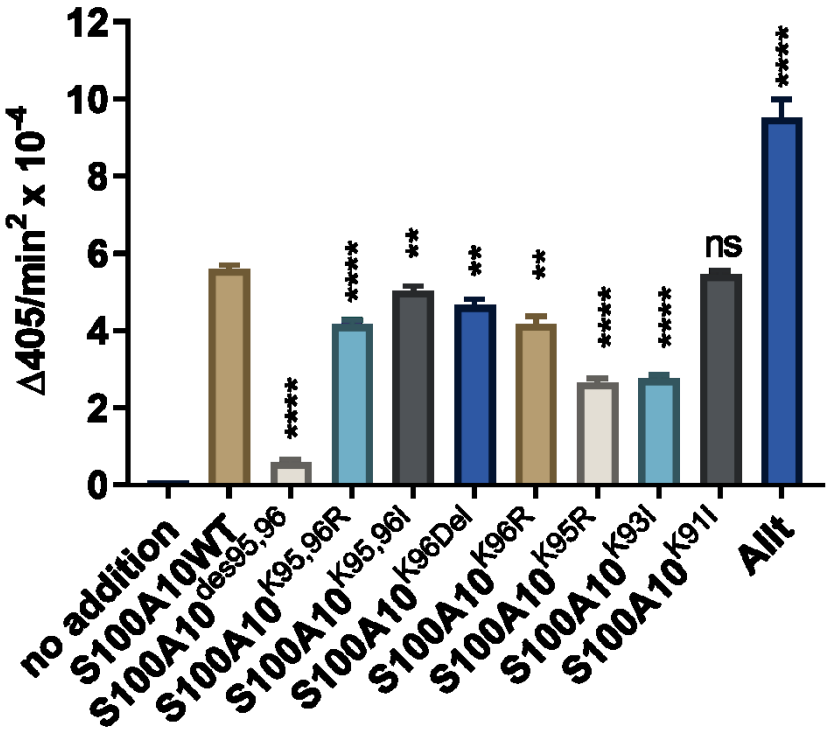

Figure 3-9 Role of the Carboxy-Terminal Domain Lysine Residue in S100A10 Accelerated Plasmin Generation

Plasmin formation was measured at 405 nm using the plasmin-specific substrate S-2251 (0.36 mM) in the presence of 4 nM tPA, 0.15 μM plasminogen, and in the absence or presence of 1 μM carboxyl-domain mutant forms of S100A10. Plasmin formation is expressed as A405 nm/min². The results are the mean ± SD of triplicate measurements, repeated at least three times. Significance refers to rate of each mutant compared to wild type.** $p < 0.01$, **** $p < 0.0001$ (one way ANOVA, Dunnet multiple comparisons test). Reproduced with permission from Miller et al. (2017) Thrombosis and Haemostasis 117, 1058–1071 via Copyright Clearance Center.

If the S100A10K95,96I construct has activity due to a processing event, caused by plasmin cleaving the receptor after a lysine or arginine residue, I would expect there to be a lag in the appearance of plasmin activity. Examination of the raw data of $S100A10^{WT}$, $S100A10^{Des95,96}$ and $S100A10^{K95,96I}$ compared to the no addition rate shows no such delay in the appearance of plasmin (Figure 3.10). Instead, the plot of A405 vs time for $S100A10^{K95,96I}$ is very similar to that of $S100A10^{WT}$.

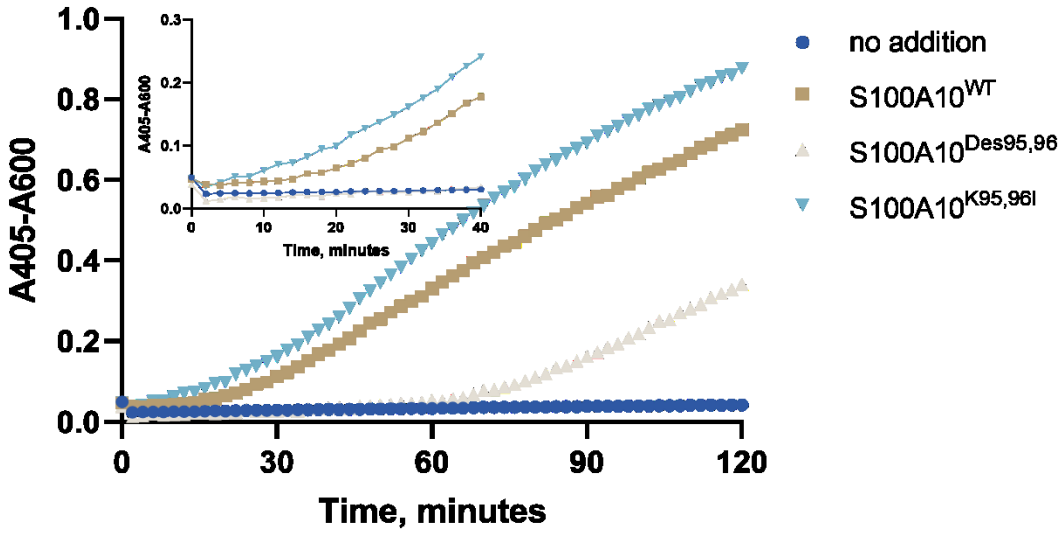

Figure 3-10 Time Course of Plasmin Substrate Cleavage, Effect of Addition of $S100A10^{WT}$, $S100A10^{K95,96I}$ or $S100A10^{Des95,96}$

Raw data of time course of plasmin substrate cleavage, A405-A600 plotted against time in minutes. 0.15 µM plasminogen with 4 nM tPA and 0.36 mM plasmin substrate in the absence or presence of 1 µM $S100A10^{WT}$, $S100A10^{K95,96I}$ or $S100A10^{Des95,96}$ in 50 mM Tris (pH7.4), 50 mM NaCl, 5 mM $CaCl_2$. Inset graph is a close-up of the data points from 0-40 minutes. The $S100A10^{Des95,96}$ is superimposable with the no addition rate during these time points.

3.2.7 SECONDARY STRUCTURE ANALYSIS OF C-TERMINAL REGION MUTANTS

Changes in the α-helical content can be approximated by analyzing the values of the circular dichroism spectra at 208 nm and 222 nm. Analysis of the circular dichroism spectra of the $S100A10^{des95,96}$ protein at 222 nm suggested that the removal of the carboxyl-terminal lysines resulted in only a small loss in the α-helical structure of about 30% (Figure 3.11). However, substituting the carboxyl-terminal lysines with isoleucine had a more profound effect on the conformation of $S100A10^{K95,96I}$, revealing an approximate loss in α-helical content of about 50% (Figure 3.11). Using the on-line CD-spectra analysis tool DiChroWeb (Whitmore and Wallace, 2008, 2004), using the K2d method determined that the $S100A10^{Des95,96}$ mutant had a loss of α-helical content of 29%. $S100A10^{K95,96I}$ had a loss in α-helical content of 39%. This loss of α-helix may result in the exposure of other lysine residues to solvent, revealing possible interaction sites for the plasminogen kringles. The X-ray crystal structure of S100A10 is incomplete, as the final 6 residues are missing from the structure- either the C-terminal region is disordered in the crystal or is missing due to proteolysis (Réty et al., 1999).

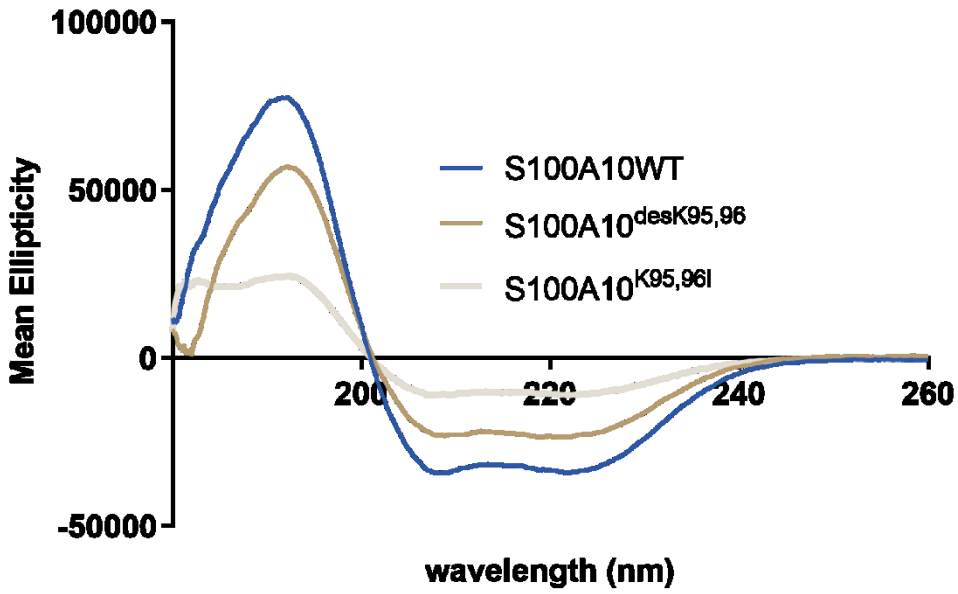

Figure 3-11 Circular Dichroism Spectroscopy of S100A10 C-Terminal Mutants

CD wavelength scans were conducted at 20 °C in the presence of 2.2 µM $S100A10^{WT}$, $S100A10^{Des95,96}$ or $S100A10^{K95,96I}$ and in buffer consisting of 10 mM phosphate, (pH 7.5), 0.15 M NaCl. The data is presented as the mean residue ellipticity. The experiment was repeated three times and representative traces of five averaged scans are presented. Reproduced with permission from Miller et al. (2017) Thrombosis and Haemostasis 117, 1058–1071 via Copyright Clearance Center.

3.2.8 TERTIARY STRUCTURE STUDY OF C-TERMINAL REGION MUTANTS

Since the denaturation of certain proteins can increase their ability to bind plasminogen (Galántai et al., 2006; Machovich and Owen, 1997), the possibility that the deletion or substitution of the carboxyl-terminal lysine of S100A10 resulted in denaturation of the molecule was also examined. This was unlikely since all mutants of S100A10 displayed identical behaviour in size exclusion chromatography, the final step in the purification of these proteins (Table 3.1).

Table 3-1 Size Exclusion Chromatography Ratios For C-terminal Lysine Mutations
The difference between means is not significant via Student t-test.

	Ratio of Elution Volume/Void Volume	
Protein Identity	Mean (n=3)	Standard Deviation
$S100A10^{WT}$	1.35	0.01
$S100A10^{Des95,96}$	1.36	0.01
$S100A10^{K95,96I}$	1.35	0.01

3.2.9 RESULTS OF INTRINSIC/TRYPTOPHAN FLUORESCENCE

The ability of the site-directed mutants of S100A10 to induce conformational changes in plasminogen was examined by measuring the intrinsic tryptophan fluorescence of Glu-plasminogen and Lys-plasminogen in the presence of S100A10. These spectra were compared to the intrinsic fluorescence spectra of Glu-plasminogen in the presence and absence of the lysine analogue, ε-aminocaproic acid (ε-ACA or 6-AH). The intrinsic fluorescence emission of plasminogen is the result of the many tryptophan residues contained in the primary sequence (Eftink, 2000; Lakowicz, 2006, chap. 16). The individual isolated kringles 1, 2, 4 and 5 bind ε-ACA which causes changes in their fluorescence emission (Kornblatt et al., 2007, 2001). As reported, the binding of ε-ACA caused an increase in the tryptophan emission of Glu-plasminogen (Figure 3.12A). It was also observed that WT S100A10, which does not contain tryptophan, caused a small but insignificant increase in the intrinsic fluorescence of plasminogen (Figure 3.12B, Figure 3.13). Interestingly, S100A10^{K95,96I} and S100A10^{des95,96} did not increase the intrinsic fluorescence of Glu-plasminogen. Furthermore, WT S100A10 did not increase the intrinsic fluorescence of Lys-plasminogen (Figure 3.13) indicating the binding of S100A10 to Lys-plasminogen causes no further relation of the plasminogen molecule.

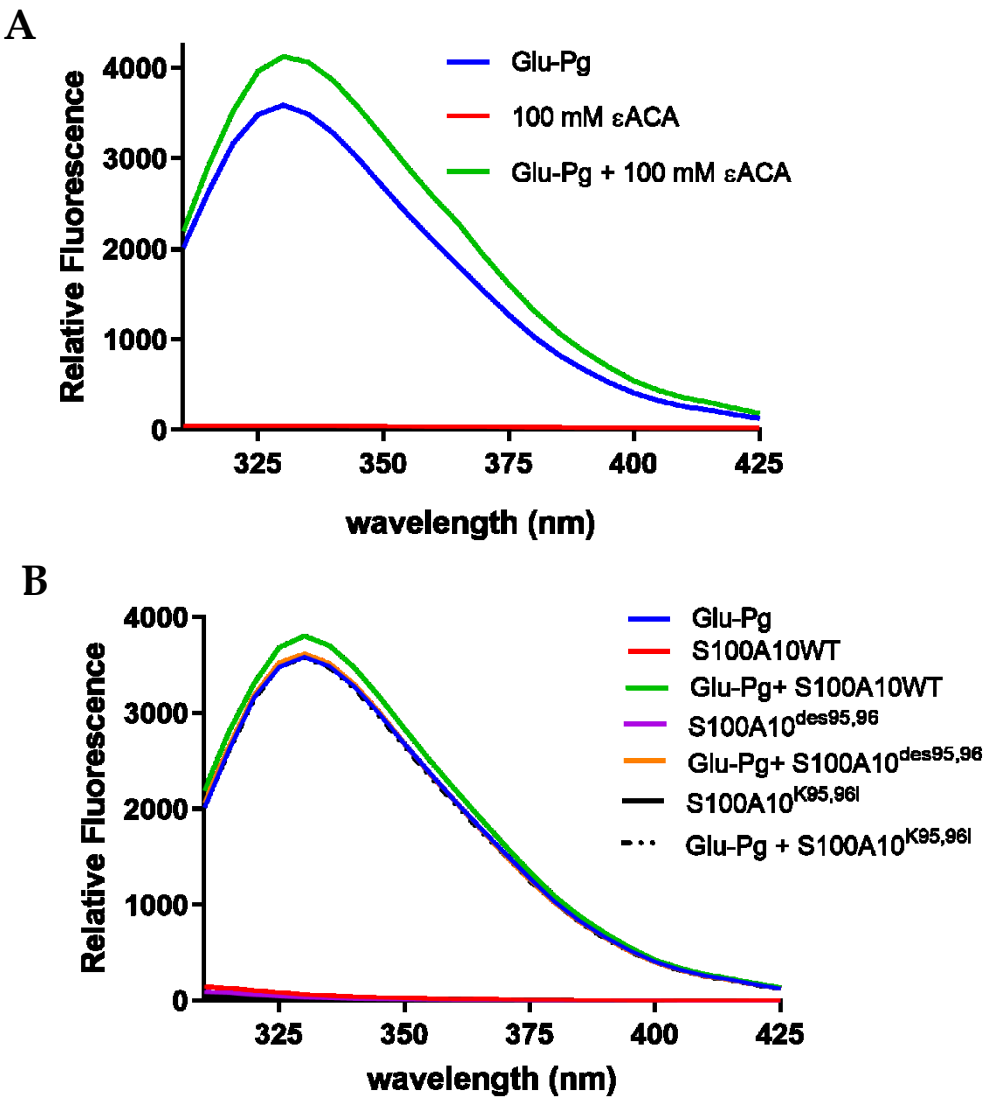

Figure 3-12 Intrinsic Fluorescence Effect of S100A10

The intrinsic protein fluorescence of Glu-plasminogen (1 μM), in the absence or presence of 100mM εACA (A). The intrinsic protein fluorescence of Glu-plasminogen (1 μM), in the absence or presence of 1 μM WT S100A10, S100A10^{des95,96} or S100A10^{K95,96I} (B). The results are the mean ± SD of triplicate measurements, repeated at least three times. Reproduced with permission from Miller et al. (2017) Thrombosis and Haemostasis 117, 1058–1071 via Copyright Clearance Center.

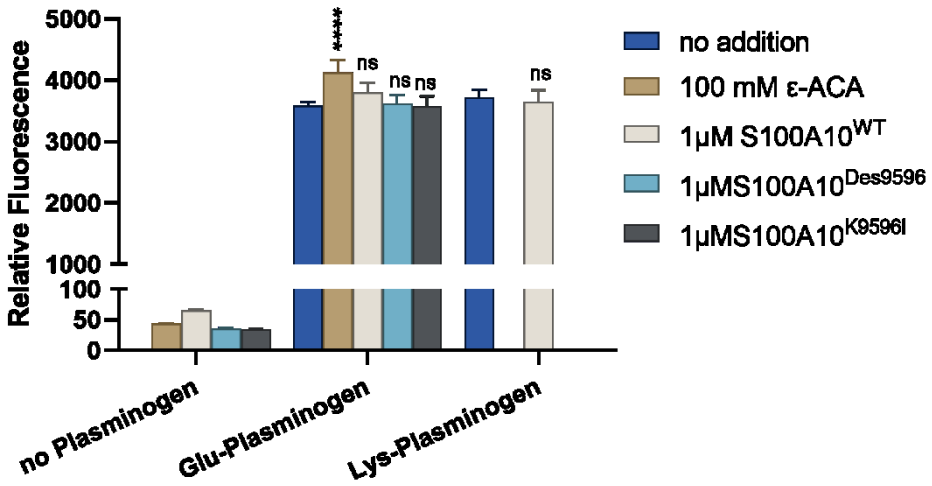

Figure 3-13 Mean Peak Intrinsic Fluorescence of Glu- or Lys-Plasminogen, S100A10, S100A10 mutants and Combinations

Plasminogen (1 μM), S100A10 (1 μM) or both were incubated in 0.2 ml PBS (pH 7.4), excited at 280 nm and the intrinsic fluorescence emission spectra were measured from 310–450 nm using a SpectraMax M3. The relative fluorescence at the peak (330 nm) is compared. The results are the mean ± SD of triplicate measurements, repeated at least three times.

3.2.10 Results of Titration of Assay Parameters on the Ability of S10A10K95,96I to Accelerate Plasmin Generation

The dose-dependency tPA-dependent plasminogen activation by WT S100A10 was compared with the $S100A10^{K95,96I}$ and $S100A10^{Des95,96}$ mutants (Figure 3.14). At lower doses of tPA, the $S100A10^{Des95,96}$ mutant retained about 10% of the activity of WT tPA which increased to about 70% at higher doses. In contrast, the $S100A10^{K95,96I}$ mutant retained about 70% of the activity of WT S100A10 over the range of tPA examined. Similarly, the $S100A10^{K95,96I}$ mutant retained about 60% of its activity over a wide range of plasminogen concentrations (Figure 3.15) though at higher concentrations of plasminogen the effect is lost, indicating a possible change in the kinetic parameters of the reaction. The observation that only the loss, not the substitution, of the carboxyl-terminal lysines of S100A10, exhibited a consistent loss of activity, presented the possibility that the carboxyl-terminal lysine was not solely responsible for the plasminogen activation activity of S100A10, especially at low, rate-limiting plasminogen concentrations. If the $S100A10^{K95,96I}$ mutant utilized an internal lysine for the acceleration of tPA-dependent plasminogen activation then its activity should be blocked by ε-ACA. As shown in Figure 3.16, the activity of the $S100A10^{K95,96I}$ mutant was blocked by ε-ACA. The addition of increasing amounts of ε-ACA increasingly interferes with the generation of plasmin for both WT and $S100A10^{K95,96I}$. The addition of ε-ACA does not affect the ability of $S100A10^{Des95,96}$ to accelerate plasmin generation. $S100A10^{K95,96I}$ is not as affected by ε-ACA, as it is possible that this S100A10 mutant is interacting with more than one plasminogen kringle or a different plasminogen kringle than the wild type, so a different ε-ACA concentration may be required to have the same effect as each kringle has its own affinity for ε-ACA. We also could not rule out the possibility that plasmin generated during S100A10-accelerated reaction resulted in the cleavage of S100A10. Therefore, the possibility of the generation of new C-terminal lysine residues by cleavage of S100A10 was

examined by SDS-PAGE. No proteolysis of WT or mutant S100A10 proteolysis was observed under these conditions (Figure 3.17).

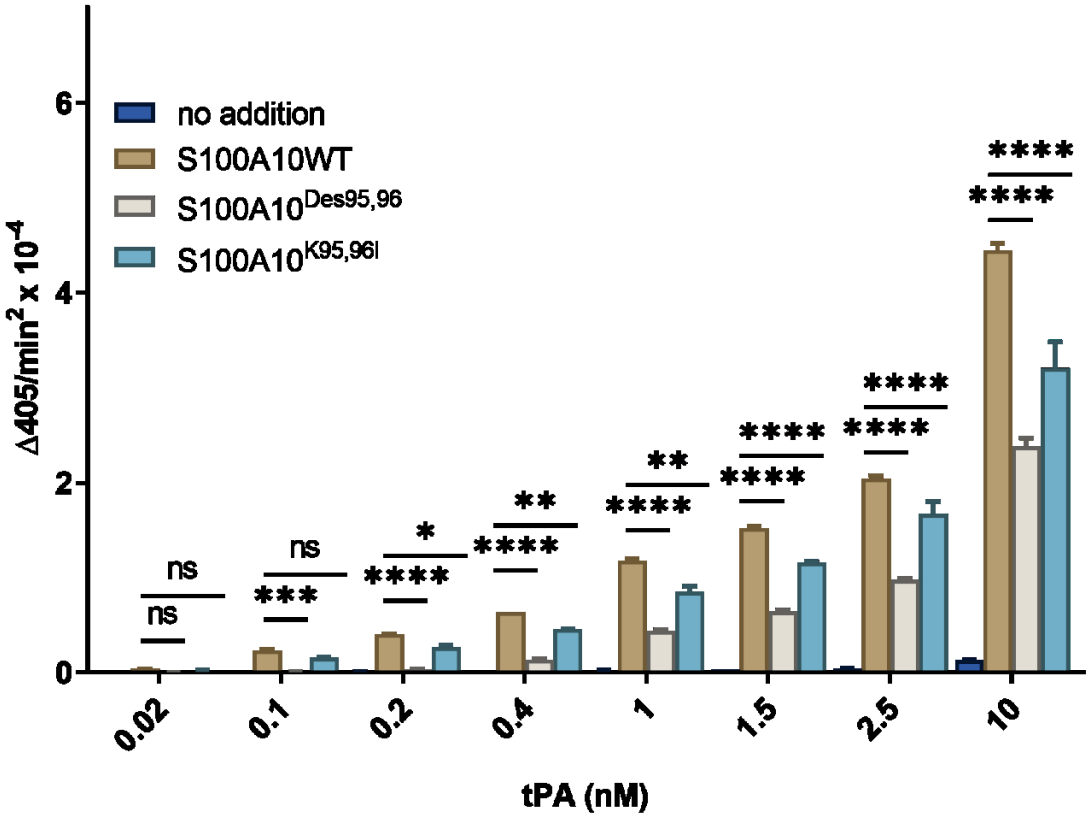

Figure 3-14 Effect of Increasing tPA Concentration on the Ability of S100A10WT and Mutants to Accelerate Plasmin Activity

Plasminogen (0.15μM) was incubated in the presence of variable concentrations of tPA and the plasmin-specific substrate S-2251 (0.36 mM) in 50 mM Tris pH 7.4, 50 mM NaCl and 5 mM $CaCl_2$. Plasmin activity was measured at 405 nm and in the absence (no addition) or presence of $S100A10^{WT}$, $S100A10^{Des95,96}$ or $S100A10^{K95,96I}$ (1 μM).

The results are the mean ± SD of triplicate measurements, repeated at least three times. * $p < 0.05$, ** $p < 0.01$, *** $p < 0.001$, **** $p < 0.0001$ (two-way ANOVA, Tukey multiple comparisons test). Reproduced with permission from Miller et al. (2017) Thrombosis and Haemostasis 117, 1058–1071 via Copyright Clearance Center.

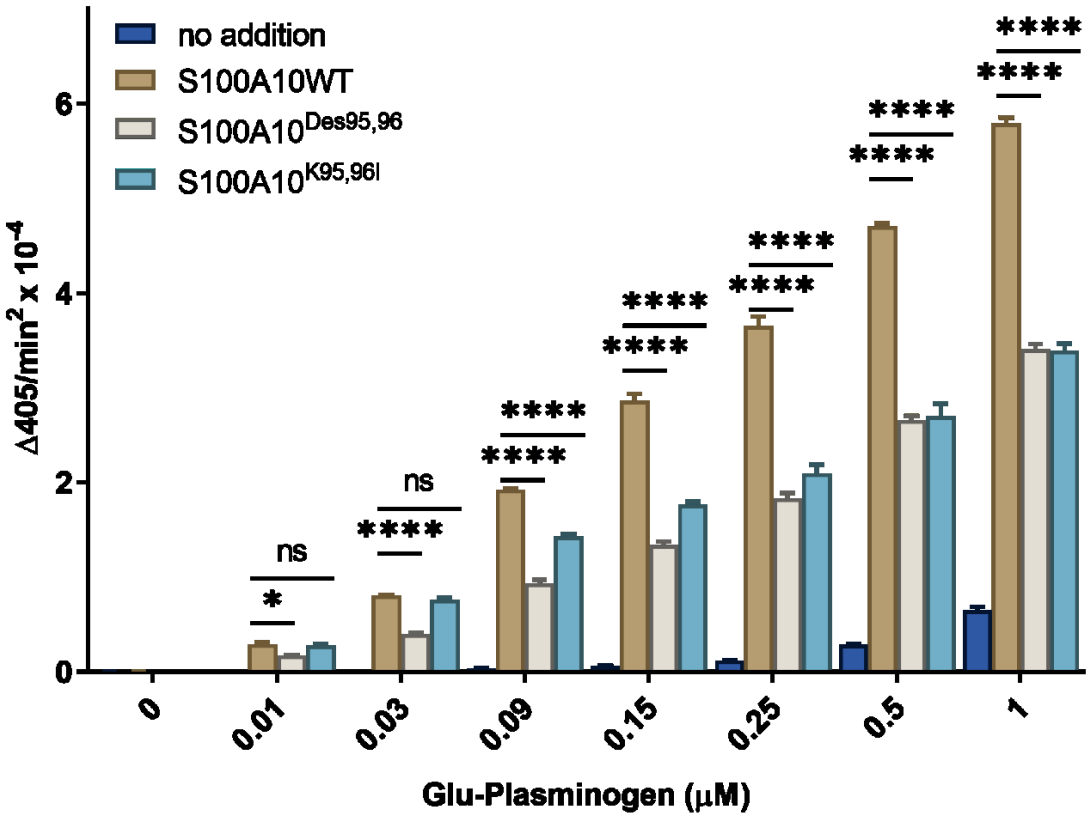

Figure 3-15 Effect of Increasing Plasminogen Concentration on the Ability of S100A10WT and Mutants to Accelerate Plasmin Activity

$S100A10^{WT}$, $S100A10^{Des95,96}$ or $S100A10^{K95,96I}$ (1 μM) was incubated in 50 mM Tris pH 7.4, 50 mM NaCl and 5 mM $CaCl_2$ and the plasmin-specific substrate S-2251 (0.36 mM). Plasmin activity was measured at 405 nm and in the absence (no addition) or presence of each S100A10 variant in the presence of variable concentrations of Glu-plasminogen with a constant concentration of tPA of 4 nM.

The results are the mean ± SD of triplicate measurements, repeated at least three times. * $p < 0.05$, ** $p < 0.01$, *** $p < 0.001$, **** $p < 0.0001$ (two-way ANOVA, Tukey multiple comparisons test). Reproduced with permission from Miller et al. (2017) Thrombosis and Haemostasis 117, 1058–1071 via Copyright Clearance Center.

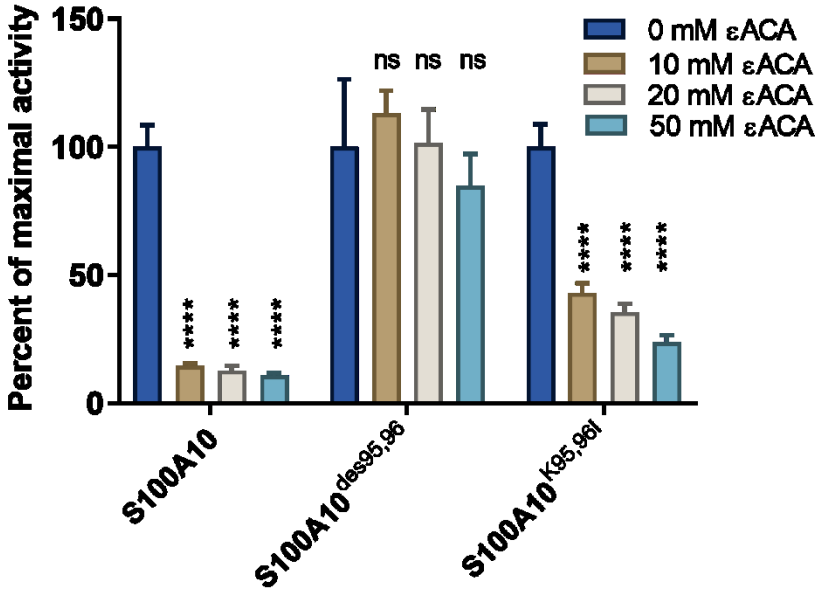

Figure 3-16 Interaction of Plasminogen with $S100A10^{K95,96I}$, Like $S100A10^{WT}$, is Lysine-Specific and Inhibited by ε-ACA

Plasminogen (0.15μM) was incubated in the absence or presence of 10, 20 or 50mM ε-ACA with 4nM tPA and the plasmin-specific substrate S-2251 (0.36 mM) and 1 μM $S100A10^{WT}$, $S100A10^{Des95,96}$ or $S100A10^{K95,96I}$ in 50 mM Tris pH 7.4, 50 mM NaCl and 5 mM $CaCl_2$. Plasmin activity was measured at 405 nm.

Data are presented as a percentage of maximum activity, not as an absolute activity. Two-way ANOVA, Tukey's multiple comparison test, **** $p < 0.0001$ Reproduced with permission from Miller et al. (2017) Thrombosis and Haemostasis 117, 1058–1071 via Copyright Clearance Center.

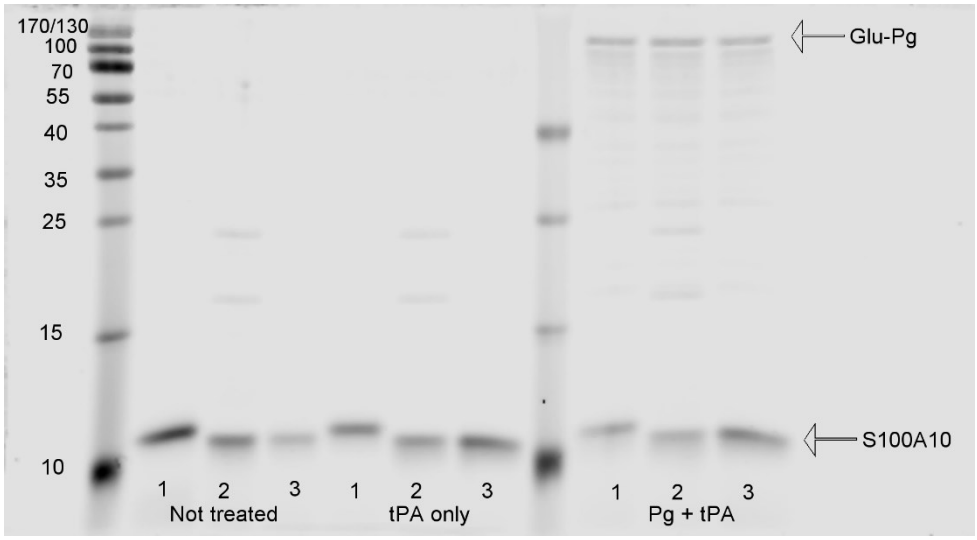

Figure 3-17 Examination of S100A10 Proteins for Evidence of Proteolysis After Exposure to Plasminogen and tPA

SDS-PAGE analysis of $S100A10^{WT}$ (1), $S100A10^{Des95,96}$ (2) and $S100A10^{K95,96I}$ (3), not treated, after treatment with tPA only or after treatment with plasminogen and tPA. Each S100A10 was exposed to the treatment for 20 minutes, the reaction stopped, then applied to a 15% acrylamide gel. Gel was stained for total protein using Coomassie Blue stain and destained until background was clear. Image was processed using Image Studio Lite (Licor). Reproduced with permission from Miller et al. (2017) Thrombosis and Haemostasis 117, 1058–1071 via Copyright Clearance Center..

3.3 Interaction of S100A10, Plasminogen and Tissue Plasminogen Activator- Internal Lysine Residues of S100A10

3.3.1 Expression and Purification of S100A10 Internal Lysine Mutants

The internal lysine mutants of S100A10 were all expressed using the same protocol as for wild type S100A10. Some of the mutant constructs are shown in an SDS-PAGE in Figure 3.18. Each of the mutants, except for $S100A10^{K56R/K95,96I}$, was purified using the same protocol as for wild type S100A10. $S100A10^{K56R/K95,96I}$ required a lower ammonium sulphate concentration (25% saturated), as it precipitated out at 50% saturated ammonium sulphate. This indicates a possible change in the overall hydrophobicity and/or conformation of this particular mutant.

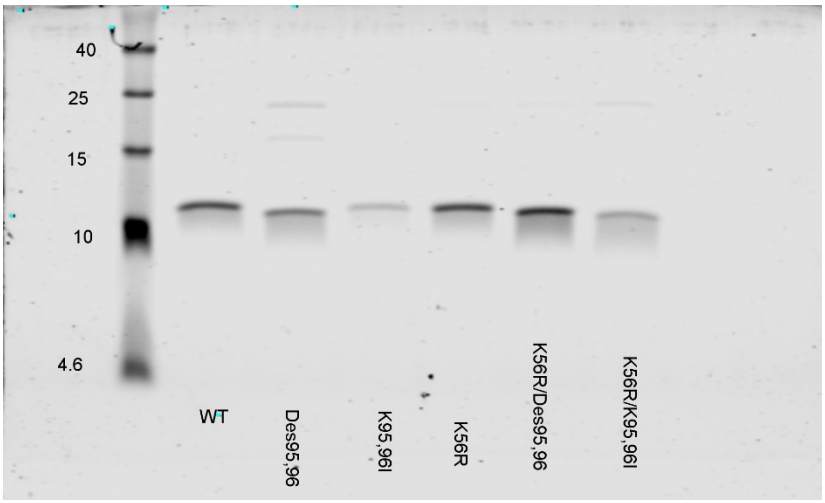

Figure 3-18 SDS-PAGE of S100A10^{WT} and Selected Mutants

One μg of S100A10 or mutant was subjected to SDS-PAGE on a 20% gel. The gel was exposed to ehe ectric current until the dye fron reached the bottom of the gel. The gel was stained with Coomassie Brilliant Blue in 30% methanol, 10% acetic acid, then destained in 30% methanol, 10% acetic acid until the background was clear. The image was obtained using a Licor Odyssey Imaging Scanner and processed with Image Suite Lite software.

3.3.2 THE ROLE OF INTERNAL LYSINE RESIDUES IN S100A10-ACCELERATED PLASMIN GENERATION

Substitution of lysine at positions, 46, 53, 56 and 65 did not affect the acceleration of plasmin generation by tPA-dependent activation of plasminogen (Figure 3.19). Since the lysine at residue 56 (human amino acid sequence) is conserved over many species (labelled as residue 62 in Figure 1.8), it is a strong candidate to be a secondary site. To explore this possibility, lysine to arginine substitution was made to S100A10^{K95,96I} as well as S100A10^{Des95,96}, producing S100A10$^{K56R/K95,96I}$ and S100A10$^{K56R/Des95,96}$ respectively. As noted in Section 3.3.1, purification of the S100A10$^{K56R/K95,96I}$ mutant required alteration of the purification protocol. A lower ammonium sulphate concentration was required to keep this mutant in solution. The ability of S100A10$^{K56R/K95,96I}$ to influence the acceleration of plasmin generation was markedly decreased compared to S100A10^{K95,96I}. (Figure 3.20) The activity of this double mutated S100A10 had a very similar plasmin generation activity to S100A10^{Des95,96}.

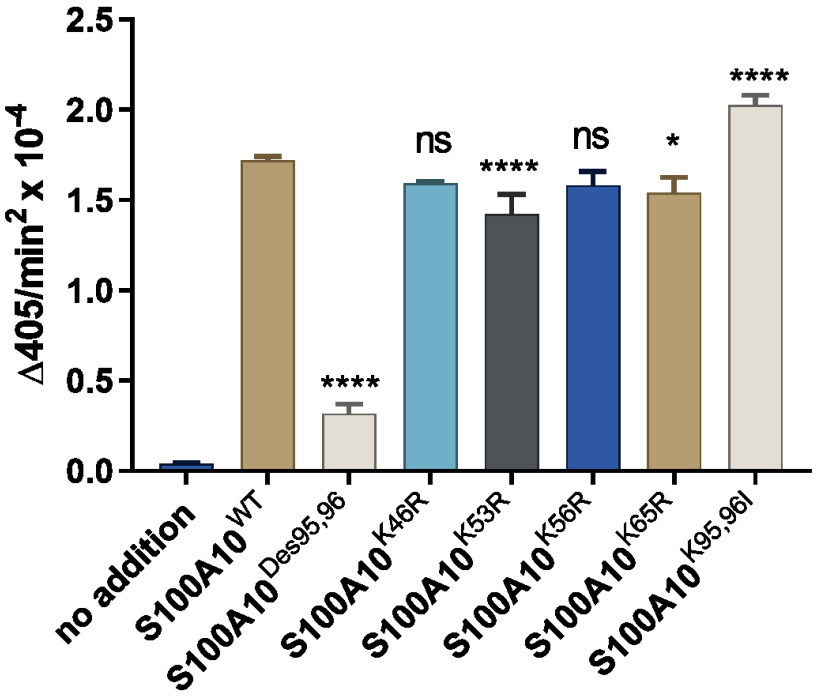

Figure 3-19 Effect of Internal Lysine Mutations on Plasmin Activity

Plasmin activity was measured at 405 nm using the plasmin-specific substrate S-2251 (0.36 mM) in the presence of 0.1 nM tPA, 0.15 µM plasminogen, and in the absence or presence of 1 µM internal mutant forms of S100A10. Plasmin activity is expressed as A405 nm/min^2. The results are the mean ± SD of triplicate measurements, repeated at least three times. Significance with respect to S100A10^{WT} is noted ** $p < 0.01$, **** $p < 0.0001$ (one-way ANOVA), Dunnet multiple comparisons test).

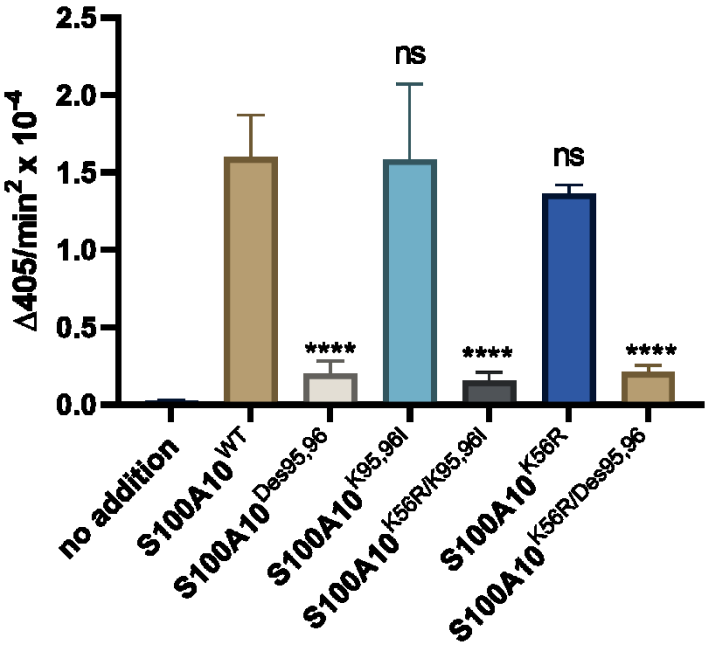

Figure 3-20 Mutating an Internal Lysine of the S100A10^{K95,96I} Mutant Results in Substantial Loss of Plasmin Activity

Plasmin activity was measured at 405 nm using the plasmin-specific substrate S-2251 (0.36 mM) in the presence of 0.1 nM tPA, 0.15 µM plasminogen, and in the absence or presence of 1 µM mutant forms of S100A10 as noted. Plasmin formation is expressed as A405 nm/min^2. The results are the mean ± SD of triplicate measurements, repeated at least three times. Significance with respect to S100A10^{WT} is noted, **** $p < 0.0001$ (one-way ANOVA, Dunnet multiple comparisons test).

3.3.3 CARBOXYPEPTIDASE TREATMENT OF MUTANTS

To determine susceptible to C-terminal cleavage by carboxypeptidase, WT and mutant S100A10 were treated with carboxypeptidase B1 (CpB1)(Worthington Biochemicals) for 30 minutes. The only S100A10 mutant constructs that were expected to be affected by the carboxypeptidase activity are those that contain a C-terminal lysine residue. These altered proteins were then examined for plasmin generation acceleration. Unexpectedly the $S100A10^{K95,96I}$ mutant also lost activity, similar to the wild type protein. The $S100A10^{K95,96I}$ mutant was re-checked for sequence, confirmed and re-expressed and the same change in activity was observed in a subsequent batch. Additionally, the CpB1-specific inhibitor (Plummer's Reagent, Calbiochem) was added prior to the addition of the CpB1, which prevented the loss of plasmin generation (Figure 3.21) indicating the change in the activity of the $S100A10^{WT}$ & $S100A10^{K95,96I}$ was due to the activity of CpB1. The loss of activity of the $S100A10^{K95,96I}$ might be due to a change in conformation that renders this mutant susceptible to carboxypeptidase activity.

Examination of the CpB1-treated S100A10WT and S100A10K95,96I revealed a decrease in the apparent molecular weight after treatment with CpB1 compared to the not treated, the protein held at 37°C, or the sample where the carboxypeptidase inhibitor, Plummer's reagent was added before CpB1 (Figure 3.22).

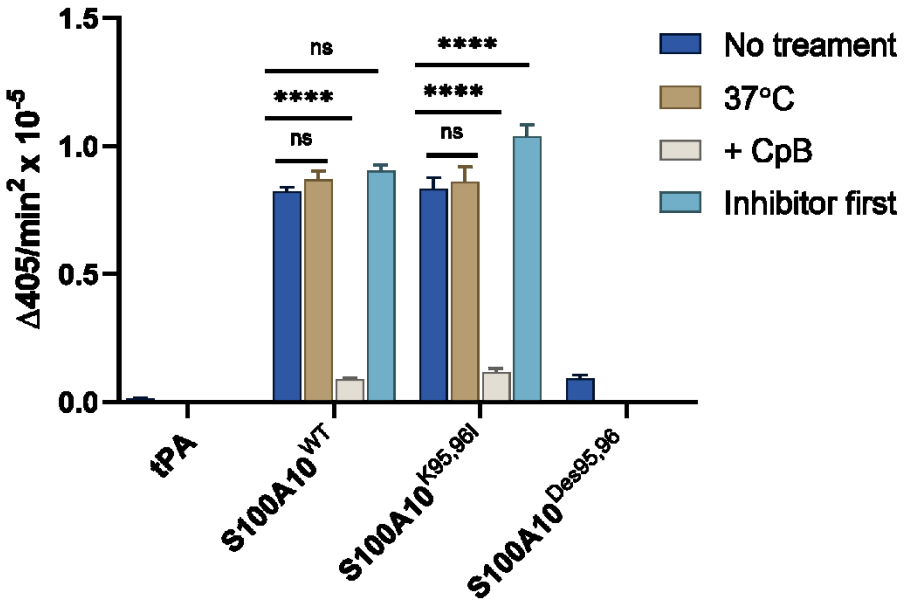

Figure 3-21 Carboxypeptidase Treatment of S100A10 and Selected Mutants

Plasmin activity was measured at 405 nm using the plasmin-specific substrate S-2251 (0.36 mM) in the presence of 0.1 nM tPA, 0.15 µM plasminogen, and in the absence or presence of 1 µM WT and mutant S100A10 as indicated. Prior to assay, S100A10 proteins were not treated (NT), held at 37°C for 30 min (37) or treated with CpB (1µM CpB1 to 380 µM S100A10) for 30 min (CpB) or had 10 µM Plummer's inhibitor added prior to the addito of CpB1. The samples marked 37 and CpB had 10 µM Plummer's inhibitor added after 30 minutes. Plasmin formation is expressed as A405 nm/min^2. The results are the mean ± SD of triplicate measurements, repeated at least three times. ** $p < 0.01$, **** $p < 0.0001$ (one-way ANOVA, Dunnet multiple comparison test.

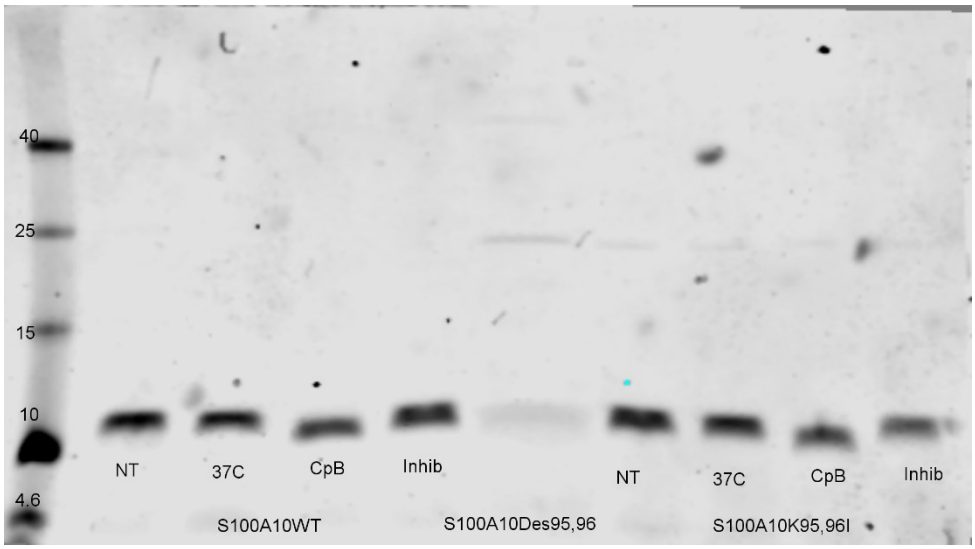

Figure 3-22 SDS-PAGE Examination of Product of CpB1 Activity on $S100A10^{WT}$ and $S100A10^{K95,96I}$

Approximately 1µg of S100A10WT or S100A10K95,96I, treated as follows: not treated, held at 37C for 30 minutes, treated with 1 µmole CpB to 340 µmole S100A10, or 10 µM Plummer's reagent added prior to addition of CpB. S100A10Des95,96 was used as a molecular weight standard. The proteins were subjected to SDS-PAGE on a 15% gel, stained with Coomassie Brilliant Blue Stain in 30%(v/v) methanol, 10% (v/v) acetic acid, then destained in 30% (v/v) methanol, 10% (v/v) acetic acid until the back ground was clear. Image captured with Licor Odyssey imaging system.

3.3.4 SECONDARY STRUCTURE STUDY OF S100A10

The CD spectra for $S100A10^{WT}$, $S100A10^{Des95,96}$, $S100A10^{K95,96I}$, $S100A10^{K56R}$, $S100A10^{K56R/Des95,96}$ and $S100A10^{K56R/K95,96I}$ were determined using circular dichroism spectroscopy as outlined in section 2.1.9. Examining the α-helical content of the 5 mutants and the wild type protein, using the on-line analysis program of DiChroWeb (Whitmore and Wallace, 2008, 2004), using the K2d method determined that the $S100A10^{Des95,96}$ mutant had a gain of α-helical content of 13%. $S100A10^{K95,96I}$ had a loss in α-helical content of 10%. Comparing the α-helical content of the $S100A10^{Des95,96}$, $S100A10^{K95,96I}$ to the values obtained earlier, shows very similar results. The α-helical content of S100A10WT is different between experiments. Adding the K56R mutation to each resulted in very small changes in the DiChroWeb's analysis of α-helical content of 1 or 2%. There is a difference in the buffers used each time, but this is not expected to cause such a change in the wild type protein (Figure 3.23).

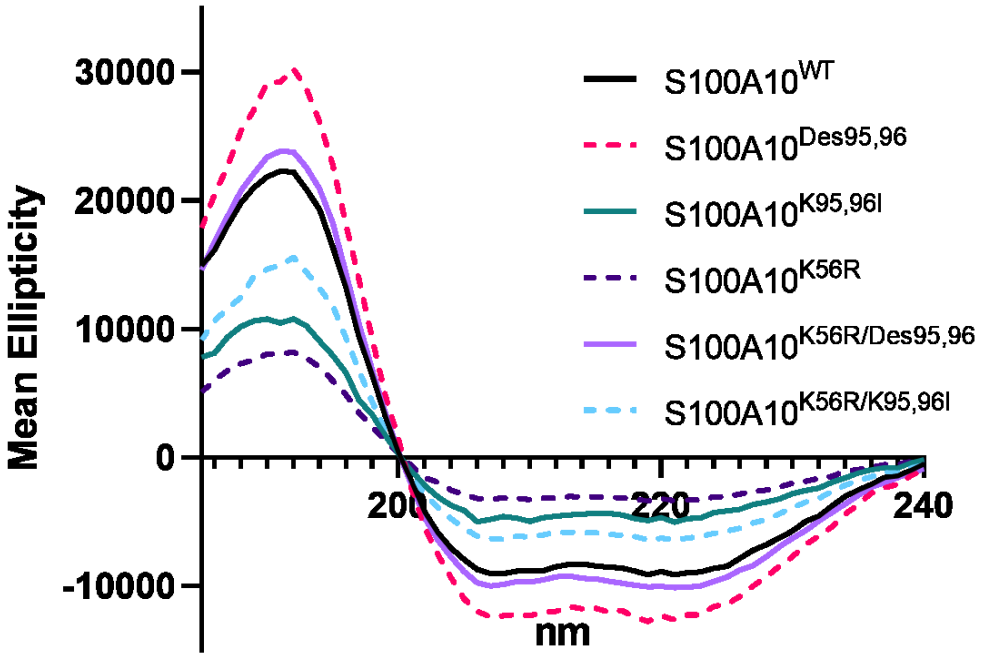

Figure 3-23 Circular Dichroism Spectra of S100A10 Mutants

CD wavelength scans were conducted at 20 °C in the presence of 2.2 µM S100A10WT, S100A10^{Des95,96,} S100A10^{K95,96I}, S100A10^{K56R}, S100A10$^{K56R/Des95,96}$ or S100A10K56R/^{K95,9I6} and in buffer consisting of 20 mM phosphate, pH7. 4. The data is presented as the mean residue ellipticity. The experiment was repeated three times and representative traces of five averaged scans are presented. The Mean Ellipticity presented is not corrected for protein content in this image.

3.3.5 TERTIARY (QUATERNARY)STRUCTURE STUDY OF S100A10

Analysis of the tertiary structure of the $S100A10^{K56R/K95,96I}$ mutant by size exclusion chromatography revealed a significant difference in the ratio of the column void volume to the eluted protein (Table 3.2). The peaks appeared superimposable but the ratio indicated a difference between the $S100A10^{WT}$ and $S100A10^{K56R/K95,96I}$. mutant behaved differently on the column. This is due to a subtle difference in hydrophobicity.

Table 3-2 Size Exclusion Chromatography Ratio of $S100A10^{K56R/K95,96I}$ Compared to $S100A10^{WT}$

There is a significant difference in the mobility of $S100A10^{K56R/K95,96I}$ compared to the wild type protein. P = 0.008 two-tailed t-test

	Ratio of Elution Volume/Void Volume	
Protein Identity	Mean (n=3)	Standard Deviation
$S100A10^{WT}$	1.39	0.01
$S100A10^{K56R/K95,96I}$	1.43	0.01

3.3.6 S100A10 IS POSSIBLY CLEAVED BY PLASMIN *IN VITRO*

Over the course of many plasmin generation assays, a shift in the activity for the S100A10^{Des95,96} mutant was noted. At times, the rate was scarcely above that of the no addition reactions, while at other times, after approximately 45 minutes, a much more accelerated rate was noted. This was also noted for the S100A10$^{K56R/Des95,96}$ and S100A10$^{K56R/K95,96I}$ mutants (Figure 3.24). To determine the cause of the delayed acceleration a small study was undertaken to determine if proteolysis of the plasminogen receptor may be responsible. Western blot analysis of the reaction revealed proteolysis of both the WT and S100A10^{Des95,96} mutant after 45 minutes of addition of plasminogen and tPA to the plasminogen receptor (Figure 3.23). The S100A10^{Des95,96} mutant showed a greater proportion of proteolyzed protein than the wild type. Either exposure of a possible new C-terminal lysine residue or the generation of a denatured protein, both known to result in acceleration of plasmin generation, resulted from the proteolysis, observable as an increase in the apparent plasmin generation after 45 minutes. The pattern of proteolysis appears to differ between the WT and S100A10^{Des95,96}.

The emergence of an additional binding site for plasminogen or the contribution of degraded protein is not evident in the wild type reaction, as the rate is already well-established by the time of proteolysis. The initial rate of the S100A10^{Des95,96} mutant is very low, so changes in the protein composition affect the rate to a greater extent. The proteolysis was not detected in earlier experiments, as the reaction was halted after 20 minutes. Additionally, the detection of the proteolyzed protein required the use of the more sensitive western blot.

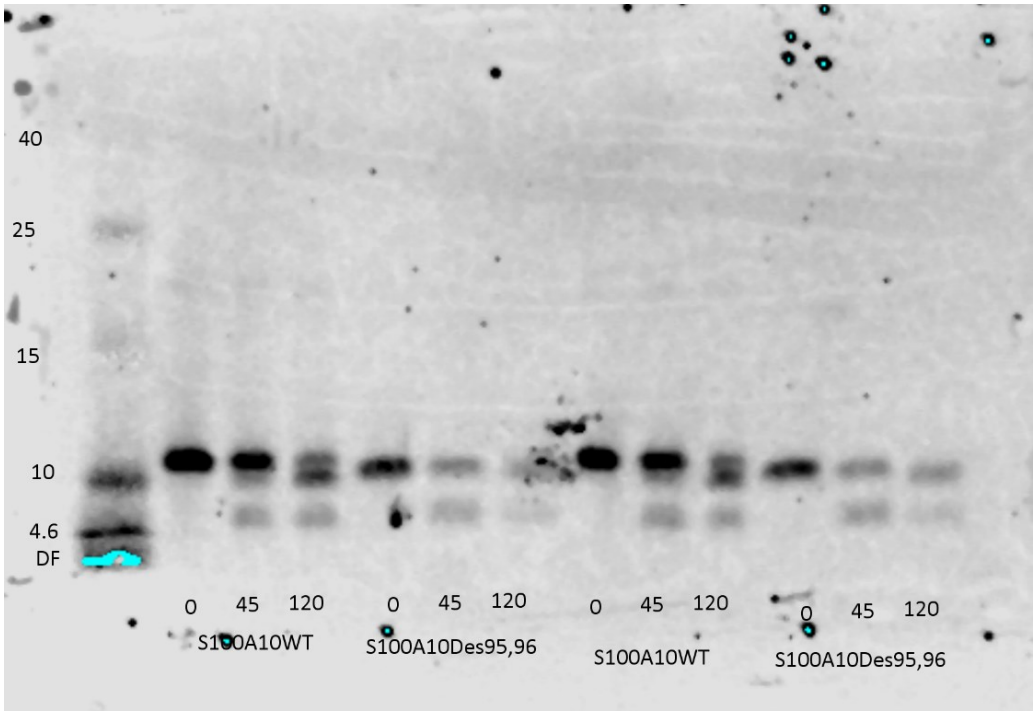

Figure 3-24 S100A10 Can Be Cleaved by Plasmin

Western blot analysis of $S100A10^{WT}$ or $S100A10^{Des95,96}$ after exposure to Plasminogen and tPA for 0, 45 or 120 minutes at the same relative concentrations as in the plasmin generation assay. Reaction mixtures were subjected to SDS-PAGE on a 15% acrylamide gel using the Laemelli buffer system. Separated proteins were then transferred to 0.2 µm nitrocellulose membrane using the Towbin's buffer system. Membranes were blocked in Licor Odyssey Blocking buffer, rinsed with TBS containing 0.5% Tween 20 (TBS-Tw) then probed with a monoclonal antibody to S100A10 (BD; 1/2000 dilution in TBS-Tw, followed by incubation with a Donkey anti-mouse IgG DyLight 800 secondary (Thermo Fisher) 1/15000 in TBS-Tw. The gel was imaged using the Licor Odyssey infrared scanner and processed using Image Studio Lite Software (Licor).

4.1 IN VITRO PROTEOLYSIS OF MYELIN BASIC PROTEIN

Examination of the products of the time-constrained proteolysis of myelin basic protein (MBP) revealed that more extensive proteolysis of MBP occurred in the presence of S100A10, regardless of tPA concentration or pre-incubation (Figure 4.1). The preincubation of plasminogen with tPA ± S100A10 results in plasmin auto-proteolysis, likely accounting for the incomplete degradation of MBP. Due to the many bands resulting from the proteolysis of MBP, in addition to the multiple isoforms present, the amount of proteolysis was defined as the total intensity of all bands below the line indicated. Quantitation of the intact (above the dotted line) and proteolyzed (below the line) protein bands is presented in Figure 4.2.

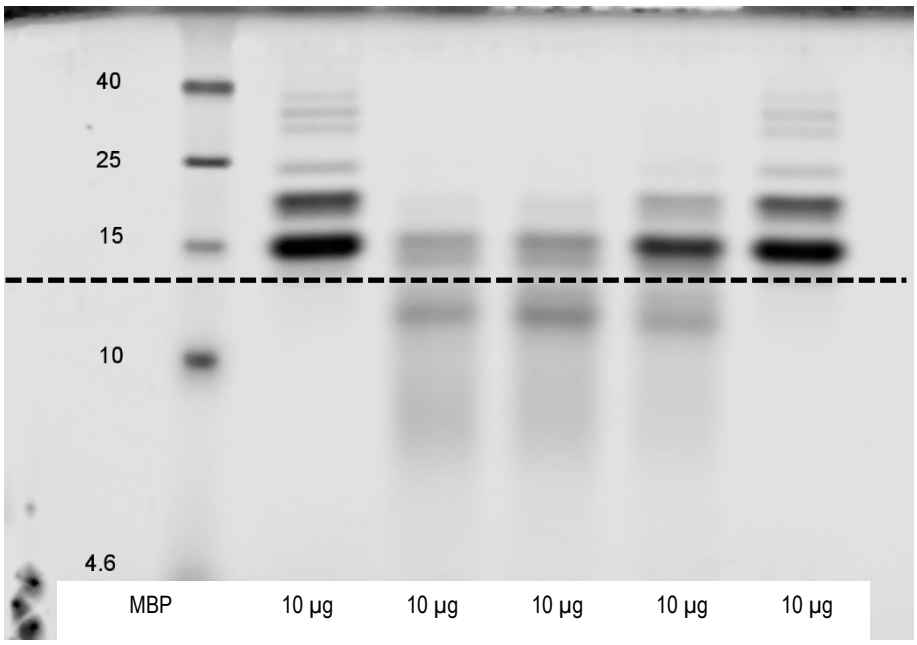

MBP	10 µg	10 µg	10 µg	10 µg	10 µg
Pg	-	30 nM	30 nM	30 nM	30 nM
tPA	-	0.8 nM	0.8 nM	0.8 nM	0.8nM
S100A10	-	-	200 nM	200 nM	-
preincubation	N/A	yes	yes	no	no

Figure 4-1 Proteolysis of Myelin Basic Protein by Plasminogen Activated by tPA in the Presence and Absence of S100A10

Myelin basic protein (10µg) was exposed for 20 minutes to 30 nM plasminogen and 0.8 nM tPA ± 200 nM S100A10, with and without preincubation (20 minutes) of the plasminogen/tPA/S100A10. The preincubation allowed for the formation of plasmin in the absence of MBP. The reaction was halted by the addition of 2X SDS-PAGE loading buffer and boiled for 5 minutes. The entire reaction was loaded onto a 20% acrylamide gel. The proteins were electrophoresed until the dye front reached the end of the gel, then was stained for total proteins with Coomassie Blue R250 and destained until the background was clear. Plasminogen (92kDa) and tPA (68 kDa) do not enter the 20% gel, and S100A10 is not clearly stained as the concentration used is below the level of detection by Coomassie Blue stain. Image was captured on Odyssey™ Imaging system (Licor™) and processed using Image Studio Lite Software (Licor™).

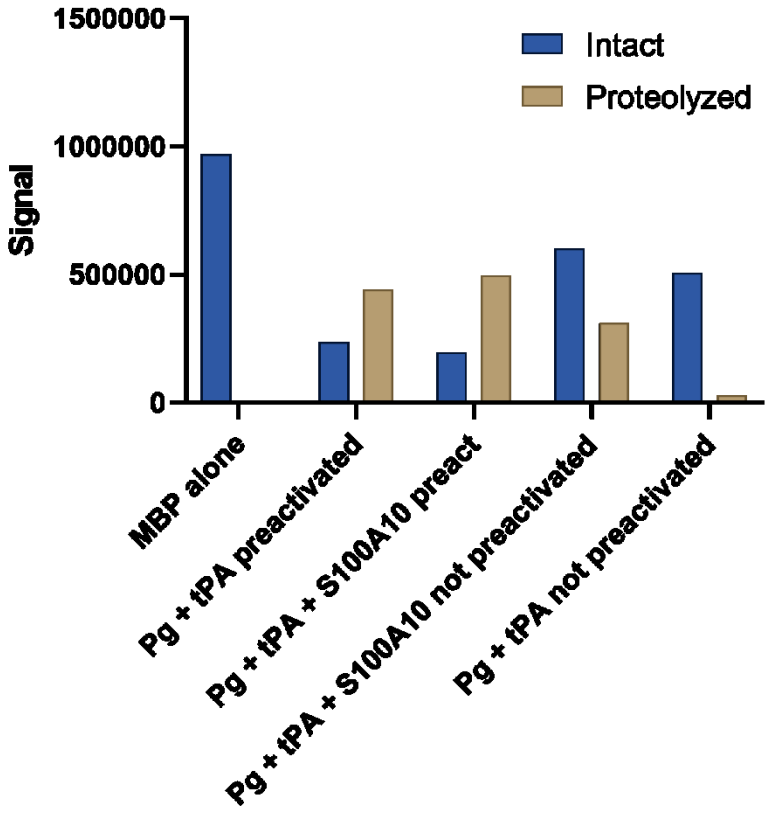

Figure 4-2 Quantitation of Intact and Proteolyzed MBP

Each lane from the gel presented in Figure 4-1 was subjected to quantitation of pixel (number and intensity) either above (intact protein) or below (proteolyzed protein) the dashed line indicated in the Figure. Quantitation was performed using pixel data determined by Image Studio Lite software. Representative experiment, n = 3

4.2 LPC INJECTION RESULTS

The LPC model of demyelination/remyelination is a well-documented model with a reproducible timeline of demyelination and remyelination in C57BL/6 mice. Maximal demyelination occurs 24 hours post-injection of LPC and remyelination occurs over the following 3-28 days (Plemel et al., 2018). This small study was undertaken to begin to understand the role S100A10 may play in the demyelination/remyelination process, with a focus on demyelination. Published data indicated an upregulation of S100A10 within the boundaries of an active lesion, as well as within sub-acute lesions, chronic lesions and in normal-appearing white matter in the MS brain. I chose to focus on the early stages of demyelination/remyelination, to determine if the S100A10 found in active lesions was there to 'help clean up' or if its presence was deleterious. Given that the presence of S100A10 marginally sped up the degradation of MBP by tPA-activated plasmin, the initial hypothesis was that the presence of S100A10 in the MS lesion resulted in a potentially more inflammatory milieu, MBP is degraded due to S100A10's plasmin generating ability.

Published reports of animals receiving LPC injections report that axons are usually not damaged in focal LPC injections (Murphy et al., 2013) limiting the probability that paralysis or other deleterious effects will be observed. As expected, no overt neurological damage was observed in either the wild type or S100A10-null cohorts. Mice were monitored 3 times daily for the first 2 days post-surgery, then daily until sacrifice. No circling behaviour, paralysis or other behaviours indicative of neurological damage was observed. Each group showed full mobility within hours of recovery from surgery, and remained fully mobile until seven days post-treatment, at the point of sacrifice.

4.3 ERIOCHROME CYANINE STAINING RESULTS

Seven days after the LPC treatment, mice were sacrificed. After processing and embedding, brain sections were stained for myelin by eriochrome cyanine and neutral red staining. The lesion area is defined as the absence of blue staining within the corpus callosum. A representative image of a wild type (top panel) and S100A10 null lesion (bottom panel)are presented in Figure 4.3. The average lesion volume was calculated for each of the sectioned brains with sufficient sections for calculation (more than one slide and more than 3 intact sections). The mean lesion volume for wild type was 0.008949 ± 0.002677 mm^3 (n = 5) compared to S100A10 null mice with a mean volume of 0.049366 ± 0.01420 mm^3 (n=9)(Figure 4.4).

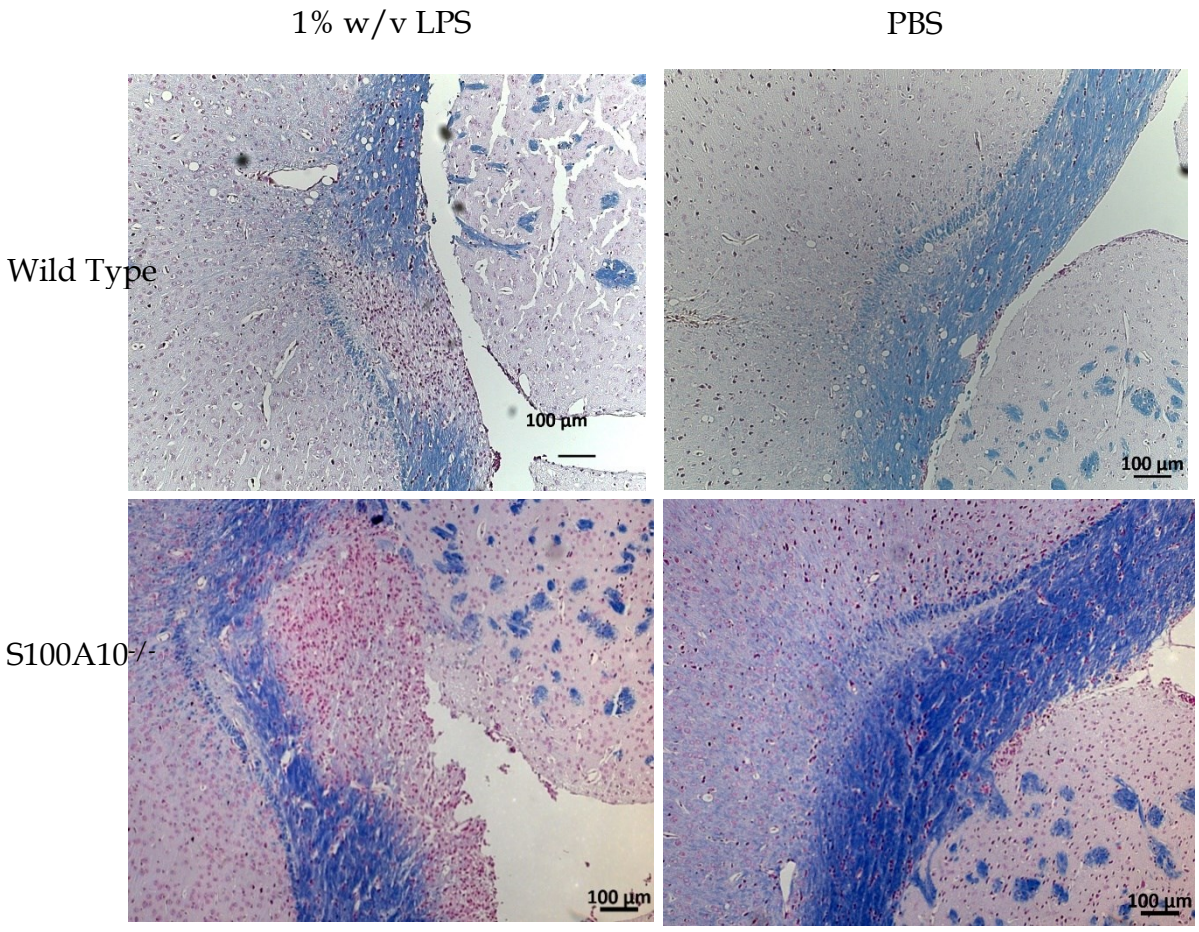

Figure 4-3 Representative Images of LPC-Induced Lesions in Wild Type and S100A10$^{-/-}$ Mice

Lesion 7 days post-injection of 1 µL 1% (w/v) lysophosphatidylcholine or the swame volume of PBS. Eriochrome cyanine with neutral red as a counterstain. Myelin is blue, cell nuclei are red. Scale bar is 100 µm.

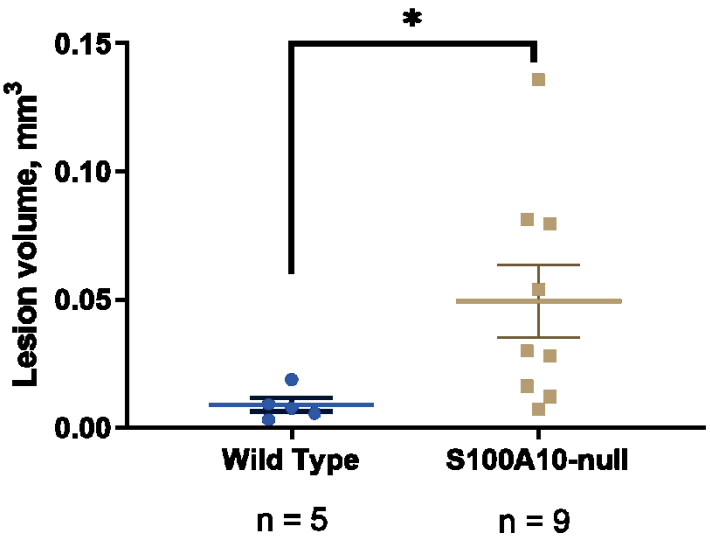

Figure 4-4 Analysis of Lesion Volume 7 Days Post-Injection of Lysophosphatidylcholine

Lesion volume of wild type and S100A10-null mice 7 days post-injection of 1µL 1% lysophosphatidylcholine. Every fifth slide was stained with eriochrome cyanine and counter stained with neutral red. The area of each lesion observed in contiguous slides was measured using imaging software Fiji. The resulting volume was extrapolated by plotting the area against accumulated section thickness and the area under the curve calculated. Data presented as mean ± SEM, unpaired t-test with Welch's correction. * $p = 0.022$.

4.4 IMMUNOFLUORESCENCE RESULTS

The unexpected finding that S100A10-null mice had larger lesion volume at day 7 prompted an analysis of both the astrocyte and microglia content in the mice. A slide from the lesioned area was selected from each of the available samples for double staining with Ionized Calcium Binding Adaptor Molecule 1 (Iba-1) to examine microglia and glial fibrillary acidic protein (GFAP) to detect astrocytes. The total fluorescence in each was quantified at either 5X or 10X magnification. If the lesion was discernible in the image, the fluorescence within this area was averaged over the lesion area. A representative image of a WT animal is shown alongside a representative image from an S100A10-null animal (Figure 4.5). Wild type is on the left, S100A10-null on the right. Merged image of panel B is Top row is Iba-1(microglia) in lesion and surrounding, middle row is lesion-vicinity GFAP (astrocytes), while the bottom row is the merged image along with DAPI for cell nuclei.

Total field fluorescence for both astrocytes and microglia was quantitated in each field of view. Aggregate data for the PBS injected and LPC injected corpus callosum imaged fields are presented in Figure 4.6 for astrocytes and Figure 4.7 for microglia. There was no significant difference in the total fluorescence between the PBS injected or LPC injected areas. Additionally, there was no significant difference between the total fluorescence of the wild type and S100A10-null animals. The S100A10-null animals have a trend toward more GFAP and Iba-1 staining, suggesting that these animals could experience more or longer-lasting inflammation.

However, there does appear to be a trend of fewer microglia within the lesion of the S100A10-null mice as presented in Figure 4.8. This suggests the possibility that there may be a difference in the activity level of the microglia, especially its ability to utilize the plasminogen activation system to degrade the extra-cellular matrix to move to sites of inflammation and damage. Further study to determine if the

Iba-1 stained cells are represented solely by microglia cells or if any peripheral macrophages present will aid in determining the role S100A10 plays in the migration of microglial cells

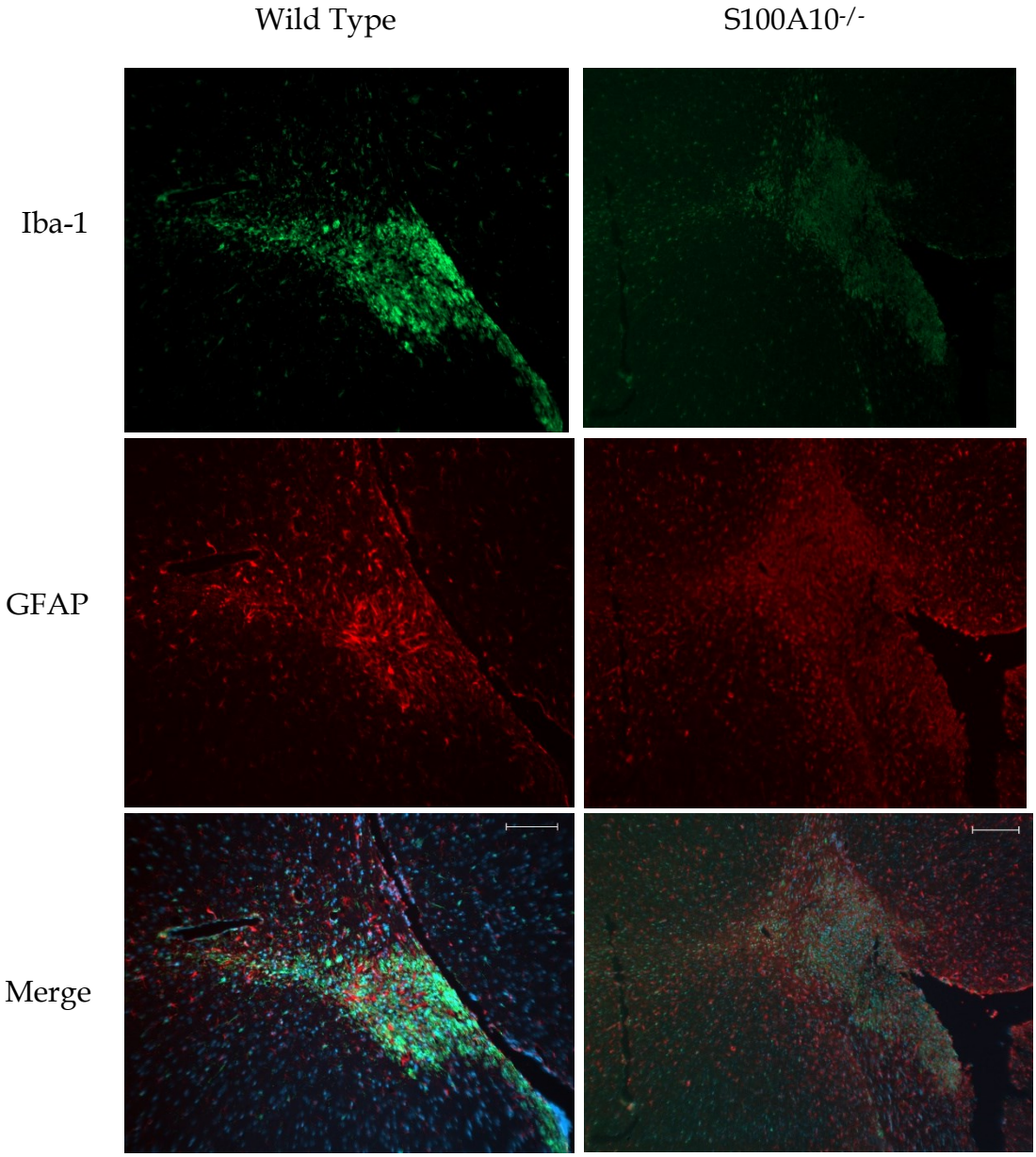

Figure 4-5 Representative Images of LPC-Induced Lesions in Wild Type and S100A10$^{-/-}$ Mice; Iba-1 and GFAP Staining

Lesion 7 days post-injection of 1 µL 1% lysophosphatidylcholine. Fluorescence immune stainingof Iba-1 for microglial cells, GFAP for astrocytes, and merged image. Scale bar is 100 µm.

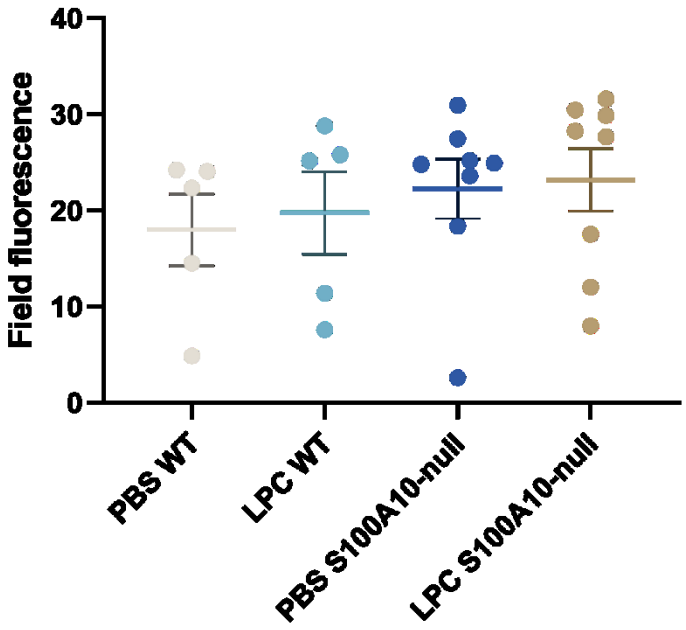

Figure 4-6 Astrocyte Staining Following LPC-Induced Demyelination

After staining with Cy3-conjugated GFAP (1:500), total field of view fluorescence was determined. No significant difference was noted. Mean ± SEM, paired t-test with Welch's correction (LPC vs PBS) or unpaired t-test with Welch's correction (WT vs S100A10-null).

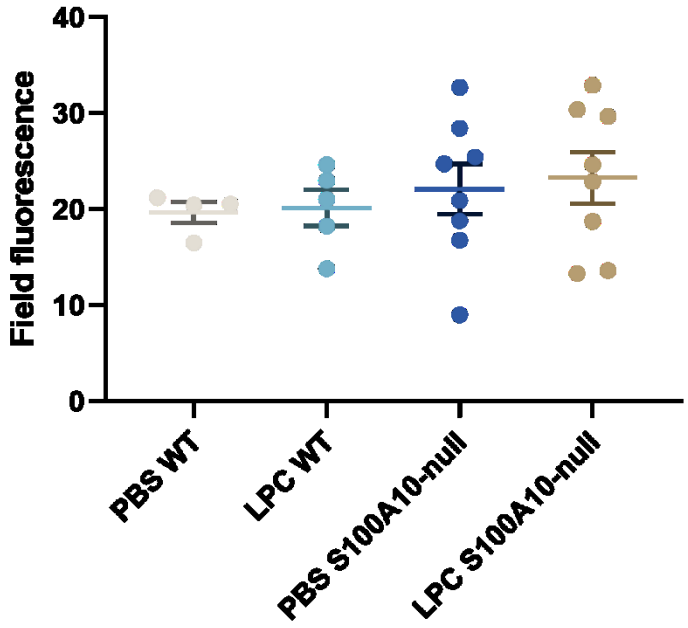

Figure 4-7 Microglia Staining Following LPC-Induced Demyelination

After staining with Iba-1 (1:500) and a anti-rabbit-EGFP secondary, total field of view fluorescence was determined. No significant difference was noted. Mean ± SEM, paired t-test with Welch's correction (LPC vs PBS) or unpaired t-test with Welch's correction (WT vs S100A10-null).

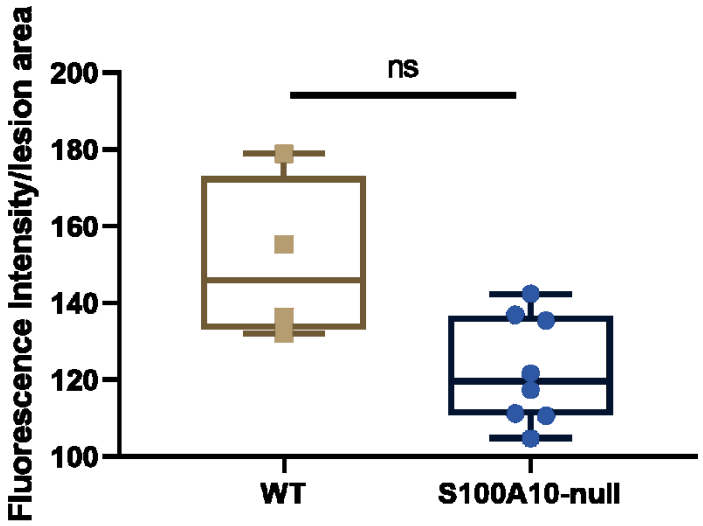

Figure 4-8 Staining Intensity of Iba-1 Within LPC-Induced Lesions

The intensity of staining containing within the area of the lesion was divided by the area, providing a fluorescence/unit area measurement. Two-tailed t-test, Welch's correction, not significant.

This thesis is divided into 3 parts. The first describes a study that explored the role of the 2 C-terminal lysines of S100A10 have in the acceleration of plasmin generation.

Plasminogen receptors are proteins found on the outside of many different types of cells, including endothelial and cancer cells. Understanding how specific plasminogen receptors interact with plasminogen and also whether it interacts with tPA may result in the identification of potential treatment targets for cancer, stroke and potentially MS. In situations where increased plasmin generation is desired, the knowledge of how the activator and receptor interact with plasminogen will lead to the identification of mechanisms that enhance the three-way binding to augment the effect of plasmin. In stroke treatment, for example, the addition of S100A10, either as the entire molecule, or more attractively, a portion of the molecule identified as the minimum required for interaction with both tPA and plasminogen, could be used as an adjunct to increase the efficacy of tPA. Adding a binding motif that helps target the complex to a fibrin clot would also increase efficacy, either in terms of decreasing the amount of tPA administered, decreasing the risk of bleeding or by increasing the treatment window by targeting the tPA to the fibrin clot, allowing more stroke sufferers to benefit from this treatment. In the case of a desired down-regulation of plasmin generation, for example in the case of cancer cells overexpressing the plasminogen receptor, knowledge of how the three proteins interact could lead to the identification of small molecules that may disrupt the interaction, leading to a reduction in local plasmin generation.

Consistent with data presented elsewhere (Fogg et al., 2002), the S100A10 mutant lacking both C-terminal lysine residues ($S100A10^{Des95,96}$) exhibited a decreased ability to accelerate plasmin generation from plasminogen. This experimental result parallels the conclusion drawn from carboxypeptidase treatment of cells

and the wild type proteins (Fogg et al., 2002), in that loss of these 2 C-terminal lysine residues severely hampers the ability of S100A10 to accelerate the conversion of plasminogen to plasmin in the presence of tPA. Unexpectedly, the mutation of these 2 lysine residues to isoleucine, which should not bind to the kringle domains of plasminogen, did not result in a similar decrease in plasmin generation. Kringle residues bind lysine residues and, to a lesser extent arginine residues (Castellino and McCance, 1997; Marti et al., 1997). The lysine binding pocket of the kringles requires interaction with a negatively charged region, a positively charged region and a hydrophobic region. Isoleucine does not possess a negative or positively charged area in the correct spatial conformation to permit binding the lysine binding site of the kringle. It is a branched hydrophobic amino acid and would not spatially interact with the binding site. Further study can be done to further investigate this remote possibility, including examination of the effect of titration of isoleucine to the fluorescence of plasminogen or binding studies using the S100A10^{K95,96I} mutant protein. Regardless of the lack of C-terminal lysine residue, this mutant was able to stimulate plasmin generation similar to the wild type protein. This raises the possibility that not only do C-terminal lysines interact, but, in the right environment, solvent-exposed lysines not at the C-terminus may also interact. In the paper revealing the X-ray crystal structure of plasminogen, the authors suggested that the lysine at residue 50 may be inserted into kringle 5 (Law et al., 2013, 2012), with a role of maintaining the tight, activation resistant formation that plasminogen usually has in circulation. This has also been demonstrated with cytokeratin 8 mutated so that the C-terminal lysine was glutamine (Q) (Gonias et al., 2001). This mutant bound plasminogen, but to a lesser extent; the K_d for WT cytokeratin 8 is 0.4 μM while with the glutamine mutant it was 1.5 μM. The final amino acid of HMGB-1 is glutamic acid (Wen et al., 1989), which, like lysine, is a charged amino acid. This data together leads to the possibility that a C-terminal lysine is not absolutely required for interaction with the lysine binding site of kringle domains.

There is the possibility that the S100A10^{K95,96I} mutant requires processing, or proteolytic cleavage of the molecule to reveal aC-terminal lysine residue. If this was the case a long lag, compared to the wild type protein, would be evident in the time course of cleavage of the plasmin substrate. Examination of a representative absorbance trace for this assay illustrating the typical plasmin substrate cleavage rates for no addition, S100A10^{WT}, S100A10^{Des95,96}, and S100A10^{K95,96I} shows no such lag time, suggesting no proteolytic processing of the S100A10 is occurring, or the activity of S100A10^{K95,96I} is not dependant on processing.

Using the tPA mutants, it was inferred that kringle 2 of tPA interacts with the C-terminal lysine residue of S100A10. Additionally, several other plasminogen receptors, including some without a C-terminal lysine also followed the same pattern. Truncation mutants of plasminogen confirmed that kringle 1 of plasminogen is required for binding/interaction with S100A10. Mutants of plasminogen lacking kringle 1 were not as efficiently converted to plasmin in the presence of tPA and S100A10 as the full length and Lys-plasminogen constructs were. There is a further loss of efficiency of plasmin generation with the loss of kringle 4 of plasminogen. This indicates that the interaction of S100A10 with plasminogen may also include some interaction with kringle 4 in addition to kringle 1. Further work using replacement kringle constructs, for instance, the mutant Kr1-Kr-3-Kr3-Kr4-Kr3-SP compared to Kr1-Kr3-Kr3-Kr3-Kr3-SP (where Kr 3 does not bind lysine) would be useful in teasing apart this potentially complicated interaction.

To further delineate the nature of the interaction of tPA and S100A10, heterotetramers consisting of annexin A2WT or annexin A2 C8S were prepared with S100A10WT, forming AIIt^{WT} and AIIt^{C8S} respectively. S100A10 is usually found complexed with annexin A2 at the cell surface (Bharadwaj et al., 2013). Agreement in the literature has shown that plasminogen interacts with S100A10

on the cell surface, not annexin A2 (Miles and Parmer, 2013). There are reports that annexin A2 is the portion of the heterotetramer that binds to tPA, and it is specifically the cysteine at position 8 that is responsible for this interaction (Jacovina et al., 2009; Roda et al., 2003). Research by Hajjar et al (1998) indicated that the amino acid, homocysteine, which is linked to stroke, interferes with the binding of tPA to annexin A2, and that binding/interaction is via the cysteine residue at position 8 of annexin A2. We hypothesized that S100A10 and annexin A2, complexed together as the heterotetramer, would both interact with tPA. Thus, if the cysteine residue at position 8 of annexin A2 was mutated to serine, this should negate the ability of that portion of the heterotetramer to bind tPA, which should result in a decrease in the rate of plasmin generation. The cysteine at position 8 is within the S100A10 binding site on annexin A2, however previous work has shown that mutation of the cysteine to serine does not affect the formation of the heterotetramer (Becker et al., 1990). Contrary to the hypothesis, the AIIt^{C8S} had a higher rate of plasmin generation compared to AIIt^{WT}. As noted in section 2.15, the heterotetramers were subjected to gel filtration to separate the dimers and monomers from the heterotetramer. Both AIIt^{WT} and AIIt^{C8S} showed an identical profile on the gel filtration, eluting at the same place in the program. This result throws doubt on the importance of the cysteine-8 residue of annexin A2 in binding tPA and suggests that the S100A10 portion of the heterotetramer is responsible for both the plasminogen and tPA binding function.

Based on the findings of the first part of the thesis, the second part of the thesis explores the role of 4 internal lysine residues in S100A10 and the possibility that they may contribute to plasminogen binding. Lysines at residues 17, 22, 27, 36, 46, 53, 56 and 65 were all individually mutated to arginine to preserve the charge and secondary/tertiary structure. All mutants expressed well in the E.coli, but only mutants at residues 46, 53, 56 and 65 were completely purified. Residues 46, 53 and 56 are all solvent-exposed, while residue 65 is buried. When substituted for the wild type protein in the plasmin generation assay, no significant decrease in

the rate of plasmin generation was noted for those mutants tested, specifically 46, 53, 56, 65; the rates were in the same range as the wild type activity. To further examine which internal lysine is likely to participate in binding plasminogen in the absence of C-terminal lysines, a further mutation of the S100A10^{K95,96I} mutant was undertaken. The lysine residue at position 56 was chosen for several reasons. First, like the C-terminal lysine, it is a highly conserved residue. As illustrated in Figure 1.9 this particular residue is conserved over 21 different species, from humans to fish. This residue is also solvent-exposed (Figure 5.1). Using a computational on-line program GETAREA (http://curie.utmb.edu/GET.html), the amino acid sequence from 1-90 was entered, accompanied by the X-ray crystal structure for the same amino acid sequence (Réty et al., 1999). The program calculates projected solvent exposure probabilities based on the information provided (Fraczkiewicz and Braun, 1998). The X-ray crystal structure of S100A10 is incomplete, as the final 6 residues are missing from the structure- either the C-terminal region is disordered in the crystal or is missing due to proteolysis (Réty et al., 1999). Residues assigned a ratio of over 50% are considered solvent-exposed and likely available for binding. Residue 56 has assigned a ratio of 85.3, indicating it is very likely exposed to the solvent. The next 2 highest scoring residues are K46 and K91.

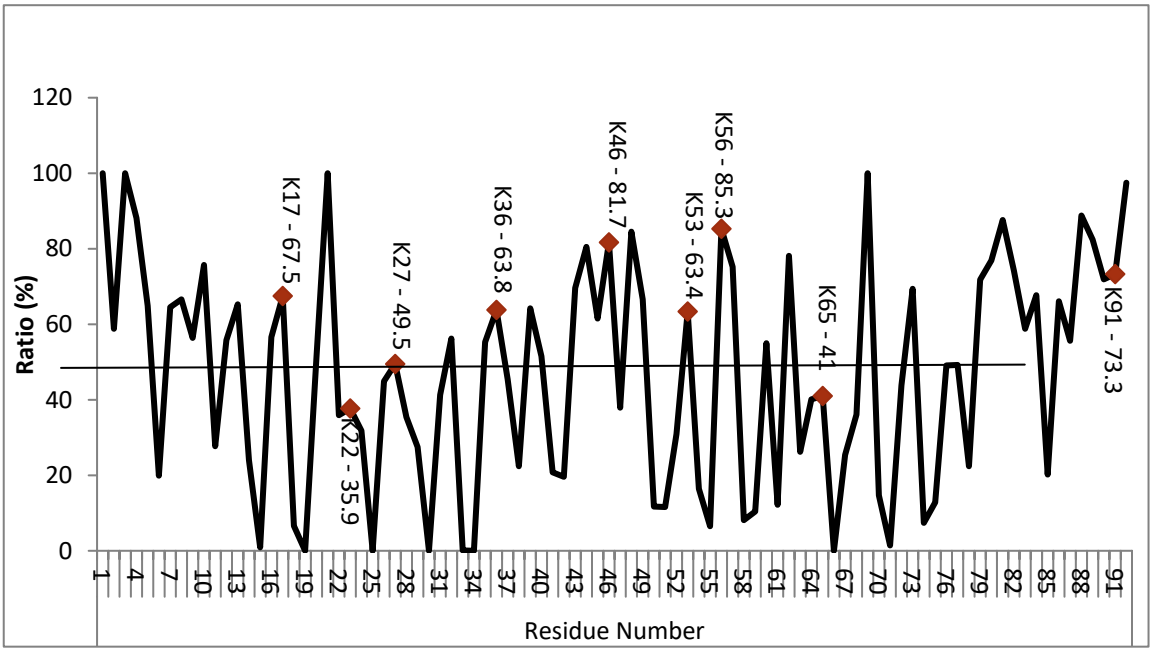

Figure 5-1 Calculated Solvent Exposure of S100A10 Amino Acids by the Program GETAREA

The GETAREA on-line computation program (http://curie.utmb.edu/GET.html) was used to calculate the potential solvent exposure based on coordinates revealed from X-ray crystallography data (Protein Database Accession1A4P). Residues are considered solvent exposed if the ratio calculated is greater than 50. The ratio is calculated by determining the ratio of side-chain surface area to "random coil" value per residue. The "random coil" value of a residue X is the average solvent-accessible surface area of X in the tripeptide Gly-X-Gly in an ensemble of 30 random conformations. For S100A10, the most solvent exposed lysine residue is K56 at 8.3, followed by K46 at 81.7 then K 91 at 73.3. Figure was produced by RW Holloway.

To examine this internal lysine residue, this –While the addition of the K to R mutation at position 56 in the S100A10^{Des95,96} mutant did not affect the purification strategy, the same addition to the S100A10^{K95,96I} mutant resulted in a change in the hydrophobicity of the molecule, resulting in the protein precipitating in the presence of 50% (w/v) ammonium sulphate. The purification protocol was altered to allow for the efficient isolation of the S100A10$^{K56R/K95,96I}$ mutant by dropping the ammonium sulphate concentration to 25% (w/v). After decreasing the ammonium sulphate concentration, the remaining purification procedure remained unchanged. Once purified, the protein eluted at approximately the same position as the WT molecule using gel filtration chromatography. Analysis of the S100A10$^{K56R/K95,96I}$ mutant in the plasmin generation assay revealed a significant drop in the rate of plasmin produced, equal or less than the rate of S100A10^{Des95,96}. The addition of K56R to S100A10^{Des95,96} yielding S100A10$^{K56R/Des95,96}$ did not further decrease the rate of plasmin generation compared to the S100A10^{Des95,96} mutant. Examination of the S100A10^{K56R}, S100A10$^{K56R/K95,96I}$, S100A10K$^{56R/Des95,96}$ by CD spectrophotometry indicated that the addition of the K56R mutation to either the S100A10^{Des95,96} or the S100A10^{K95,96I} mutant did not result in extreme changes in secondary structure. More interestingly, the size exclusion chromatography analysis of S100A10$^{K56R/K95,96I}$ revealed an increase in the retention volume compared to the wild type molecule. No changes had been seen with either the S100A10^{Des95,96} nor S100A10^{K96,96I} mutants. This suggests that, like the change required for the purification from the crude extract, the small change in the amino acids exposed to solvent in this mutant may have caused a larger change in overall protein conformation. Gel filtration chromatography has been used to evaluate the 3D structure of proteins (Uversky, 2012). Changes in the globular form of the protein, possibly caused by changes in the amount of alpha-helical content, may affect which amino acid residues are solvent-exposed and available for interaction.

In the absence of a C-terminal lysine residue, Kr 1 of Glu-plasminogen may interact with an internal lysine. This interaction appears to be conformation-specific. Deletion of the C-terminal lysine, by mutation or by carboxypeptidase cleavage of the C-terminal lysines may not result in the same conformational changes that occur when the C-terminus is mutated to isoleucine. The conformational shift that may occur when the C-terminus is isoleucine may be enough to allow kringle 1 of plasminogen to interact with the internal residue, likely lysine 56. As noted previously, the lysine at residue 50 of plasminogen is thought to interact with kringle 5 of plasminogen, helping to keep the molecule in the closed, activation resistant form. If an internal lysine of plasminogen is able to interact with kringle 5, then an internal lysine on a plasminogen receptor may be also able to interact with a kringle. The other kringle domains of plasminogen may also play a role in the interaction.

Also leading to great curiosity is the repeated finding that carboxypeptidase B1 (CpB1) treatment of S100A10^{K95,96I} caused a loss of plasmin activation, similar to the result seen with the wild type S100A10. CpB1 is classified as an exopeptidase, with specificity for C-terminal lysine and arginine residues (Folk and Gladner, 1958; Wintersberger et al., 1962). The CpB1 treatment of S100A10^{WT} and selected mutants was performed at pH 7.4. It is possible that the assay conditions used were sub-optimal for the exopeptidase, however, an effect of less cleavage rather than non-C-terminal cleavage would be more likely. It is possible that the CpB1 interaction with S100A10K95,96I prevents interaction with either plasminogen, tPA or both. This could also cause a decrease in plasmin generation. Much further work is required to tease apart the exact process that results in the CpB1-specific loss of plasmin generation activity of S100A10^{K95,96I}. CD spectra after treatment with CpB1 may reveal further conformational changes. Mass spectrometry analysis of S100A10^{K95,96I} before and after treatment by CpB1 will reveal if the carboxypeptidase is truly cleaving the S100A10 mutant, or is causing a change in spatial conformation that results in the plasminogen receptor's inability to

facilitate plasminogen cleavage to plasmin. Additionally, repeating the CpB1 treatment using the heterotetramers formed with annexin A2 and either $S100A10^{WT}$ or $S100A10^{K95,96I}$ will also reveal more about the potential interaction of S100A10 and CpB1. The mutant S100A10 protein or the wild type could also be over-expressed in a cell line and the resulting cells expressing the respective heterotetramer on the surface treated with the CpB. This would also reveal if the mutation affects heterotetramer formation and/or movement to the cell surface, as the mechanism controlling the extracellular expression of the heterotetramer sill remain elusive.

The third portion of this thesis revolves around the potential role of S100A10 in demyelination events in Multiple Sclerosis. Published work from Gverić et al. (2005) identified both S100A10 and its binding partner Annexin A2 as being present in established lesions in autopsy samples from individuals with MS. Along with publications showing that plasmin degrades myelin basic protein (Cammer et al., 1978; Law et al., 1985), this led to the hypothesis that S100A10 would accelerate MBP degradation and worsen the outcome, i.e. the MS-like lesions would be larger in the presence of S100A10, so the loss of the protein would be protective. *In vitro*, plasmin activation resulted in the degradation of MBP, which was increased in the presence of S100A10 (Figure 4.1 and 4.2). Most of the previous work examining plasmin degradation of MBP was performed using uPA as the plasminogen activator. tPA is known to be present in the brain (Ortolano and Spuch, 2012) as it has roles in neuroplasticity as well as neurotoxicity, which lead to the choice of tPA as the plasminogen activator, as it is more likely to be relevant *in vivo*. Previous results of this thesis also suggest that tPA may interact with S100A10, giving further credibility to the choice of tPA in this model of MBP degradation.

Lysophosphatidylcholine was injected into the corpus callosum of both wild type C57BL/6 mice and age-matched S100A10-null mice. Day 7 was chosen as the

endpoint as substantial remyelination occurs by this time (Plemel et al., 2018; Warford et al., 2018). Unexpectedly, when the total lesion volume was calculated, the wild type lesion volumes clustered tightly with an average volume of 0.0089 ± 0.0027 mm^3, while the S100A10-null lesions spread over a large range, with an average of 0.0494 ± 0.0142 mm^3 (Figure 4.4).

This result was unexpected in that it was initially hypothesized that loss of S100A10 would be protective, that removing the potential of S100A10 to enhance the generation of plasmin would result in less myelin basic protein degradation by plasmin, leaving more of the myelin intact. The data showed the opposite effect; loss of S100A10 resulted in lesions that were, on average, larger in volume.

When Lewis lung carcinoma cells were injected into either wild type or S100A10-null C57BL/6 mice, the tumours that resulted after 18 days of growth were dramatically smaller in the S100A10-null mice than in the wild type mice (Phipps et al., 2011). Further exploration of this phenomenon revealed that it was due in part to the inability of macrophages to infiltrate the tumour in the S100A10-null mice. In this case, the macrophages used the S100A10 on their surface to focus proteolytic activity and to enhance migration. Although the macrophages in the xenograft-tumour study have a different physiologic role than the microglia and recruited macrophages in the role of myelin debris removal, the same processes apply for migration to the site of inflammation.

The presence of the brain macrophages – known as microglia - within the lesion was quantified in both the wild type and S100A10-null mice using immunofluorescent staining of a single slide from each of the mice. This slide selected was from within the centre of the lesion. This selection should permit a reasonable estimation of the cross-section of the lesion, however, differences in intensity may be present depending on the localization of the two cell types, microglia and astrocytes, that were examined. Mice lacking S100A10 had a lower intensity of Iba-1 staining within the lesion, with an overall larger lesion. The level

of Iba-1 expression increases when the microglia, as well as recruited macrophages, are activated(Imai et al., 1996; Sasaki et al., 2001). indicating fewer microglia/macrophages present within the lesion or that there were fewer activated microglial cells within the lesion. Macrophages utilize S100A10 mediated generation of plasmin to facilitate movement through the extracellular matrix (O'Connell et al., 2010; Phipps et al., 2011; Surette et al., 2011). Thus, in mice without S100A10 present, the activated microglia and any recruited peripheral macrophages may have a more challenging task to get to the site of demyelination. Macrophages and microglia phagocytose debris; this mode of action would be required for efficient removal of MBP-debris created by the action of the LPC If fewer macrophage and microglial cells are present within the lesion, then any myelin degraded by the action of the lysophosphatidylcholine will not be efficiently phagocytosed by this critical cell type for debris clean up, and remyelination is delayed (Griffin et al., 1992; Ousman and David, 2000).

I propose a model of the interplay between S100A10, lesion formation and possible fibrin deposition in the development of MS-like lesions based on the preliminary results observed in WT and S100A10-null mice, (Figures 5.2, 5.3 and 5.4). In the WT brain (Figure 5.2), the requisite surveillance occurs. Any fibrinogen leaking into the brain parenchyma is detected and converted to fibrin. Resident microglia and peripheral macrophage are able to respond, binding via their cell surface CD11b/CD18 integrin to the now-exposed binding site on fibrinogen. The microglia use the S100A10 on their cell surface to aid in their movement to the site of injury, and once there, the S100A10 will localize both plasminogen and tPA to expedite the removal of any fibrin deposition and further degrade myelin debris. In the S100A10-null mouse (Figure 5.3), the LPC injection is a two-fold injury; both the BBB is disrupted by the needle (physical injury), and myelin is disrupted by LPC. WT mice are subject to the same injury, but have the necessary processes to mitigate the damage; microglia and infiltrating macrophage migrate to the site of injury, and utilize plasmin generated on their cell surface to further degrade the

myelin and phagocytose it. The S100A10-null mice lack S100A10 on the surface of microglia and infiltrating macrophages, putting these cells at disadvantage to reach the site of injury and use S100A10 to aid in the degradation of fibrin and any myelin debris, potentially resulting in a lesion that cannot be remyelinated, due to the debris still present. The continued presence of fibrin may also perpetuate an area of inflammation, resulting in continued exposure of the local tissue to cytokine and chemokines resulting in continued damage (Figure 5.3).

Extrapolating to the MS brain, (Figure 5.4) although S100A10 and its binding partner are found to be upregulated/concentrated in lesions, the activity is somehow diminished, likely by upregulation of PAI-1 and subsequent inhibition of tPA (East et al., 2005; Gverić et al., 2005, 2003).

Additionally, a study by Dugas et al (Dugas et al., 2006) and found that S100A10 is downregulated on mature oligodendrocytes (OL) compared to oligodendrocyte precursor cells (OPC). Once OPCs differentiate into oligodendrocytes, expression of S100A10 drops dramatically. This result is corroborated by Milosevic et al (Milosevic et al., 2017) who catalogue the location of S100A10 in the mouse. These researchers found that in addition to discrete areas of the brain and specific neuronal cell types, S100A10 was expressed in astrocytes, microglial cells, but not mature oligodendrocytes. S100A10 was expressed in oligodendrocyte precursor cells, but only those that expressed the marker Neural/glial antigen 2 (NG2), found in white matter tracts(Milosevic et al., 2017). The OPCs may use S100A10 and the plasminogen activation system to allow them to move through the brain to sites requiring remyelination. Further work to delineate the possible role of OPC migration to the site of injury and the differentiation to OL is required to capture the full story of the role of S100A10 in demyelination/remyelination. Initially, immunofluorescence staining for OPCs using NG2 as a marker to determine if S100A10 is up-regulated in NG2 positive cells in the wild type mice should be interrogated. The relative number of NG2 positive cells in wild type mice

compared to S100A10$^{-/-}$ mice will also aid in determining the role. If OPCs are not migrating in the S100A10$^{-/-}$ mice, then mice utilize S100A10 for migration towards a site requiring remyelination. This will be difficult to interrogate the same way in human subjects, as samples of newly demyelinating tissue are not readily available.

S100A10 levels are inversely correlated with the risk of depression (Milosevic et al., 2017; Svenningsson et al., 2006). The prevalence of depression is higher in MS patients than in the general population (Boeschoten et al., 2017; Marrie et al., 2017; Patten et al., 2017). S100A10 regulates the expression of the 5-HT1B receptor (Egeland et al., 2011; Svenningsson et al., 2006), which could contribute to the higher rate of depression in some MS patients. There is some evidence that in the EAE model of MS, some animals exhibit depressive-like symptoms (Pollak et al., 2002). Much further study is required to explore the possibility that a low level of S100A10 in the brain is a potential biomarker for the risk of developing MS.

Figure 5-2 Hypothetical Model of the Role of S100A10 in Normal Brain in a Demyelination Event

Under normal conditions if the blood-brain barrier is disrupted fibrinogen (Fg) enters the brain parenchyma, along with other plasma proteins and peripheral immune cells. Tissue factor, (TF) expressed on pericytes and astrocyte end feet, initiates the coagulation cascade, terminating in active thrombin (IIa) which cleaves soluble fibrinogen to fibrin (Fn). S100A10, expressed on the surface of microglia and infiltrating macrophages accelerates the conversion of plasminogen (Pg) to active plasmin (Pm), which degrades Fn to fibrin degradation products (FDP) which are cleared by microglial cells. Oligodendrocytes (OL) support the myelinated axon. In the case of LPC injection, the LPC integrates into the myelin, disrupting the myelin structure, resulting in loss of myelin structure. Peripheral macrophages migrate to the area of damage, and phagocytose the degraded myelin, and have the ability to further break down the myelin debris prior to phagocytosing it.

On this and following figures, S100A10 is abbreviated p11.

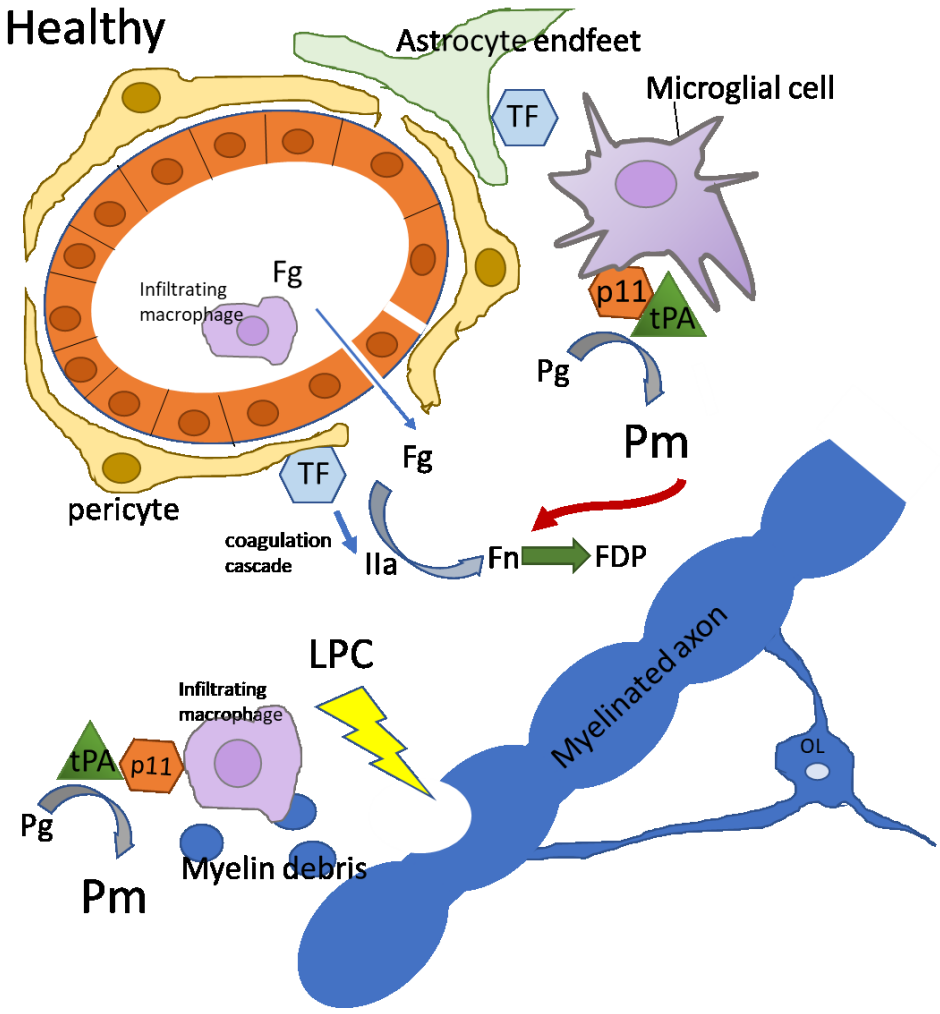
Healthy
Astrocyte endfeet
Microglial cell
TF
Infiltrating
macrophage
Fg
p11
tPA
Pg
Pm
Fg
TF
pericyte
coagulation
cascade
IIa
Fn
FDP
LPC
Infiltrating
macrophage
tPA
p11
Pg
Pm
Myelin debris
Myelinated axon
OL

Figure 5-3 Hypothetical Model of the Effect of Loss of S100A10 in a Demyelination Event

The S100A10 null mouse lacks S100A10 on the surface of microglia and peripheral macrophages. When demyelination is triggered by LPC, the myelin sheath is degraded, astrocytes migrate to the site of damage, and microglia in the vicinity of the damage are activated. The absence of S100A10 on macrophage cell surface diminishes migration. Myelin debris is ineffiently phagocytosed and remains at the site of damagae, inhibiting remyelination. There is also the potential for fibrinogen to enter the parenchyma and be converted into fibrin. Prompt degradation of the fibrin mesh does not occur because of diminished plasmin production resulting in a persistent fibrin mesh. Plasmin production is diminished due to the absence of S100A10 and inhibition of plasmin production by PAI-1. The limited recruitment of immune cells by the fibrin mesh leads to destruction of the myelin sheath. Myelin and OLs are destroyed. A limited number of Oligodendrocyte Precursor Cells (OPC) able to migrate to the site of injury, proliferate, differentiate to OLs, and remyelinate the damage.

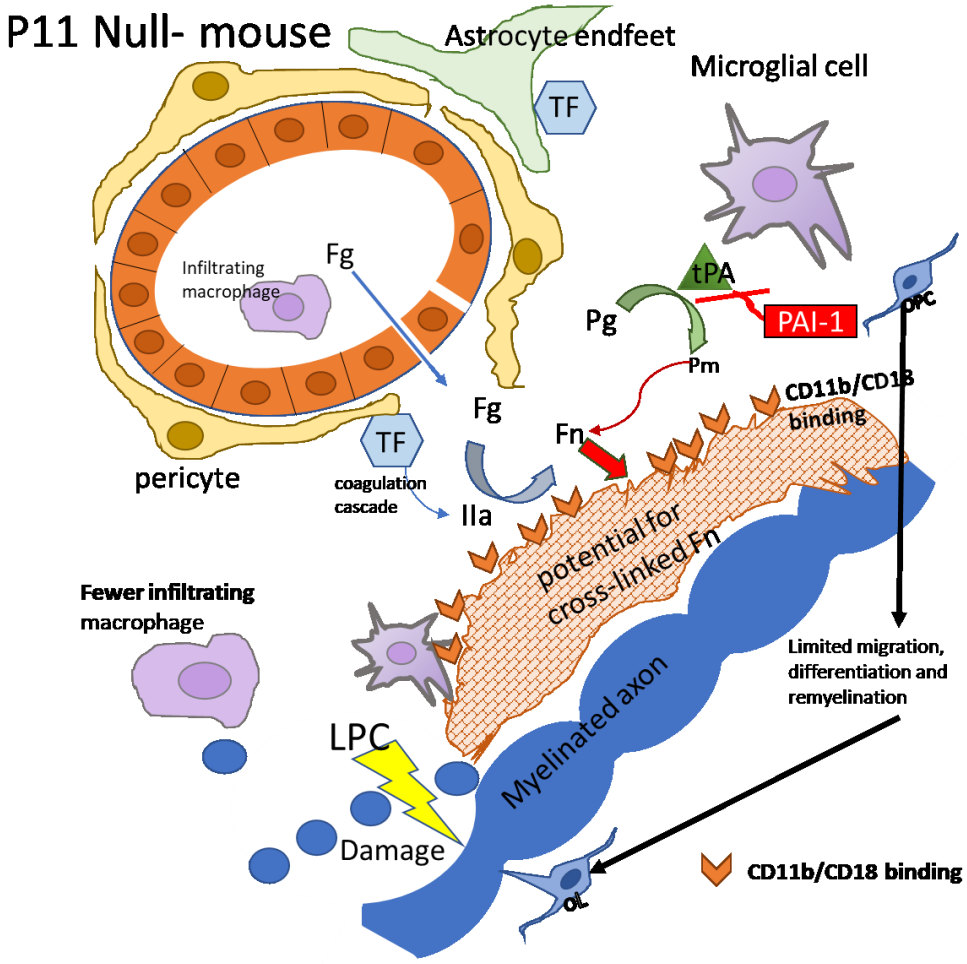
P11 Null- mouse
Astrocyte endfeet
Microglial cell
TF
Infiltrating macrophage
Fg
tPA
Pg
PAI-1
OPC
Pm
CD11b/CD18 binding
Fg
Fn
TF
pericyte
coagulation cascade
IIa
potential for cross-linked Fn
Fewer infiltrating macrophage
Limited migration, differentiation and remyelination
LPC
Myelinated axon
Damage
oL
CD11b/CD18 binding

Figure 5-4 Hypothetical Model of the Role of S100A10 in MS/Demyelination

Extrapolating to a potential role of S100A10 in multiple sclerosis, a breach in the blood brain barrier results in the movement of fibrinogen into the brain parenchyma. This fibrinogen is cleaved into fibrin, however, the presence of abnormally high PAI-1 blocks plasmin generation and fibrinolysis. As a result, a fibrin mesh is formed in proximity to the myelinated axons. A cryptic epitope (γ377-395), present on fibrin, but not fibrinogen, interacts with CD11b/CD18 receptor of microglial cells causing their activation and release of cytokines which results in the recruitment of peripheral macrophages and cytotoxic T-cells and inflammatory demyelination. We therefore predict that S100A10 plays a key role in fibrin surveillance in MS, a role that is attenuated by the abnormal levels of PAI-1 present in MS lesions. Myelin and OLs are destroyed. A limited number of Oligodendrocyte Precursor Cells (OPC) migrate to the site of injury, proliferate, differentiate to OLs, and remyelinate the damage.

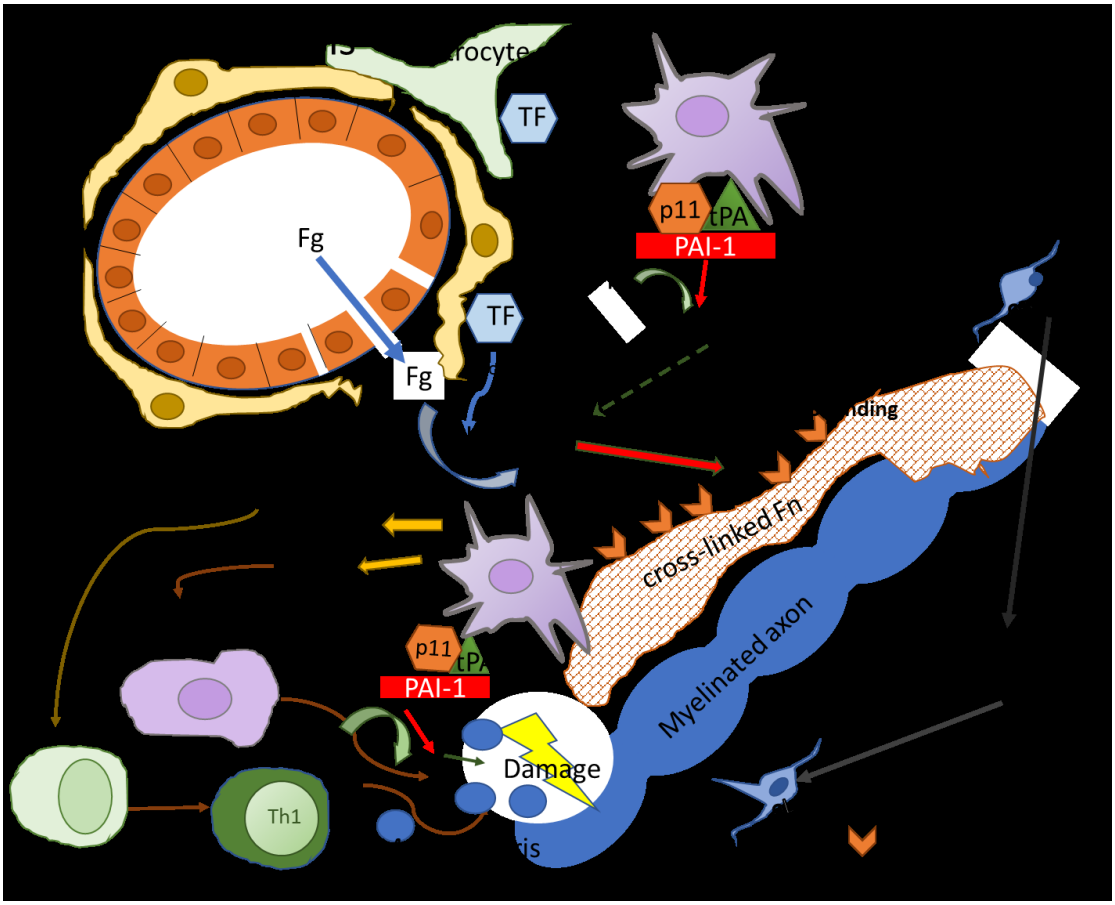
TF
p11
tPA
PAI-1
Fg
TF
Fg
cross-linked Fn
Myelinated axon
p11
PAI-1
Damage
Th1

6.1 CONCLUSION

Plasminogen receptors function to facilitate the activation of plasminogen by specific plasminogen activators. S100A10 is an established plasminogen receptor that has a classic kringle binding C-terminal lysine residue. Loss of the C-terminal lysine residues, by either mutation or by carboxypeptidase directed removal results in a profound loss of the ability of S100A10 to accelerate plasmin generation. Mutation of the 2 lysine residues at the C-terminus of S100A10 to isoleucine unexpectedly did not result in a decrease in the rate of plasmin generated. This result suggested the possibility that an internal lysine residue was utilized by this mutant. Further mutations revealed that the mutation of internal residues alone did not result in any plasmin generation decrease, however, mutating lysine at position 56 in addition to position 95 and 96 (C-terminus) resulted in a 75-90% decrease in the rate of plasmin generated, suggesting that the internal lysine may be that at position 56. Further work to confirm this is required, as outlined in the future directions, however, evidence that this residue is solvent-exposed, as well as conserved over several species gives this conclusion weight. Additionally, work confirmed that the kringle 1 of plasminogen interacts with the plasminogen receptor, as well as kringle 2 of tPA.

Preliminary work presented on the potential role of S100A10 in the mechanics of demyelination supports a key role for this plasminogen receptor. Animals lacking S100A10 had larger lesions than animals with S100A10 present. The S100A10-null mice had a lower concentration of Iba-1 staining within the lesion, suggesting a lower total number of microglia or an inefficient activation. This finding parallels with an earlier finding that S100A10-null mice had fewer macrophages infiltrating a xenograft tumour than wild type mice. It is postulated that the microglia/macrophages use S100A10 to enhance plasmin generation to both

increase MMP-9 activation as well as directly proteolyze the extra-cellular matrix. Additionally, remyelination cannot proceed unless the area of insult is cleared of myelin and other debris, so if microglia and peripheral macrophages cannot be recruited to the site, the remyelination will be delayed. As outlined in future directions, much more work is required to confirm differences between the S100A10-null and the wild type mice in the LPC model and to fully understand the potential role for S100A10 in demyelinating diseases in general.

6.2 FUTURE DIRECTIONS

As in any area of scientific inquiry, this thesis is in no way a complete answer to any question. Further mutagenesis work needs to be done including additional mutations to the $S100A10^{K95,96I}$ construct to determine if the same drop in plasmin generation is due specifically to the loss of K56 or if any further change in the α helix regions will result in the same loss in plasmin generation. To further delineate binding, surface plasmon resonance assays can be performed with each of the key mutant S100A10 proteins. Ideally, this work should use immobilized S100A10, and flow Glu-plasminogen over it at various concentrations to determine if differences in the K_D, Km or other binding constants with mutant proteins. Additionally, the use of tPA mutants in SPR would also be informative. If the activity levels reflect binding ability, the S100A10 mutants with low activity ($S100A10^{Des95,96}$, $S100A10^{K56R/K95,96I}$ and $S100A10^{K56R/Des95,96}$, should show decreased binding of plasminogen and tPA in SPR, or use of affinity column (with either plasminogen or tPA bound to the column support. The further interrogation of activity of the tPA mutants and the Pg mutants with the S100A10 mutants would also be informative. Each of the mutant versions of S100A10 should follow a similar trend, with lower activity seen with both wild type and mutant plasminogen and tPA preparations. Kringle 4 of plasminogen may also play a role in the interaction, thus securing plasminogen lacking kringles 1-4 would be informative. Mutants of plasminogen that keep the full length of the molecule. But

substitute kringle 3 for combinations of the 5 kringles will also tease out which kringles are involved in binding with S100A10. A matrix of plasminogen mutants with S100A10 mutants would result in comprehensive data to completely delineate the binding of plasminogen with the plasminogen receptor S100A10. $S100A10^{Des95,96}$ and $S100A10^{K95,96I}$ both form heterotetramers with annexin A2. The double mutants, $S100A10^{K56R/Des95,96}$ and $S100A10^{K56R/K95,96I}$ should both be examined for the formation of the heterotetramer with annexin A2, and if successful, determine whether the mutant AIIt still supports accelerated plasmin generation.

Unexpectedly, carboxypeptidase treatment of $S100A10^{K95,96I}$ resulted in a decrease in plasmin generation, similar to the result observed with the wild type S100A10. Does the AIIt form of $S100A10^{K95,96I}$ still lose activity upon carboxypeptidase treatment? Expression of this and other mutant proteins in a cellular context, using overexpression vectors would also reveal if the heterotetramer can be formed and if it can be exported to the exterior of the cell. Additionally, the treatment of each of the mutants expressed in cells with CpB1 or another carboxypeptidase would also prove informative. The $S100A10^{K95,96I}$ mutant shows signs of proteolysis in the presence of CpB1 that is rescued by the addition of the CpB1 inhibitor, Plummer's reagent (Figure 3.20). Examination of the mutant pre and post-CpB1 treatment by mass spectrometry would be key in determining the cause of the decrease in plasmin generation.

The role of S100A10 in remyelination is the least complete of the work presented. To further explore the role S100A10 could play in demyelination/remyelination, a full time-course after demyelination should be undertaken. Additional data points to determine lesion size, at days 2, 14, and 21 should be determined to ensure the maximum lesion size usually observed at day 2, is the same between wild type and S100A10-null mice. as well as to determine whether the S100A10-null mice ever 'catch up' to the wild type in terms of maximum remyelination. The

contribution of astrocytes and microglia should be explored at these time points, in addition to any changes in oligodendrocyte precursor cells, as well as the potential for fibrin deposition. In addition to more time points with the LPC model, the use of the cuprizone model of demyelination/remyelination may be a useful confirmatory model to compare the wild type and S100A10$^{-/-}$ mice, as the demyelination occurs in this model in the absence of physical injury. Similar time course experiments would be required to confirm the timeline with this model. More intensive staining to find all areas of demyelination would be required.

To further explore the role of S100A10 in MS, EAE experiments utilizing immunization of both wild type and S100A10-/- C57BL/6 mice with MOG35-55 antigen would initiate the exploration of how S100A10 may fit into the immunological environment of MS would be useful in filling in the rest of the story on why MS plaques have high levels of S100A10 within them. The use of human autopsy samples would be useful for validating molecules or cell types identified through the EAE model comparison between wild type and S100A10$^{-/-}$ mice.

Adams, R., Passin, M., Sachs, B., Nuriel, T., Akassoglou, K., 2004. Fibrin Mechanisms and Functions in Nervous System Pathology. Mol Interv 4, 163–176.

Akassoglou, K., Adams, R.A., Bauer, J., Mercado, P., Tseveleki, V., Lassmann, H., Probert, L., Strickland, S., 2004. Fibrin depletion decreases inflammation and delays the onset of demyelination in a tumor necrosis factor transgenic mouse model for multiple sclerosis. PNAS 101, 6698–6703. https://doi.org/10.1073/pnas.0303859101

Andreasen, P.A., Egelund, R., Petersen, H.H., 2000. The plasminogen activation system in tumor growth, invasion, and metastasis. Cell. Mol. Life Sci. 57, 25–40. https://doi.org/10.1007/s000180050497

Andreasen, P.A., Kjøller, L., Christensen, L., Duffy, M.J., 1997. The urokinase-type plasminogen activator system in cancer metastasis: a review. Int. J. Cancer 72, 1–22.

Andreone, B.J., Chow, B.W., Tata, A., Lacoste, B., Ben-Zvi, A., Bullock, K., Deik, A.A., Ginty, D.D., Clish, C.B., Gu, C., 2017. Blood-Brain Barrier Permeability Is Regulated by Lipid Transport-Dependent Suppression of Caveolae-Mediated Transcytosis. Neuron 94, 581-594.e5. https://doi.org/10.1016/j.neuron.2017.03.043

Andronicos, N.M., Ranson, M., 2001. The topology of plasminogen binding and activation on the surface of human breast cancer cells. British Journal of Cancer 85, 909–916. https://doi.org/10.1054/bjoc.2001.2022

Ascherio, A., Munger, K.L., 2016. Epidemiology of Multiple Sclerosis: From Risk Factors to Prevention-An Update. Semin Neurol 36, 103–114. https://doi.org/10.1055/s-0036-1579693

Ayala-Sanmartin, J., Gouache, P., Henry, J.-P., 2000. N-Terminal Domain of Annexin 2 Regulates Ca2+-Dependent Membrane Aggregation by the Core Domain: A Site Directed Mutagenesis Study. Biochemistry 39, 15190–15198. https://doi.org/10.1021/bi000764r

Baecher-Allan, C., Kaskow, B.J., Weiner, H.L., 2018. Multiple Sclerosis: Mechanisms and Immunotherapy. Neuron 97, 742–768. https://doi.org/10.1016/j.neuron.2018.01.021

Bailey, O.T., Pappenheimer, A.M., Cheever, F.S., Daniels, J.B., 1949. A Murine Virus (JHM) Causing Disseminated Encephalomyelitis With Extensive Destruction of Myelin: II. Pathology. J. Exp. Med. 90, 195–212. https://doi.org/10.1084/jem.90.3.195

Bardehle, S., Rafalski, V.A., Akassoglou, K., 2015. Breaking boundaries—coagulation and fibrinolysis at the neurovascular interface. Frontiers in Cellular Neuroscience 354. https://doi.org/10.3389/fncel.2015.00354

Becher, B., Spath, S., Goverman, J., 2017. Cytokine networks in neuroinflammation. Nat. Rev. Immunol. 17, 49–59. https://doi.org/10.1038/nri.2016.123

Becker, T., Weber, K., Johnsson, N., 1990. Protein-protein recognition via short amphiphilic helices; a mutational analysis of the binding site of annexin II for p11. EMBO J 9, 4207–4213.

Bettum, I.J., Vasiliauskaite, K., Nygaard, V., Clancy, T., Pettersen, S.J., Tenstad, E., Mælandsmo, G.M., Prasmickaite, L., 2014. Metastasis-associated protein S100A4 induces a network of inflammatory cytokines that activate stromal cells to acquire pro-tumorigenic properties. Cancer Letters 344, 28–39. https://doi.org/10.1016/j.canlet.2013.10.036

Bharadwaj, A., Bydoun, M., Holloway, R., Waisman, D., 2013. Annexin A2 heterotetramer: structure and function. Int J Mol Sci 14, 6259–6305. https://doi.org/10.3390/ijms14036259

Boer, A.G. de, Gaillard, P.J., 2006. Blood–brain barrier dysfunction and recovery. J Neural Transm 113, 455–462. https://doi.org/10.1007/s00702-005-0375-4

Boeschoten, R.E., Braamse, A.M.J., Beekman, A.T.F., Cuijpers, P., van Oppen, P., Dekker, J., Uitdehaag, B.M.J., 2017. Prevalence of depression and anxiety in Multiple Sclerosis: A systematic review and meta-analysis. J. Neurol. Sci. 372, 331–341. https://doi.org/10.1016/j.jns.2016.11.067

Briens, A., Bardou, I., Lebas, H., Miles, L.A., Parmer, R.J., Vivien, D., Docagne, F., 2017. Astrocytes regulate the balance between plasminogen activation and plasmin clearance via cell-surface actin. Cell Discovery 3, 17001. https://doi.org/10.1038/celldisc.2017.1

Browne, B.C., Hochgräfe, F., Wu, J., Millar, E.K.A., Barraclough, J., Stone, A., McCloy, R.A., Lee, C.S., Roberts, C., Ali, N.A., Boulghourjian, A., Schmich, F., Linding, R., Farrow, L., Gee, J.M.W., Nicholson, R.I., O'Toole, S.A., Sutherland, R.L., Musgrove, E.A., Butt, A.J., Daly, R.J., 2013. Global characterization of signalling networks associated with tamoxifen resistance in breast cancer. The FEBS Journal 280, 5237–5257. https://doi.org/10.1111/febs.12441

Buchholz, M., Biebl, A., Neesse, A., Wagner, M., Iwamura, T., Leder, G., Adler, G., Gress, T.M., 2003. SERPINE2 (protease nexin I) promotes extracellular matrix production and local invasion of pancreatic tumors in vivo. Cancer Res. 63, 4945–4951.

Bugge, T.H., Flick, M.J., Daugherty, C.C., Degen, J.L., 1995. Plasminogen deficiency causes severe thrombosis but is compatible with development and reproduction. Genes Dev. 9, 794–807. https://doi.org/10.1101/gad.9.7.794

Burrows, D.J., McGown, A., Jain, S.A., De Felice, M., Ramesh, T.M., Sharrack, B., Majid, A., 2018. Animal models of multiple sclerosis: From rodents to zebrafish. Mult Scler 25, 306–324. https://doi.org/10.1177/1352458518805246

Buzzard, K., Chan, W.H., Kilpatrick, T., Murray, S., 2017. Multiple Sclerosis: Basic and Clinical, in: Beart, P., Robinson, M., Rattray, M., Maragakis, N.J. (Eds.), Neurodegenerative Diseases: Pathology, Mechanisms, and Potential Therapeutic Targets, Advances in Neurobiology. Springer International Publishing, Cham, pp. 211–252. https://doi.org/10.1007/978-3-319-57193-5_8

Bydoun, M., Sterea, A., Liptay, H., Uzans, A., Huang, W.-Y., Rodrigues, G.J., Weaver, I.C.G., Gu, H., Waisman, D.M., 2018. S100A10, a novel biomarker in pancreatic ductal adenocarcinoma. Mol Oncol 12, 1895–1916. https://doi.org/10.1002/1878-0261.12356

Cammer, W., Bloom, B.R., Norton, W.T., Gordon, S., 1978. Degradation of basic protein in myelin by neutral proteases secreted by stimulated macrophages: A possible mechanism of inflammatory demyelination. Proc Natl Acad Sci U S A 75, 1554–1558.

Cammer, W., Brosnan, C.F., Bloom, B.R., Norton, W.T., 1981. Degradation of the P0, P1, and Pr proteins in peripheral nervous system myelin by plasmin: implications regarding the role of macrophages in demyelinating diseases. J. Neurochem. 36, 1506–1514.

Capello, M., Ferri-Borgogno, S., Cappello, P., Novelli, F., 2011. α-enolase: a promising therapeutic and diagnostic tumor target. The FEBS Journal 278, 1064–1074. https://doi.org/10.1111/j.1742-4658.2011.08025.x

Castellino, F.J., McCance, S.G., 1997. The kringle domains of human plasminogen. Ciba Found. Symp. 212, 46–60; discussion 60-65. https://doi.org/10.1002/9780470515457.ch4

Ceruti, P., Principe, M., Capello, M., Cappello, P., Novelli, F., 2013. Three are better than one: plasminogen receptors as cancer theranostic targets. Experimental Hematology & Oncology 2, 12. https://doi.org/10.1186/2162-3619-2-12

Cesarman, G.M., Guevara, C.A., Hajjar, K.A., 1994. An endothelial cell receptor for plasminogen/tissue plasminogen activator (t-PA). II. Annexin II-mediated enhancement of t-PA-dependent plasminogen activation. Journal of Biological Chemistry 269:, 21198–21203.

Chodobski, A., Zink, B.J., Szmydynger-Chodobska, J., 2011. Blood-brain barrier pathophysiology in traumatic brain injury. Transl Stroke Res 2, 492–516. https://doi.org/10.1007/s12975-011-0125-x

Choi, K.-S., Fogg, D.K., Yoon, C.-S., Waisman, D.M., 2003. p11 Regulates extracellular plasmin production and invasiveness of HT1080 fibrosarcoma cells. The FASEB Journal 17, 235–246. https://doi.org/10.1096/fj.02-0697com

Christen, M.T., Frank, P., Schaller, J., Llinás, M., 2010. Human Plasminogen Kringle 3: Solution Structure, Functional Insights, Phylogenetic Landscape,. Biochemistry 49, 7131–7150. https://doi.org/10.1021/bi100687f

Craner, M.J., Lo, A.C., Black, J.A., Baker, D., Newcombe, J., Cuzner, M.L., Waxman, S.G., 2003. Annexin II/p11 is up-regulated in Purkinje cells in EAE and MS. NeuroReport 14, 555–558.
Crawford, A.H., Chambers, C., Franklin, R.J.M., 2013. Remyelination: the true regeneration of the central nervous system. J. Comp. Pathol. 149, 242–254. https://doi.org/10.1016/j.jcpa.2013.05.004
Crooks, G.E., Hon, G., Chandonia, J.-M., Brenner, S.E., 2004. WebLogo: a sequence logo generator. Genome Res. 14, 1188–1190. https://doi.org/10.1101/gr.849004
Cubellis, M.V., Wun, T.C., Blasi, F., 1990. Receptor-mediated internalization and degradation of urokinase is caused by its specific inhibitor PAI-1. EMBO J. 9, 1079–1085.
Das, R., Burke, T., Plow, E.F., 2007. Histone H2B as a functionally important plasminogen receptor on macrophages. Blood 110, 3763–3772.
Davalos, D., Akassoglou, K., 2011. Fibrinogen as a key regulator of inflammation in disease. Semin Immunopathol 34, 43–62. https://doi.org/10.1007/s00281-011-0290-8
Davalos, D., Mahajan, K.R., Trapp, B.D., 2019. Brain fibrinogen deposition plays a key role in MS pathophysiology – Yes. Mult Scler 1352458519852723. https://doi.org/10.1177/1352458519852723
de Boer, J.P., Creasey, A.A., Chang, A., Abbink, J.J., Roem, D., Eerenberg, A.J., Hack, C.E., Taylor, F.B., 1993. Alpha-2-macroglobulin functions as an inhibitor of fibrinolytic, clotting, and neutrophilic proteinases in sepsis: studies using a baboon model. Infect. Immun. 61, 5035–5043.
de Vos, A.M., Ultsch, M.H., Kelley, R.F., Padmanabhan, K., Tulinsky, A., Westbrook, M.L., Kossiakoff, A.A., 1992. Crystal structure of the kringle 2 domain of tissue plasminogen activator at 2.4-A resolution. Biochemistry 31, 270–279.
de Vries, C., Veerman, H., Pannekoek, H., 1989. Identification of the domains of tissue-type plasminogen activator involved in the augmented binding to fibrin after limited digestion with plasmin. J. Biol. Chem. 264, 12604–12610.
Deutsch, D.G., Mertz, E.T., 1970. Plasminogen: Purification from Human Plasma by Affinity Chromatography. Science 170, 1095–1096.
Doeing, D.C., Borowicz, J.L., Crockett, E.T., 2003. Gender dimorphism in differential peripheral blood leukocyte counts in mice using cardiac, tail, foot, and saphenous vein puncture methods. BMC Clin Pathol 3, 3. https://doi.org/10.1186/1472-6890-3-3
Dohgu, S., Takata, F., Matsumoto, J., Oda, M., Harada, E., Watanabe, T., Nishioku, T., Shuto, H., Yamauchi, A., Kataoka, Y., 2011. Autocrine and paracrine up-regulation of blood–brain barrier function by plasminogen activator inhibitor-1. Microvascular Research 81, 103–107. https://doi.org/10.1016/j.mvr.2010.10.004

Donato, R., 2001. S100: a multigenic family of calcium-modulated proteins of the EF-hand type with intracellular and extracellular functional roles. Int. J. Biochem. Cell Biol. 33, 637–668.
Donato, R., 1999. Functional roles of S100 proteins, calcium-binding proteins of the EF-hand type. Biochimica et Biophysica Acta (BBA) - Molecular Cell Research 1450, 191–231. https://doi.org/10.1016/S0167-4889(99)00058-0
Dugas, J.C., Tai, Y.C., Speed, T.P., Ngai, J., Barres, B.A., 2006. Functional Genomic Analysis of Oligodendrocyte Differentiation. J. Neurosci. 26, 10967–10983. https://doi.org/10.1523/JNEUROSCI.2572-06.2006
Dupont, D.M., Madsen, J.B., Kristensen, T., Bodker, J.S., Blouse, G.E., Wind, T., Andreasen, P.A., 2009. Biochemical properties of plasminogen activator inhibitor-1. Front Biosci (Landmark Ed) 14, 1337–1361.
Dvorak, H.F., Senger, D.R., Dvorak, A.M., Harvey, V.S., McDonagh, J., 1985. Regulation of extravascular coagulation by microvascular permeability. Science 227, 1059–1061. https://doi.org/10.1126/science.3975602
East, E., Baker, D., Pryce, G., Lijnen, H.R., Cuzner, M.L., Gverić, D., 2005. A Role for the Plasminogen Activator System in Inflammation and Neurodegeneration in the Central Nervous System during Experimental Allergic Encephalomyelitis. The American Journal of Pathology 167, 545–554. https://doi.org/10.1016/S0002-9440(10)62996-3
East, E., Gverić, D., Baker, D., Pryce, G., Lijnen, H.R., Cuzner, M.L., 2008. Chronic relapsing experimental allergic encephalomyelitis (CREAE) in plasminogen activator inhibitor-1 knockout mice: the effect of fibrinolysis during neuroinflammation. Neuropathology and Applied Neurobiology 34, 216–230. https://doi.org/10.1111/j.1365-2990.2007.00889.x
Eaton, D.L., Baker, J.B., 1983. Evidence that a variety of cultured cells secrete protease nexin and produce a distinct cytoplasmic serine protease-binding factor. Journal of Cellular Physiology 117, 175–182. https://doi.org/10.1002/jcp.1041170207
Eftink, M.R., 2000. Intrinsic Fluorescence of Proteins, in: Lakowicz, J.R. (Ed.), Topics in Fluorescence Spectroscopy: Volume 6: Protein Fluorescence, Topics in Fluorescence Spectroscopy. Springer US, Boston, MA, pp. 1–15. https://doi.org/10.1007/0-306-47102-7_1
Egeland, M., Warner-Schmidt, J., Greengard, P., Svenningsson, P., 2011. Co-expression of serotonin 5-HT1B and 5-HT4 receptors in p11 containing cells in cerebral cortex, hippocampus, caudate-putamen and cerebellum. Neuropharmacology 61, 442–450. https://doi.org/10.1016/j.neuropharm.2011.01.046
Egeland, M., Warner-Schmidt, J., Greengard, P., Svenningsson, P., 2010. Neurogenic Effects of Fluoxetine Are Attenuated in p11 (S100A10) Knockout Mice. Biological Psychiatry, Synaptic Development in Mood Disorders 67, 1048–1056. https://doi.org/10.1016/j.biopsych.2010.01.024

Ellis, V., Behrendt, N., Danø, K., 1991. Plasminogen activation by receptor-bound urokinase. A kinetic study with both cell-associated and isolated receptor. J. Biol. Chem. 266, 12752–12758.

Ellis, V., Scully, M.F., Kakkar, V.V., 1989. Plasminogen activation initiated by single-chain urokinase-type plasminogen activator. Potentiation by U937 monocytes. J. Biol. Chem. 264, 2185–2188.

Felez, J., Chanquia, C., Fabregas, P., Plow, E., Miles, L., 1993. Competition between plasminogen and tissue plasminogen activator for cellular binding sites. Blood 82, 2433.

Flaumenhaft, R., Koseoglu, S., 2016. Platelet Contents, in: Schulze, H., Italiano, J. (Eds.), Molecular and Cellular Biology of Platelet Formation: Implications in Health and Disease. Springer International Publishing, Cham, pp. 133–152. https://doi.org/10.1007/978-3-319-39562-3_6

Fogg, D.K., Bridges, D.E., Cheung, K.K.-T., Kassam, G., Filipenko, N.R., Choi, K.-S., Fitzpatrick, S.L., Nesheim, M., Waisman, D.M., 2002. The p11 Subunit of Annexin II Heterotetramer Is Regulated by Basic Carboxypeptidase. Biochemistry 41, 4953–4961. https://doi.org/10.1021/bi012045y

Folk, J.E., Gladner, J.A., 1958. Carboxypeptidase B: I. Purification of the Zymogen and Specificity of the Enzyme. Journal of Biological Chemistry 231, 379–391.

Fraczkiewicz, R., Braun, W., 1998. Exact and efficient analytical calculation of the accessible surface areas and their gradients for macromolecules. Journal of Computational Chemistry 19, 319–333. https://doi.org/10.1002/(SICI)1096-987X(199802)19:3<319::AID-JCC6>3.0.CO;2-W

Franklin, R.J.M., Zhao, C., Sim, F.J., 2002. Ageing and CNS remyelination. NeuroReport 13, 923.

Fugate, J.E., Rabinstein, A.A., 2014. Update on intravenous recombinant tissue plasminogen activator for acute ischemic stroke. Mayo Clin. Proc. 89, 960–972. https://doi.org/10.1016/j.mayocp.2014.03.001

Galántai, R., Módos, K., Fidy, J., Kolev, K., Machovich, R., 2006. Structural basis of the cofactor function of denatured albumin in plasminogen activation by tissue-type plasminogen activator. Biochem. Biophys. Res. Commun. 341, 736–741. https://doi.org/10.1016/j.bbrc.2006.01.027

Gall, L.S., Vulliamy, P., Gillespie, S., Jones, T.F., Pierre, R.S.J., Breukers, S.E., Gaarder, C., Juffermans, N.P., Maegele, M., Stensballe, J., Johansson, P.I., Davenport, R.A., Brohi, K., Targeted Action for Curing Trauma-Induced Coagulopathy (TACTIC) partners, 2018. The S100A10 Pathway Mediates an Occult Hyperfibrinolytic Subtype in Trauma Patients. Ann. Surg. https://doi.org/10.1097/SLA.0000000000002733

Garcia-Ferrer, I., Marrero, A., Gomis-Rüth, F.X., Goulas, T., 2017. α2-Macroglobulins: Structure and Function. Subcell. Biochem. 83, 149–183. https://doi.org/10.1007/978-3-319-46503-6_6

Godier, A., Hunt, B.J., 2013. Plasminogen receptors and their role in the pathogenesis of inflammatory, autoimmune and malignant disease. Journal of Thrombosis and Haemostasis 11, 26–34. https://doi.org/10.1111/jth.12064

Gong, Y., Kim, S.-O., Felez, J., Grella, D.K., Castellino, F.J., Miles, L.A., 2001. Conversion of Glu-Plasminogen to Lys-Plasminogen Is Necessary for Optimal Stimulation of Plasminogen Activation on the Endothelial Cell Surface. J. Biol. Chem. 276, 19078–19083.

Gonias, S.L., Hembrough, T.A., Sankovic, M., 2001. Cytokeratin 8 functions as a major plasminogen receptor in select epithelial and carcinoma cells. Front. Biosci. 6, D1403-1411.

Gonzalez-Gronow, M., Gawdi, G., Pizzo, S.V., 2002. Tissue factor is the receptor for plasminogen type 1 on 1-LN human prostate cancer cells. Blood 99, 4562–4567. https://doi.org/10.1182/blood.V99.12.4562

Griffin, J.W., George, R., Lobato, C., Tyor, W.R., Yan, L.C., Glass, J.D., 1992. Macrophage responses and myelin clearance during Wallerian degeneration: relevance to immune-mediated demyelination. J. Neuroimmunol. 40, 153–165. https://doi.org/10.1016/0165-5728(92)90129-9

Gu, S.X., Lentz, S.R., 2018. Fibrin films: overlooked hemostatic barriers against microbial infiltration. J. Clin. Invest. 128, 3243–3245. https://doi.org/10.1172/JCI121858

Gudi, V., Gingele, S., Skripuletz, T., Stangel, M., 2014. Glial response during cuprizone-induced de- and remyelination in the CNS: lessons learned. Front. Cell. Neurosci. 8. https://doi.org/10.3389/fncel.2014.00073

Gverić, D., Herrera, B., Petzold, A., Lawrence, D.A., Cuzner, M.L., 2003. Impaired fibrinolysis in multiple sclerosis: a role for tissue plasminogen activator inhibitors. Brain 126, 1590–1598. https://doi.org/10.1093/brain/awg167

Gverić, D., Herrera, B.M., Cuzner, M.L., 2005. tPA Receptors and the Fibrinolytic Response in Multiple Sclerosis Lesions. The American Journal of Pathology 166, 1143–1151. https://doi.org/10.1016/S0002-9440(10)62334-6

Hajjar, K.A., Jacovina, A.T., Chacko, J., 1994. An endothelial cell receptor for plasminogen/tissue plasminogen activator. I. Identity with annexin II. Journal of Biological Chemistry 269:, 21191–21197.

Hajjar, K.A., Mauri, L., Jacovina, A.T., Zhong, F., Mirza, U.A., Padovan, J.C., Chait, B.T., 1998. Tissue plasminogen activator binding to the annexin II tail domain. Direct modulation by homocysteine. J. Biol. Chem. 273, 9987–9993.

Hall, S.W., Humphries, J.E., Gonias, S.L., 1991. Inhibition of cell surface receptor-bound plasmin by alpha 2-antiplasmin and alpha 2-macroglobulin. J. Biol. Chem. 266, 12329–12336.

Han, M.H., Hwang, S.-I., Roy, D.B., Lundgren, D.H., Price, J.V., Ousman, S.S., Fernald, G.H., Gerlitz, B., Robinson, W.H., Baranzini, S.E., Grinnell, B.W.,

Raine, C.S., Sobel, R.A., Han, D.K., Steinman, L., 2008. Proteomic analysis of active multiple sclerosis lesions reveals therapeutic targets. Nature 451, 1076–1081. https://doi.org/10.1038/nature06559

Harder, T., Kube, E., Gerke, V., 1992. Cloning and characterization of the human gene encoding p11: structural similarity to other members of the S-100 gene family. Gene 113, 269–274. https://doi.org/10.1016/0378-1119(92)90406-F

Hastings, G.A., Coleman, T.A., Haudenschild, C.C., Stefansson, S., Smith, E.P., Barthlow, R., Cherry, S., Sandkvist, M., Lawrence, D.A., 1997. Neuroserpin, a brain-associated inhibitor of tissue plasminogen activator is localized primarily in neurons. Implications for the regulation of motor learning and neuronal survival. J. Biol. Chem. 272, 33062–33067. https://doi.org/10.1074/jbc.272.52.33062

Hawley, S.B., Tamura, T., Miles, L.A., 2001. Purification, Cloning, and Characterization of a Profibrinolytic Plasminogen-binding Protein, TIP49a. J. Biol. Chem. 276, 179–186. https://doi.org/10.1074/jbc.M004919200

Hébert, M., Lesept, F., Vivien, D., Macrez, R., 2016. The story of an exceptional serine protease, tissue-type plasminogen activator (tPA). Revue Neurologique 172, 186–197. https://doi.org/10.1016/j.neurol.2015.10.002

Heremans, H., Dillen, C., Groenen, M., Martens, E., Billiau, A., 1996. Chronic relapsing experimental autoimmune encephalomyelitis (CREAE) in mice: enhancement by monoclonal antibodies against interferon-gamma. Eur. J. Immunol. 26, 2393–2398. https://doi.org/10.1002/eji.1830261019

Hermel, M., Dailey, W., Hartzer, M.K., 2010. Efficacy of plasmin, microplasmin, and streptokinase-plasmin complex for the in vitro degradation of fibronectin and laminin- implications for vitreoretinal surgery. Curr. Eye Res. 35, 419–424. https://doi.org/10.3109/02713680903572517

Herren, T., Burke, T.A., Das, R., Plow, E.F., 2006. Identification of Histone H2B as a Regulated Plasminogen Receptor†. Biochemistry 45, 9463–9474. https://doi.org/doi: 10.1021/bi060756w

Holloway, R.W., Thomas, M.L., Cohen, A.M., Bharadwaj, A.G., Rahman, M., Marcato, P., Marignani, P.A., Waisman, D.M., 2018. Regulation of cell surface protease receptor S100A10 by retinoic acid therapy in acute promyelocytic leukemia (APL)☆. Cell Death Dis 9, 920. https://doi.org/10.1038/s41419-018-0954-6

Hoylaerts, M., Rijken, D.C., Lijnen, H.R., Collen, D., 1982. Kinetics of the activation of plasminogen by human tissue plasminogen activator. Role of fibrin. J. Biol. Chem. 257, 2912–2919.

Huang, D., Yang, Y., Sun, J., Dong, X., Wang, J., Liu, H., Lu, C., Chen, X., Shao, J., Yan, J., 2017. Annexin A2-S100A10 heterotetramer is upregulated by PML/RARα fusion protein and promotes plasminogen-dependent

fibrinolysis and matrix invasion in acute promyelocytic leukemia. Front Med 11, 410–422. https://doi.org/10.1007/s11684-017-0527-6
Ikota, H., Iwasaki, A., Kawarai, M., Nakazato, Y., 2010. Neuromyelitis optica with intraspinal expansion of Schwann cell remyelination. Neuropathology 30, 427–433. https://doi.org/10.1111/j.1440-1789.2009.01071.x
Imai, Y., Ibata, I., Ito, D., Ohsawa, K., Kohsaka, S., 1996. A novel gene iba1 in the major histocompatibility complex class III region encoding an EF hand protein expressed in a monocytic lineage. Biochem. Biophys. Res. Commun. 224, 855–862. https://doi.org/10.1006/bbrc.1996.1112
Ito, D., Imai, Y., Ohsawa, K., Nakajima, K., Fukuuchi, Y., Kohsaka, S., 1998. Microglia-specific localisation of a novel calcium binding protein, Iba1. Molecular Brain Research 57, 1–9. https://doi.org/10.1016/S0169-328X(98)00040-0
Jacovina, A.T., Deora, A.B., Ling, Q., Broekman, M.J., Almeida, D., Greenberg, C.B., Marcus, A.J., Smith, J.D., Hajjar, K.A., 2009. Homocysteine inhibits neoangiogenesis in mice through blockade of annexin A2–dependent fibrinolysis. J Clin Invest 119, 3384–3394.
Jennewein, C., Tran, N., Paulus, P., Ellinghaus, P., Eble, J.A., Zacharowski, K., 2011. Novel Aspects of Fibrin(ogen) Fragments during Inflammation. Mol Med 17, 568–573. https://doi.org/10.2119/molmed.2010.00146
Johansson, H.J., Sanchez, B.C., Forshed, J., Stål, O., Fohlin, H., Lewensohn, R., Hall, P., Bergh, J., Lehtiö, J., Linderholm, B.K., 2015. Proteomics profiling identify CAPS as a potential predictive marker of tamoxifen resistance in estrogen receptor positive breast cancer. Clin Proteom 12, 1–10. https://doi.org/10.1186/s12014-015-9080-y
Joshi, K.K., Nanda, J.S., Kumar, P., Sahni, G., 2012. Substrate kringle-mediated catalysis by the streptokinase-plasmin activator complex: critical contribution of kringle-4 revealed by the mutagenesis approaches. Biochim. Biophys. Acta 1824, 326–333. https://doi.org/10.1016/j.bbapap.2011.10.010
Kang, H.M., Kassam, G., Jarvis, S.E., Fitzpatrick, S.L., Waisman, D.M., 1997. Characterization of human recombinant annexin II tetramer purified from bacteria: role of N-terminal acetylation. Biochemistry 36, 2041–2050. https://doi.org/10.1021/bi962569b
Kassam, G., Choi, K.S., Ghuman, J., Kang, H.M., Fitzpatrick, S.L., Zackson, T., Zackson, S., Toba, M., Shinomiya, A., Waisman, D.M., 1998. The role of annexin II tetramer in the activation of plasminogen. J. Biol. Chem. 273, 4790–4799. https://doi.org/10.1074/jbc.273.8.4790
Kassam, G., Kwon, M., Yoon, C.S., Graham, K.S., Young, M.K., Gluck, S., Waisman, D.M., 2001. Purification and characterization of A61. An angiostatin-like plasminogen fragment produced by plasmin

autodigestion in the absence of sulfhydryl donors. J. Biol. Chem. 276, 8924–8933. https://doi.org/10.1074/jbc.M009071200
Kassam, Geetha, Le, B.-H., Choi, K.-S., Kang, H.-M., Fitzpatrick, S.L., Louie, P., Waisman, D.M., 1998. The p11 Subunit of the Annexin II Tetramer Plays a Key Role in the Stimulation of t-PA-Dependent Plasminogen Activation†. Biochemistry 37, 16958–16966. https://doi.org/10.1021/bi981713l
Kassam, G., Manro, A., Braat, C.E., Louie, P., Fitzpatrick, S.L., Waisman, D.M., 1997. Characterization of the Heparin Binding Properties of Annexin II Tetramer. J. Biol. Chem. 272, 15093–15100. https://doi.org/10.1074/jbc.272.24.15093
Katono, K., Sato, Y., Jiang, S.-X., Kobayashi, M., Saito, K., Nagashio, R., Ryuge, S., Satoh, Y., Saegusa, M., Masuda, N., 2016. Clinicopathological Significance of S100A10 Expression in Lung Adenocarcinomas. Asian Pac. J. Cancer Prev. 17, 289–294. https://doi.org/10.7314/apjcp.2016.17.1.289
Kattula, S., Byrnes, J.R., Wolberg, A.S., 2017. Fibrinogen and Fibrin in Hemostasis and Thrombosis. Arteriosclerosis, Thrombosis, and Vascular Biology 37, e13–e21. https://doi.org/10.1161/ATVBAHA.117.308564
Kaur, J., Tuor, U.I., Zhao, Z., Barber, P.A., 2011. Quantitative MRI reveals the elderly ischemic brain is susceptible to increased early blood-brain barrier permeability following tissue plasminogen activator related to claudin 5 and occludin disassembly. J. Cereb. Blood Flow Metab. 31, 1874–1885. https://doi.org/10.1038/jcbfm.2011.79
Khanna, N.C., Helwig, E.D., Ikebuchi, N.W., Fitzpatrick, S., Bajwa, R., Waisman, D.M., 1990. Purification and characterization of annexin proteins from bovine lung. Biochemistry 29, 4852–4862.
Kipp, M., 2016. Remyelination strategies in multiple sclerosis: a critical reflection. Expert Review of Neurotherapeutics 16, 1–3. https://doi.org/10.1586/14737175.2016.1116387
Kipp, M., Nyamoya, S., Hochstrasser, T., Amor, S., 2017. Multiple sclerosis animal models: a clinical and histopathological perspective. Brain Pathol. 27, 123–137. https://doi.org/10.1111/bpa.12454
Klingelhöfer, J., Grum-Schwensen, B., Beck, M.K., Knudsen, R.S.P., Grigorian, M., Lukanidin, E., Ambartsumian, N., 2012. Anti-S100A4 Antibody Suppresses Metastasis Formation by Blocking Stroma Cell Invasion. Neoplasia 14, 1260-IN47. https://doi.org/10.1593/neo.121554
Knaust, A., Weber, M.V.R., Hammerschmidt, S., Bergmann, S., Frosch, M., Kurzai, O., 2007. Cytosolic proteins contribute to surface plasminogen recruitment of Neisseria meningitidis. J. Bacteriol. 189, 3246–3255. https://doi.org/10.1128/JB.01966-06
Ko, Y.-P., Flick, M.J., 2016. Fibrinogen Is at the Interface of Host Defense and Pathogen Virulence in Staphylococcus aureus Infection. Semin Thromb Hemost 42, 408–421. https://doi.org/10.1055/s-0036-1579635

Köhler, S., Schmid, F., Settanni, G., 2015. The Internal Dynamics of Fibrinogen and Its Implications for Coagulation and Adsorption. PLOS Computational Biology 11, e1004346. https://doi.org/10.1371/journal.pcbi.1004346

Kornblatt, J.A., Barretto, T.A., Chigogidze, K., Chirwa, B., 2007. Canine Plasminogen: Spectral Responses to Changes in 6-Aminohexanoate and Temperature. Anal Chem Insights 2, 17–29.

Kornblatt, J.A., Rajotte, I., Heitz, F., 2001. Reaction of canine plasminogen with 6-aminohexanoate: a thermodynamic study combining fluorescence, circular dichroism, and isothermal titration calorimetry. Biochemistry 40, 3639–3647.

Kumar, V., Abbas, A.K., Aster, J.C., 2015. Robbins and Cotran Pathologic Basis of Disease, 9th ed. Elsevier.

Kwon, M., MacLeod, T.J., Zhang, Y., Waisman, D.M., 2005. S100A10, annexin A2, and annexin a2 heterotetramer as candidate plasminogen receptors. Front. Biosci. 10, 300–325.

Kwon, M., Yoon, C.S., Fitzpatrick, S., Kassam, G., Graham, K.S., Young, M.K., Waisman, D.M., 2001. p22 is a novel plasminogen fragment with antiangiogenic activity. Biochemistry 40, 13246–13253. https://doi.org/10.1021/bi0113420

Laemmli, U.K., 1970. Cleavage of Structural Proteins during the Assembly of the Head of Bacteriophage T4. Nature 227, 680–685. https://doi.org/10.1038/227680a0

Lakowicz, J.R., 2006. Protein Fluorescence, in: Principles of Fluorescence Spectroscopy. Springer US, Boston, MA, pp. 529–575. https://doi.org/10.1007/978-0-387-46312-4_16

Lassmann, H., Bradl, M., 2017. Multiple sclerosis: experimental models and reality. Acta Neuropathol 133, 223–244. https://doi.org/10.1007/s00401-016-1631-4

Law, M.J., Deibler, G.E., Martenson, R.E., Krutzsch, H.C., 1985. Cleavage of rabbit myelin basic protein by plasmin: isolation and identification of the major products. J. Neurochem. 45, 1232–1243.

Law, R.H.P., Abu-Ssaydeh, D., Whisstock, J.C., 2013. New insights into the structure and function of the plasminogen/plasmin system. Curr. Opin. Struct. Biol. 23, 836–841. https://doi.org/10.1016/j.sbi.2013.10.006

Law, R.H.P., Caradoc-Davies, T., Cowieson, N., Horvath, A.J., Quek, A.J., Encarnacao, J.A., Steer, D., Cowan, A., Zhang, Q., Lu, B.G.C., Pike, R.N., Smith, A.I., Coughlin, P.B., Whisstock, J.C., 2012. The X-ray Crystal Structure of Full-Length Human Plasminogen. Cell Reports 1, 185–190. https://doi.org/10.1016/j.celrep.2012.02.012

Lecander, I., Astedt, B., 1986. Isolation of a new specific plasminogen activator inhibitor from pregnancy plasma. Br. J. Haematol. 62, 221–228.

Lee, T.W., Tsang, V.W.K., Loef, E.J., Birch, N.P., 2017. Physiological and pathological functions of neuroserpin: Regulation of cellular responses through multiple mechanisms. Semin. Cell Dev. Biol. 62, 152–159. https://doi.org/10.1016/j.semcdb.2016.09.007

Leung, L.L.K., Morser, J., 2018. Carboxypeptidase B2 and carboxypeptidase N in the crosstalk between coagulation, thrombosis, inflammation, and innate immunity. Journal of Thrombosis and Haemostasis 16, 1474–1486. https://doi.org/10.1111/jth.14199

Lijnen, H.R., Collen, D., 2003. Role of the Plasminogen and MMP Systems in Wound Healing, in: Waisman, D.M. (Ed.), Plasminogen: Structure, Activation, and Regulation. Springer US, Boston, MA, pp. 189–200. https://doi.org/10.1007/978-1-4615-0165-7_11

Lijnen, H.R., Collen, D., 1995. 1 Mechanisms of physiological fibrinolysis. Baillière's Clinical Haematology, Fibrinolysis 8, 277–290. https://doi.org/10.1016/S0950-3536(05)80268-9

Lokman, N.A., Pyragius, C.E., Ruszkiewicz, A., Oehler, M.K., Ricciardelli, C., 2016. Annexin A2 and S100A10 are independent predictors of serous ovarian cancer outcome. Transl Res 171, 83-95.e1–2. https://doi.org/10.1016/j.trsl.2016.02.002

Longstaff, C., Kolev, K., 2015. Basic mechanisms and regulation of fibrinolysis. Journal of Thrombosis and Haemostasis 13, S98–S105. https://doi.org/10.1111/jth.12935

Longstaff, C., Thelwell, C., Williams, S.C., Silva, M.M.C.G., Szabó, L., Kolev, K., 2011. The interplay between tissue plasminogen activator domains and fibrin structures in the regulation of fibrinolysis: kinetic and microscopic studies. Blood 117, 661–668. https://doi.org/10.1182/blood-2010-06-290338

Lord, S.T., 2007. Fibrinogen and fibrin: scaffold proteins in hemostasis: Current Opinion in Hematology 14, 236–241. https://doi.org/10.1097/MOH.0b013e3280dce58c

Lublin, F.D., Knobler, R.L., Kalman, B., Goldhaber, M., Marini, J., Perrault, M., D'Imperio, C., Joseph, J., Alkan, S.S., Korngold, R., 1993. Monoclonal anti-gamma interferon antibodies enhance experimental allergic encephalomyelitis. Autoimmunity 16, 267–274. https://doi.org/10.3109/08916939309014645

Machovich, R., Owen, W.G., 1997. Denatured proteins as cofactors for plasminogen activation. Arch. Biochem. Biophys. 344, 343–349. https://doi.org/10.1006/abbi.1997.0221

MacLeod, T.J., Kwon, M., Filipenko, N.R., Waisman, D.M., 2003. Phospholipid-associated annexin A2-S100A10 heterotetramer and its subunits: characterization of the interaction with tissue plasminogen activator, plasminogen, and plasmin. J. Biol. Chem. 278, 25577–25584. https://doi.org/10.1074/jbc.M301017200

Madureira, P.A., O'Connell, P.A., Surette, A.P., Miller, V.A., Waisman, D.M., 2012. The biochemistry and regulation of S100A10: a multifunctional plasminogen receptor involved in oncogenesis. J. Biomed. Biotechnol. 2012, 353687. https://doi.org/10.1155/2012/353687

Madureira, P.A., Surette, A.P., Phipps, K.D., Taboski, M.A.S., Miller, V.A., Waisman, D.M., 2011. The Role of the Annexin A2 Heterotetramer in Vascular Fibrinolysis. Blood 118, 4789–4797. https://doi.org/10.1182/blood-2011-06-334672

Malleshappa Gowder, S., Chatterjee, J., Chaudhuri, T., Paul, K., 2014. Prediction and Analysis of Surface Hydrophobic Residues in Tertiary Structure of Proteins [WWW Document]. The Scientific World Journal. https://doi.org/10.1155/2014/971258

Malpass, K., 2012. "Outside-in" demyelination in MS. Nat Rev Neurol 8, 61–61. https://doi.org/10.1038/nrneurol.2011.217

Marik, C., Felts, P.A., Bauer, J., Lassmann, H., Smith, K.J., 2007. Lesion genesis in a subset of patients with multiple sclerosis: a role for innate immunity? Brain 130, 2800–2815. https://doi.org/10.1093/brain/awm236

Marrie, R.A., Walld, R., Bolton, J.M., Sareen, J., Walker, J.R., Patten, S.B., Singer, A., Lix, L.M., Hitchon, C.A., El-Gabalawy, R., Katz, A., Fisk, J.D., Bernstein, C.N., CIHR Team in Defining the Burden and Managing the Effects of Psychiatric Comorbidity in Chronic Immunoinflammatory Disease, 2017. Estimating annual prevalence of depression and anxiety disorder in multiple sclerosis using administrative data. BMC Res Notes 10, 619. https://doi.org/10.1186/s13104-017-2958-1

Marti, D.N., Hu, C.-K., An, S.S.A., von Haller, P., Schaller, J., Llinás, M., 1997. Ligand Preferences of Kringle 2 and Homologous Domains of Human Plasminogen: Canvassing Weak, Intermediate, and High-Affinity Binding Sites by 1H-NMR. Biochemistry 36, 11591–11604. https://doi.org/10.1021/bi971316v

Mehra, A., Ali, C., Parcq, J., Vivien, D., Docagne, F., 2016. The plasminogen activation system in neuroinflammation. Biochimica et Biophysica Acta (BBA) - Molecular Basis of Disease, NEUROINFLAMMATION: A common denominator for stroke, multiple sclerosis and Alzheimer's disease 1862, 395–402. https://doi.org/10.1016/j.bbadis.2015.10.011

Melchor, J.P., Pawlak, R., Strickland, S., 2003. The Tissue Plasminogen Activator-Plasminogen Proteolytic Cascade Accelerates Amyloid-β (Aβ) Degradation and Inhibits Aβ-Induced Neurodegeneration. J. Neurosci. 23, 8867–8871.

Melchor, J.P., Strickland, S., 2005. Tissue plasminogen activator in central nervous system physiology and pathology. Thromb Haemost 93, 655–660. https://doi.org/10.1160/TH04-12-0838

Mestas, J., Hughes, C.C.W., 2004. Of mice and not men: differences between mouse and human immunology. J. Immunol. 172, 2731–2738. https://doi.org/10.4049/jimmunol.172.5.2731
Miles, L.A., Andronicos, N.M., Chen, E.I., Baik, N., Bai, H., Parmer, C.M., Lighvani, S., Nangia, S., Kiosses, W.B., Kamps, M.P., Iii, J.R.Y., Parmer, R.J., 2012. Identification of the Novel Plasminogen Receptor, Plg-RKT. https://doi.org/10.5772/31113
Miles, L.A., Dahlberg, C.M., Plescia, J., Felez, J., Kato, K., Plow, E.F., 1991. Role of cell-surface lysines in plasminogen binding to cells: identification of .alpha.-enolase as a candidate plasminogen receptor. Biochemistry 30, 1682–1691. https://doi.org/10.1021/bi00220a034
Miles, L.A., Dahlberg, C.M., Plow, E.F., 1988. The cell-binding domains of plasminogen and their function in plasma. J. Biol. Chem. 263, 11928–11934.
Miles, L.A., Parmer, R.J., 2013. Plasminogen receptors: the first quarter century. Semin. Thromb. Hemost. 39, 329–337. https://doi.org/10.1055/s-0033-1334483
Miller, R.H., Fyffe-Maricich, S., Caprariello, A.C., 2017. Chapter 37 - Animal Models for the Study of Multiple Sclerosis, in: Conn, P.M. (Ed.), Animal Models for the Study of Human Disease (Second Edition). Academic Press, pp. 967–988. https://doi.org/10.1016/B978-0-12-809468-6.00037-1
Miller, V.A., Madureira, P.A., Kamaludin, A.A., Komar, J., Sharma, V., Sahni, G., Thelwell, C., Longstaff, C., Waisman, D.M., 2017. Mechanism of plasmin generation by S100A10. Thromb. Haemost. 117, 1058–1071. https://doi.org/10.1160/TH16-12-0936
Milosevic, A., Liebmann, T., Knudsen, M., Schintu, N., Svenningsson, P., Greengard, P., 2017. Cell- and Region-Specific Expression of Depression-Related Protein p11 (S100A10) in the Brain. Journal of Comparative Neurology 525, 955–975. https://doi.org/10.1002/cne.24113
Montagne, A., Barnes, S.R., Sweeney, M.D., Halliday, M.R., Sagare, A.P., Zhao, Z., Toga, A.W., Jacobs, R.E., Liu, C.Y., Amezcua, L., Harrington, M.G., Chui, H.C., Law, M., Zlokovic, B.V., 2015. Blood-Brain Barrier Breakdown in the Aging Human Hippocampus. Neuron 85, 296–302. https://doi.org/10.1016/j.neuron.2014.12.032
Muradashvili, N., Tyagi, S.C., Lominadze, D., 2017. Localization of Fibrinogen in the Vasculo-Astrocyte Interface after Cortical Contusion Injury in Mice. Brain Sci 7. https://doi.org/10.3390/brainsci7070077
Murphy, R.P., Murphy, K.J., Pickering, M., 2013. The development of myelin repair agents for treatment of multiple sclerosis. Bioengineered 4, 140–146. https://doi.org/10.4161/bioe.22835
Myrvang, H.K., Guo, X., Li, C., Dekker, L.V., 2013. Protein interactions between surface annexin A2 and S100A10 mediate adhesion of breast cancer cells

to microvascular endothelial cells. FEBS Letters 587, 3210–3215. https://doi.org/10.1016/j.febslet.2013.08.012
Nagashima, M., Yin, Z.-F., Broze, G.J., Morser, J., 2002. Thrombin-activatable fibrinolysis inhibitor (TAFI) deficient mice. Front. Biosci. 7, d556-568.
Nexø, B.A., Jensen, S.B., Nissen, K.K., Hansen, B., Laska, M.J., 2016. Two endogenous retroviral loci appear to contribute to Multiple Sclerosis. BMC Neurology 16, 57. https://doi.org/10.1186/s12883-016-0580-9
Niego, B., Freeman, R., Puschmann, T.B., Turnley, A.M., Medcalf, R.L., 2012. t-PA–specific modulation of a human blood-brain barrier model involves plasmin-mediated activation of the Rho kinase pathway in astrocytes. Blood 119, 4752–4761. https://doi.org/10.1182/blood-2011-07-369512
Norton, W.T., Cammer, W., Bloom, B.R., Gordon, S., 1978. Neutral proteinases secreted by macrophages degrade basic protein: a possible mechanism of inflammatory demyelination. Adv. Exp. Med. Biol. 100, 365–381.
Noye, T.M., Lokman, N.A., Oehler, M.K., Ricciardelli, C., 2018. S100A10 and Cancer Hallmarks: Structure, Functions, and its Emerging Role in Ovarian Cancer. Int J Mol Sci 19. https://doi.org/10.3390/ijms19124122
Obermeier, B., Verma, A., Ransohoff, R.M., 2016. The blood-brain barrier. Handb Clin Neurol 133, 39–59. https://doi.org/10.1016/B978-0-444-63432-0.00003-7
O'Connell, P.A., Surette, A.P., Liwski, R.S., Svenningsson, P., Waisman, D.M., 2010. S100A10 Regulates Plasminogen-Dependent Macrophage Invasion. Blood 116, 1136–1146. https://doi.org/10.1182/blood-2010-01-264754
Oleszak, E.L., Chang, J.R., Friedman, H., Katsetos, C.D., Platsoucas, C.D., 2004. Theiler's Virus Infection: a Model for Multiple Sclerosis. Clin Microbiol Rev 17, 174–207. https://doi.org/10.1128/CMR.17.1.174-207.2004
Ortolano, S., Spuch, C., 2012. tPA in the Central Nervous System: Relations Between tPA and Cell Surface LRPs. Recent Patents on Endocrine, Metabolic & Immune Drug Discovery 7, 65–76. https://doi.org/10.2174/1872214811307010065
Ousman, S.S., David, S., 2000. Lysophosphatidylcholine induces rapid recruitment and activation of macrophages in the adult mouse spinal cord. Glia 30, 92–104. https://doi.org/10.1002/(SICI)1098-1136(200003)30:1<92::AID-GLIA10>3.0.CO;2-W
Panitch, H.S., Hirsch, R.L., Haley, A.S., Johnson, K.P., 1987. Exacerbations of multiple sclerosis in patients treated with gamma interferon. Lancet 1, 893–895. https://doi.org/10.1016/s0140-6736(87)92863-7
Parkkinen, J., Rauvala, H., 1991. Interactions of plasminogen and tissue plasminogen activator (t-PA) with amphoterin. Enhancement of t-PA-catalyzed plasminogen activation by amphoterin. J. Biol. Chem. 266, 16730–16735.

Patibandla, P.K., Tyagi, N., Dean, W.L., Tyagi, S.C., Roberts, A.M., Lominadze, D., 2009. Fibrinogen induces alterations of endothelial cell tight junction proteins. J. Cell. Physiol. 221, 195–203. https://doi.org/10.1002/jcp.21845

Patten, S.B., Marrie, R.A., Carta, M.G., 2017. Depression in multiple sclerosis. Int Rev Psychiatry 29, 463–472. https://doi.org/10.1080/09540261.2017.1322555

Paul, J., Strickland, S., Melchor, J.P., 2007. Fibrin deposition accelerates neurovascular damage and neuroinflammation in mouse models of Alzheimer's disease. J Exp Med 204, 1999–2008. https://doi.org/10.1084/jem.20070304

Petersen, M.A., Ryu, J.K., Akassoglou, K., 2018. Fibrinogen in neurological diseases: mechanisms, imaging and therapeutics. Nature Reviews Neuroscience 19, 283. https://doi.org/10.1038/nrn.2018.13

Phipps, K.D., Surette, A.P., O'Connell, P.A., Waisman, D.M., 2011. Plasminogen Receptor S100A10 Is Essential for the Migration of Tumor-Promoting Macrophages into Tumor Sites. Cancer Res 71, 6676–6683. https://doi.org/10.1158/0008-5472.CAN-11-1748

Pieters, M., Wolberg, A.S., 2019. Fibrinogen and fibrin: An illustrated review. Research and Practice in Thrombosis and Haemostasis 3, 161–172. https://doi.org/10.1002/rth2.12191

Plemel, J.R., Michaels, N.J., Weishaupt, N., Caprariello, A.V., Keough, M.B., Rogers, J.A., Yukseloglu, A., Lim, J., Patel, V.V., Rawji, K.S., Jensen, S.K., Teo, W., Heyne, B., Whitehead, S.N., Stys, P.K., Yong, V.W., 2018. Mechanisms of lysophosphatidylcholine-induced demyelination: A primary lipid disrupting myelinopathy. Glia 66, 327–347. https://doi.org/10.1002/glia.23245

Ploplis, V.A., Carmeliet, P., Vazirzadeh, S., Van Vlaenderen, I., Moons, L., Plow, E.F., Collen, D., 1995. Effects of Disruption of the Plasminogen Gene on Thrombosis, Growth, and Health in Mice. Circulation 92, 2585–2593. https://doi.org/10.1161/01.cir.92.9.2585

Plow, E.F., Herren, T., Redlitz, A., Miles, L.A., Hoover-Plow, J.L., 1995. The Cell Biology of the Plasminogen System. FASEB Journal 9, 939–945.

Poddar, N.K., Maurya, S.K., Saxena, V., 2017. Role of Serine Proteases and Inhibitors in Cancer, in: Chakraborti, S., Dhalla, N.S. (Eds.), Proteases in Physiology and Pathology. Springer Singapore, Singapore, pp. 257–287. https://doi.org/10.1007/978-981-10-2513-6_12

Pollak, Y., Orion, E., Goshen, I., Ovadia, H., Yirmiya, R., 2002. Experimental autoimmune encephalomyelitis-associated behavioral syndrome as a model of 'depression due to multiple sclerosis.' Brain, Behavior, and Immunity 16, 533–543. https://doi.org/10.1016/S0889-1591(02)00010-7

Procaccini, C., De Rosa, V., Pucino, V., Formisano, L., Matarese, G., 2015. Animal models of Multiple Sclerosis. Eur. J. Pharmacol. 759, 182–191. https://doi.org/10.1016/j.ejphar.2015.03.042

Rahmanzadeh, R., Moghadasi, A.N., Navardi, S., Minagar, A., Sahraian, M.A., 2018. Chapter 1 - Multiple Sclerosis: Clinical Features, Pathophysiology, Diagnosis, and Management, in: Minagar, A. (Ed.), Neuroinflammation (Second Edition). Academic Press, pp. 1–20. https://doi.org/10.1016/B978-0-12-811709-5.00001-6

Ranson, M., Andronicos, N.M., 2003. Plasminogen binding and cancer: promises and pitfalls. Front. Biosci. 8, s294-304. https://doi.org/10.2741/1044

Réty, S., Sopkova, J., Renouard, M., Osterloh, D., Gerke, V., Tabaries, S., Russo-Marie, F., Lewit-Bentley, A., 1999. The crystal structure of a complex of p11 with the annexin II N-terminal peptide. Nat. Struct. Biol. 6, 89–95. https://doi.org/10.1038/4965

Rijken, D.C., Lijnen, H.R., 2009. New insights into the molecular mechanisms of the fibrinolytic system. Journal of Thrombosis and Haemostasis 7, 4–13. https://doi.org/10.1111/j.1538-7836.2008.03220.x

Roda, O., Valero, M.L., Peiró, S., Andreu, D., Real, F.X., Navarro, P., 2003. New insights into the tPA-annexin A2 interaction. Is annexin A2 CYS8 the sole requirement for this association? J. Biol. Chem. 278, 5702–5709. https://doi.org/10.1074/jbc.M207605200

Ryu, J.K., McLarnon, J.G., 2009. A leaky blood–brain barrier, fibrinogen infiltration and microglial reactivity in inflamed Alzheimer's disease brain. Journal of Cellular and Molecular Medicine 13, 2911–2925. https://doi.org/10.1111/j.1582-4934.2008.00434.x

Ryu, J.K., Petersen, M.A., Murray, S.G., Baeten, K.M., Meyer-Franke, A., Chan, J.P., Vagena, E., Bedard, C., Machado, M.R., Coronado, P.E.R., Prod'homme, T., Charo, I.F., Lassmann, H., Degen, J.L., Zamvil, S.S., Akassoglou, K., 2015. Blood coagulation protein fibrinogen promotes autoimmunity and demyelination via chemokine release and antigen presentation. Nat Commun 6, 8164. https://doi.org/10.1038/ncomms9164

Ryu, J.K., Rafalski, V.A., Meyer-Franke, A., Adams, R.A., Poda, S.B., Coronado, P.E.R., Pedersen, L.Ø., Menon, V., Baeten, K.M., Sikorski, S.L., Bedard, C., Hanspers, K., Bardehle, S., Mendiola, A.S., Davalos, D., Machado, M.R., Chan, J.P., Plastira, I., Petersen, M.A., Pfaff, S.J., Ang, K.K., Hallenbeck, K.K., Syme, C., Hakozaki, H., Ellisman, M.H., Swanson, R.A., Zamvil, S.S., Arkin, M.R., Zorn, S.H., Pico, A.R., Mucke, L., Freedman, S.B., Stavenhagen, J.B., Nelson, R.B., Akassoglou, K., 2018. Fibrin-targeting immunotherapy protects against neuroinflammation and neurodegeneration. Nature Immunology 1. https://doi.org/10.1038/s41590-018-0232-x

Sasaki, Y., Ohsawa, K., Kanazawa, H., Kohsaka, S., Imai, Y., 2001. Iba1 is an actin-cross-linking protein in macrophages/microglia. Biochem. Biophys. Res. Commun. 286, 292–297. https://doi.org/10.1006/bbrc.2001.5388

Sato, F., Omura, S., Martinez, N.E., Tsunoda, I., 2018. Chapter 3 - Animal Models of Multiple Sclerosis, in: Minagar, A. (Ed.), Neuroinflammation (Second Edition). Academic Press, pp. 37–72. https://doi.org/10.1016/B978-0-12-811709-5.00003-X

Sato, K., Saiki, Y., Arai, K., Ishizawa, K., Fukushige, S., Aoki, K., Abe, J., Takahashi, S., Sato, I., Sakurada, A., Okada, Y., Horii, A., 2018. S100A10 upregulation associates with poor prognosis in lung squamous cell carcinoma. Biochem. Biophys. Res. Commun. 505, 466–470. https://doi.org/10.1016/j.bbrc.2018.09.118

Schaller, J., Gerber, S.S., 2011. The Plasmin–Antiplasmin System: Structural and Functional Aspects. Cellular and Molecular Life Sciences 68, 785–801. https://doi.org/10.1007/s00018-010-0566-5

Schindelin, J., Arganda-Carreras, I., Frise, E., Kaynig, V., Longair, M., Pietzsch, T., Preibisch, S., Rueden, C., Saalfeld, S., Schmid, B., Tinevez, J.-Y., White, D.J., Hartenstein, V., Eliceiri, K., Tomancak, P., Cardona, A., 2012. Fiji: an open-source platform for biological-image analysis. Nat. Methods 9, 676–682. https://doi.org/10.1038/nmeth.2019

Schmitt, M., Goretzki, L., Jänicke, F., Calvete, J., Eulitz, M., Kobayashi, H., Chucholowski, N., Graeff, H., 1991. Biological and clinical relevance of the urokinase-type plasminogen activator (uPA) in breast cancer. Biomed. Biochim. Acta 50, 731–741.

Schneider, C.A., Rasband, W.S., Eliceiri, K.W., 2012. NIH Image to ImageJ: 25 years of image analysis. Nat. Methods 9, 671–675. https://doi.org/10.1038/nmeth.2089

Schneider, T.D., Stephens, R.M., 1990. Sequence logos: a new way to display consensus sequences. Nucleic Acids Res. 18, 6097–6100. https://doi.org/10.1093/nar/18.20.6097

Schuh, C., Wimmer, I., Hametner, S., Haider, L., Van Dam, A.-M., Liblau, R.S., Smith, K.J., Probert, L., Binder, C.J., Bauer, J., Bradl, M., Mahad, D., Lassmann, H., 2014. Oxidative tissue injury in multiple sclerosis is only partly reflected in experimental disease models. Acta Neuropathol. 128, 247–266. https://doi.org/10.1007/s00401-014-1263-5

Semov, A., Moreno, M.J., Onichtchenko, A., Abulrob, A., Ball, M., Ekiel, I., Pietrzynski, G., Stanimirovic, D., Alakhov, V., 2005. Metastasis-associated protein S100A4 induces angiogenesis through interaction with Annexin II and accelerated plasmin formation. J. Biol. Chem. 280, 20833–20841. https://doi.org/10.1074/jbc.M412653200

Sharif, Y., Jumah, F., Coplan, L., Krosser, A., Sharif, K., Tubbs, R.S., 2018. Blood brain barrier: A review of its anatomy and physiology in health and disease. Clin Anat 31, 812–823. https://doi.org/10.1002/ca.23083

Shaw, M.A., Gao, Z., McElhinney, K.E., Thornton, S., Flick, M.J., Lane, A., Degen, J.L., Ryu, J.K., Akassoglou, K., Mullins, E.S., 2017. Plasminogen Deficiency Delays the Onset and Protects from Demyelination and Paralysis in

Autoimmune Neuroinflammatory Disease. J. Neurosci. 37, 3776–3788. https://doi.org/10.1523/JNEUROSCI.2932-15.2017
Simmons, S.B., Pierson, E.R., Lee, S.Y., Goverman, J.M., 2013. Modeling the heterogeneity of multiple sclerosis in animals. Trends in Immunology 34, 410–422. https://doi.org/10.1016/j.it.2013.04.006
Sofroniew, M.V., Vinters, H.V., 2010. Astrocytes: biology and pathology. Acta Neuropathol 119, 7–35. https://doi.org/10.1007/s00401-009-0619-8
Stephens, R.W., Pöllänen, J., Tapiovaara, H., Leung, K.C., Sim, P.S., Salonen, E.M., Rønne, E., Behrendt, N., Danø, K., Vaheri, A., 1989. Activation of pro-urokinase and plasminogen on human sarcoma cells: a proteolytic system with surface-bound reactants. J. Cell Biol. 108, 1987–1995. https://doi.org/10.1083/jcb.108.5.1987
Stoppelli, M.P., 2013. The Plasminogen Activation System in Cell Invasion. Landes Bioscience.
Su, E.J., Fredriksson, L., Geyer, M., Folestad, E., Cale, J., Andrae, J., Gao, Y., Pietras, K., Mann, K., Yepes, M., Strickland, D.K., Betsholtz, C., Eriksson, U., Lawrence, D.A., 2008. Activation of PDGF-CC by tissue plasminogen activator impairs blood-brain barrier integrity during ischemic stroke. Nat. Med. 14, 731–737. https://doi.org/10.1038/nm1787
Suenson, E., Petersen, L.C., 1986. Fibrin and Plasminogen Structures Essential to Stimulation of Plasmin Formation by Tissue-Type Plasminogen Activator - PubMed. Biochim Biophys Acta 870, 510–519.
Sun, Z., Chen, Y., Wang, P., Zhang, J., Gurewich, V., Zhang, P., Liu, J.-N., 2002. The blockage of the high-affinity lysine binding sites of plasminogen by EACA significantly inhibits prourokinase-induced plasminogen activation. Biochimica et Biophysica Acta (BBA) - Protein Structure and Molecular Enzymology 1596, 182–192. https://doi.org/10.1016/S0167-4838(02)00233-9
Surette, A.P., Madureira, P.A., Phipps, K.D., Miller, V.A., Svenningsson, P., Waisman, D.M., 2011. Regulation of Fibrinolysis by S100A10 in Vivo. Blood 118, 3172–3181. https://doi.org/10.1182/blood-2011-05-353482
Suzuki, S., Yamayoshi, Y., Nishimuta, A., Tanigawara, Y., 2011. S100A10 protein expression is associated with oxaliplatin sensitivity in human colorectal cancer cells. Proteome Sci 9, 1–12. https://doi.org/10.1186/1477-5956-9-76
Svenningsson, P., Chergui, K., Rachleff, I., Flajolet, M., Zhang, X., Yacoubi, M.E., Vaugeois, J.-M., Nomikos, G.G., Greengard, P., 2006. Alterations in 5-HT1B Receptor Function by P11 in Depression-Like States. Science 311, 77–80. https://doi.org/10.1126/science.1117571
Sweeney, M.D., Sagare, A.P., Zlokovic, B.V., 2018. Blood-brain barrier breakdown in Alzheimer disease and other neurodegenerative disorders. Nat Rev Neurol 14, 133–150. https://doi.org/10.1038/nrneurol.2017.188
Takada, Y., Makino, Y., Takada, A., 1985. Glu-plasminogen I and II: Their activation by urokinase and streptokinase in the presence of fibrin and

fibrinogen. Thrombosis Research 39, 289–296. https://doi.org/10.1016/0049-3848(85)90224-5
Tennent, G.A., Brennan, S.O., Stangou, A.J., O'Grady, J., Hawkins, P.N., Pepys, M.B., 2007. Human plasma fibrinogen is synthesized in the liver. Blood 109, 1971–1974. https://doi.org/10.1182/blood-2006-08-040956
Thompson, A.J., Baranzini, S.E., Geurts, J., Hemmer, B., Ciccarelli, O., 2018. Multiple sclerosis. The Lancet 391, 1622–1636. https://doi.org/10.1016/S0140-6736(18)30481-1
Tjärnlund-Wolf, A., Brogren, H., Lo, E.H., Wang, X., 2012. Plasminogen Activator Inhibitor-1 and Thrombotic Cerebrovascular Diseases. Stroke 43, 2833–2839. https://doi.org/10.1161/STROKEAHA.111.622217
Towbin, H., Staehelin, T., Gordon, J., 1979. Electrophoretic Transfer of Proteins from Polyacrylamide Gels to Nitrocellulose Sheets: Procedure and Some Applications. Proceedings of the National Academy of Sciences 76, 4350–4354.
Tyagi, N., Roberts, A.M., Dean, W.L., Tyagi, S.C., Lominadze, D., 2008. Fibrinogen induces endothelial cell permeability. Mol. Cell. Biochem. 307, 13–22. https://doi.org/10.1007/s11010-007-9579-2
Uversky, V.N., 2012. Size-exclusion chromatography in structural analysis of intrinsically disordered proteins. Methods Mol. Biol. 896, 179–194. https://doi.org/10.1007/978-1-4614-3704-8_11
van der Vorm, L.N., Remijn, J.A., de Laat, B., Huskens, D., 2018. Effects of Plasmin on von Willebrand Factor and Platelets: A Narrative Review. TH Open 2, e218–e228. https://doi.org/10.1055/s-0038-1660505
van Oijen, M., Witteman, J.C., Hofman, A., Koudstaal, P.J., Breteler, M.M.B., 2005. Fibrinogen is associated with an increased risk of Alzheimer disease and vascular dementia. Stroke 36, 2637–2641. https://doi.org/10.1161/01.STR.0000189721.31432.26
Wakefield, A.J., More, L.J., Difford, J., McLaughlin, J.E., 1994. Immunohistochemical study of vascular injury in acute multiple sclerosis. J Clin Pathol 47, 129–133.
Wang, H., Karlsson, A., Sjöström, I., Wiman, B., 2006. The interaction between plasminogen and antiplasmin variants as studied by surface plasmon resonance. Biochimica et Biophysica Acta (BBA) - Proteins and Proteomics 1764, 1730–1734. https://doi.org/10.1016/j.bbapap.2006.09.009
Wang, H., Yu, A., Wiman, B., Pap, S., 2003. Identification of amino acids in antiplasmin involved in its noncovalent 'lysine-binding-site'-dependent interaction with plasmin. Eur. J. Biochem. 270, 2023–2029. https://doi.org/10.1046/j.1432-1033.2003.03578.x
Warford, J.R., Lamport, A.-C., Clements, D.R., Malone, A., Kennedy, B.E., Kim, Y., Gujar, S.A., Hoskin, D.W., Easton, A.S., 2018. Surfen, a proteoglycan binding agent, reduces inflammation but inhibits remyelination in murine

models of Multiple Sclerosis. Acta Neuropathologica Communications 6, 4. https://doi.org/10.1186/s40478-017-0506-9
Weisel, J.W., 2005. Fibrinogen and Fibrin, in: Chemistry, B.-A. in P. (Ed.), Fibrous Proteins: Coiled-Coils, Collagen and Elastomers. Academic Press, pp. 247–299.
Weisel, J.W., Medved, L., 2001. The Structure and Function of the αC Domains of Fibrinogen. Annals of the New York Academy of Sciences 936, 312–327.
Wen, L., Huang, J.K., Johnson, B.H., Reeck, G.R., 1989. A human placental cDNA clone that encodes nonhistone chromosomal protein HMG-1. Nucleic Acids Res. 17, 1197–1214. https://doi.org/10.1093/nar/17.3.1197
Whitmore, L., Wallace, B.A., 2008. Protein secondary structure analyses from circular dichroism spectroscopy: methods and reference databases. Biopolymers 89, 392–400. https://doi.org/10.1002/bip.20853
Whitmore, L., Wallace, B.A., 2004. DICHROWEB, an online server for protein secondary structure analyses from circular dichroism spectroscopic data. Nucleic Acids Res 32, W668–W673. https://doi.org/10.1093/nar/gkh371
Wiman, B., Lijnen, H.R., Collen, D., 1979. On the specific interaction between the lysine-binding sites in plasmin and complementary sites in α2-antiplasmin and in fibrinogen. Biochimica et Biophysica Acta (BBA) - Protein Structure 579, 142–154. https://doi.org/10.1016/0005-2795(79)90094-1
Wingerchuk, D.M., 2011. Environmental factors in multiple sclerosis: Epstein-Barr virus, vitamin D, and cigarette smoking. Mt. Sinai J. Med. 78, 221–230. https://doi.org/10.1002/msj.20240
Winter, W.E., Flax, S.D., Harris, N.S., 2017. Coagulation Testing in the Core Laboratory. Lab Med 48, 295–313. https://doi.org/10.1093/labmed/lmx050
Wintersberger, E., Cox, D.J., Neurath, H., 1962. Bovine pancreatic procarboxypeptidase B. I. Isolation, properties, and activation. Biochemistry 1, 1069–1078. https://doi.org/10.1021/bi00912a017
Wolberg, A.S., 2007. Thrombin generation and fibrin clot structure. Blood Reviews 21, 131–142. https://doi.org/10.1016/j.blre.2006.11.001
Yepes, M., Lawrence, D.A., 2004. Neuroserpin: a selective inhibitor of tissue-type plasminogen activator in the central nervous system. Thromb. Haemost. 91, 457–464. https://doi.org/10.1160/TH03-12-0766
Zhang, L., Fogg, D.K., Waisman, D.M., 2004. RNA Interference-mediated Silencing of the S100A10 Gene Attenuates Plasmin Generation and Invasiveness of Colo 222 Colorectal Cancer Cells. J. Biol. Chem. 279, 2053–2062.